SINGLE-CELL AND SINGLE-MOLECULE STUDIES OF BACTERIOPHAGE LAMBDA POST-INFECTION DECISION-MAKING

A Dissertation

by

QIUYAN SHAO

Submitted to the Office of Graduate and Professional Studies of
Texas A&M University
in partial fulfillment of the requirements for the degree of

DOCTOR OF PHILOSOPHY

Chair of Committee,	Lanying Zeng
Committee Members,	Deborah Siegele
	Jean-Philippe Pellois
	Ryland F. Young
Head of Department,	Gregory Reinhart

December 2017

Major Subject: Biochemistry

ABSTRACT

Cellular decision making is a ubiquitous process among all life forms, and a key step that organisms take to integrate the environmental signals to choose an optimal response to improve their overall fitness. The genetic circuits selected to carry out this task determine the cell fate in a seemingly probabilistic way, either due to the inherent stochasticity of the system, or our inability to characterize the factors with deterministic impacts. To gain a better understanding of the mechanisms underlying cell-fate selection, we utilize a well-established system for cellular decision-making, the paradigm of bacteriophage lambda infection, which leads to two distinct outcomes – lysis and lysogeny. Recent studies of this system using higher resolution techniques suggested that different phage decisions are partially determined by pre-existing difference and the complex *in vivo* phage-phage interactions. Therefore, characterizing more 'hidden' deterministic factors and dissecting the intracellular behaviors of phage components, such as DNA, RNA and proteins are central to a more complete understanding of the phage decision-making strategies. One commonly overlooked but potentially important factor is phage DNA replication, which could result in not only more templates for gene expression but also introduce gene copy number variations. Meanwhile, although theoretical work has long predicted that noise arising from stochastic gene expression can be propagated through the gene networks to result in phenotypic variance, experimental characterization is still lacking, impeding the assessment of its contributions to phage decision-making.

In this work, we provided direct experimental evidence that different phage DNAs are capable of making decisions independently. DNA integration, a characteristic event for phage lysogenization, can also be detected in lytic cells. Moreover, through single phage DNA labeling technique, we revealed great heterogeneity in intracellular DNA motions, which could partially explain the complex phage-phage interactions. Furthermore, we found that DNA replication is important for the enforcement of decisions. Instead of affecting the transcription of early lysis-lysogeny decision-making genes, DNA replication exerts its effect on the expression of the decision effectors, CI. Lastly, a mathematical model is built to provide comprehensive understanding of the decision making network.

ACKNOWLEDGEMENTS

I would like to thank my thesis advisor, Dr. Lanying Zeng, for her guidance, support and encouragement over the past 6 years at Texas A&M University on research work. I also greatly appreciate the opportunities that she provided for scientific trainings, collaborations, and the freedom to explore. Without her help and guidance, I wouldn't have become as confident and independent as I am now. I am also thankful to my committee members, Dr. Deborah Siegele, Dr. Jean-Philippe Pellois, and Dr. Ry Young, for their great suggestions and efforts to promote the ongoing of my research and to improve my presentation skills. I also want to give my special thanks to Dr. Ry Young for many informative discussions, helpful suggestions, and motivating remarks. He was willing to spend a lot of time sharing his knowledge with me, to help me in trouble-shooting, and to provide great suggestions for project developments. His enthusiasm and love for science would continue to motivate me to explore. I also want to thank Dr. Gábor Balázsi and Michael Cortes for great collaborations and valuable advice on mathematical modeling. I also thank the past and present members of the Zeng laboratory, Alex Hawkins, Jimmy T. Trinh, Jinbai Guo, Xu Shi, Chanda Bhat, Jingwen Guan, Kailun Zhang and Laith Harb, for their help and great discussions. I am also greatly thankful to the members of the Young Laboratory, especially Karthik Reddy Chamakura, Rohit Kongari, Irina Chen, Manoj Rajaure, and Adriana Carolina Hernandez, for sharing protocols, reagents and a lot of helpful suggestions. I also want to thank the undergraduate students, Laura Moehlman, Dat Nguyen, Jaynish Amin,

Colby McIntosh, and James Corban, for their help with experiments and bringing more fun to lab.

Thanks to my family and friends for their support and confidence in me. Thanks also go to my friends and colleagues here and the department faculty and staff for making my time at Texas A&M University a great experience.

Finally, thanks to my parents for their love and patience in me.

CONTRIBUTORS AND FUNDING SOURCES

Contributors

This work was supervised by a dissertation committee consisting of Dr. Lanying Zeng, Dr. Jean-Philippe Pellois, Dr. Ryland F. Young of the Department of Biochemistry and Biophysics and Dr. Deborah Siegele of the Department of Biology.

The SeqA DNA labeling system in Chapter II is constructed by Alex Hawkins and Dr. Lanying Zeng, data analysis and paper writing was in part done by Dr. Lanying Zeng. The WT fluorescent phage and the *E. coli* strain with *tetO* repeats reported in Chapter III were in part constructed by Jimmy T. Trinh. Colby McIntosh helps with the data analysis in Chapter III. The mathematical modeling in Chapter IV were mainly done by Michael Cortes in Dr. Gábor Balázsi's lab in Laufer Center for Physical & Quantitative Biology, Stony Brook University. The real-time live-cell imaging of the WT and P^- phage mutants were in part conducted by Jimmy T. Trinh, and the smFISH probe for *cII* were designed and labeled by Jingwen Guan.

All other work conducted for the dissertation was completed by the student independently.

Funding Sources

This work was made possible in part by Texas A&M AgriLife Research and National Institutes of Health under Grant Number R01GM107597.

Its contents are solely the responsibility of the authors and do not necessarily represent the official views of the Texas A&M AgriLife Research and National Institute of Health.

TABLE OF CONTENTS

Page

ABSTRACT ii

ACKNOWLEDGEMENTS iv

CONTRIBUTORS AND FUNDING SOURCES vi

TABLE OF CONTENTS vii

LIST OF FIGURES x

LIST OF TABLES xiii

CHAPTER I INTRODUCTION AND LITERATURE REVIEW 1

Introduction 1
Players of the Lambda Decision Making 2
CI and Cro 5
CII and CIII 9
Q 12
Phage DNA replication 16
Deterministic Factors Affecting the Lysis-Lysogeny Decision Making 21
Multiplicity of infection (MOI), cell size and phage voting 21
Position of phage infection 24
Stochastic Factors Affecting the Lysis-Lysogeny Decision Making 26
Stochastic gene expression 28
Heterogeneity of the bacterial cytoplasm 31
Heterogeneity in the timing of phage DNA ejection 40
The Thesis Overview 42

CHAPTER II PHAGE DNA DYNAMICS IN CELLS WITH DIFFERENT FATES 44

Introduction 44
Materials and Methods 47
Bacterial strains, plasmids, phages and primers 47
Construction of the plasmid pACYC177-PLate*D-eyfp 47
Fully methylated fluorescent phages 50
Construction of the SeqA-ECFP 51
Fully methylated fluorescent phage shows the same lysogenic response in different hosts in bulk 52

Microscopy and imaging 52
Results 58
A plasmid-based approach for the construction of stable, well-behaved and fluorescent phage lambda 58
Phage DNA detection 60
Phage DNA dynamics during the immediately early stage of phage infection in living cells 63
Phage DNA shows different patterns of motions during the late stage of phage infection in lytic and lysogenic cells 65
Phage DNA locates at similar positions for both lytic and lysogenic cells 74
Discussion 79

CHAPTER III LYSIS-LYSOGENY COEXISTENCE: PROPHAGE INTEGRATION DURING LYTIC DEVELOPMENT 84

Introduction 84
Materials and Methods 86
Bacterial strains 86
Plasmid construction 86
Phage strains 89
Phage lysate preparation 90
Bulk lysogenization assay 90
PCR and qPCR 91
Quantifying percentage of multiple prophage integration 94
Microscopy 94
Data analysis 95
Results 97
Reporter system for phage DNA integration: E. coli attB and phage DNA labeling 97
Lyso-lysis: cell lysis with phage DNA integration 100
E. coli attB migrates towards the cell pole in lytic cells, leading to more co-localization with lambda DNA 104
Lyso-lysis: a process regulated by CII 106
Discussion 109

CHAPTER IV CRO AND DNA REPLICATION REGULATE STOCHASTIC CELL-FATE SELECTION BY BACTERIOPHAGE LAMBDA 116

Introduction 116
Materials and Methods 118
Plasmid, bacterial and phage strains 118
RNA smFISH 121
qPCR for quantifying phage DNA and RNA level 124
Microscopy 124

mRNA number quantification 126
Results 129
Single-molecule characterization of pR transcription activity after phage infection 129
Lytic-lysogenic bifurcation requires negative regulation by Cro 130
Lysogenic establishment requires multiple copies of phage DNA 140
Transient pRE activation and DNA replication mediate proper cI expression for lysogenic establishment 148
Discussion 153

CHAPTER V SUMMARY AND CONCLUSIONS 156

Phage DNA Dynamics *in vivo* 156
Lysis-lysogeny Coexistence 157
DNA Replication and Cro Regulated Cell-fate Bifurcation 157

REFERENCES 159

LIST OF FIGURES

Page

Figure 1.1 Simplified genetic map of the phage regulatory region. 3

Figure 1.2 Regulation of pR, pL and pRM by CI and Cro. 4

Figure 1.3 Structure and regulation of CII. 8

Figure 1.4 Q regulates transcription from pR'. 11

Figure 1.5 A schematic for phage DNA replication. 15

Figure 1.6 The effect of MOI, cell size, and phage voting on lambda lysis-lysogeny decision making. 20

Figure 1.7 LamB and ManY. 23

Figure 1.8 Noise at different levels. 27

Figure 1.9 Replication driven DNA integration. 33

Figure 2.1 Fluorescently labeled phage and the control lysogenization experiment in bulk. 49

Figure 2.2 Assaying the phage infection process. 55

Figure 2.3 Histograms of phage intensity. 56

Figure 2.4 Phage bands after ultracentrifuge and the DNA packaging efficiency test of the fluorescent phages. 57

Figure 2.5 Intensity of phage DNA focus and the timing of phage DNA appearance. 62

Figure 2.6 Subdiffusive motion for phage DNA particles. 62

Figure 2.7 Phage DNA particles exhibit both localized motion and motion spanning the whole cell. 67

Figure 2.8 Cell division time. 68

Figure 2.9 Motion of phage particles in lytic and lysogenic cells. 69

Figure 2.10 Cell size partially accounts for the MSD plateau. 70

Figure 2.11 Phage and phage DNA locations. 73

Figure 2.12 Phage DNA locations for the whole population. 78

Figure 2.13 Effect of *dam*$^{-}$ mutation and phage labeling on the lysogenization frequency. 79

Figure 3.1 The validation of the reporter system. 88

Figure 3.2 Lambda DNA and *E. coli attB* fluorescent reporters allow DNA tracking in lytic and lysogenic cells. 96

Figure 3.3 Lysogenization frequency of λ*int*$^{-}$*-Kan* is much lower compared to λWT... 101

Figure 3.4 Apparent DNA integration is observed in some lytic cells. 102

Figure 3.5 *E. coli attB* migrates to the polar region in lytic cells where lambda DNA preferentially locates. 103

Figure 3.6 Probability of lyso-lysis increases with API and CII activity. 107

Figure 3.7 The *cII*, *int* and *xis* mRNA levels along time for cells infected by λcII_{68}, λWT and λcII_{stable} 112

Figure 3.8 Division inhibition, compromised host DNA replication and length extension during the λWT-FP lytic development. 115

Figure 4.1 Calculation of single mRNA intensity for *cII*. 127

Figure 4.2 The simplified genetic diagram of lambda lysis-lysogenic decision making and the characterization of *cII* mRNA expression. 128

Figure 4.3 Comparison of average cII mRNA level by qRT-PCR and smFISH. 131

Figure 4.4 Lack of Cro results in defective lytic development. 132

Figure 4.5 Lack of Cro results in higher frequency of lysogenization. 133

Figure 4.6 *cII* mRNA expression after infection. 134

Figure 4.7 The effect of Cro on the lytic-lysogenic decision. 135

Figure 4.8 *SRRz* mRNA expression after λWT and λ*cro*$^{-}$ phage infection. 136

Figure 4.9 Distribution of *SRRz* mRNA number over time for different phages. 137

Figure 4.10 DNA replication is important for the lysogenization decision by lambda. 142

Figure 4.11 DNA replication is important for the lysogenic decision. 143

Figure 4.12 The lysogenization frequency of λ*cro*$^{-}$*P*$^{-}$ is lower than λWT. 143

Figure 4.13 The expression level of *SRRz* for different phages. 144

Figure 4.14 Lack of DNA replication results in failure in lysogenic establishment. 147

Figure 4.15 Average phage DNA copy number along time after infection. 150

Figure 4.16 The *cI* expression patterns for different phages. 151

Figure 4.17 A schematic model for the lysis-lysogeny process. 152

LIST OF TABLES

Page

Table 2.1 Bacterial strains, plasmids, phages, and primers used in this work. 48

Table 3.1 Bacterial strains, plasmids, phages, and primers used in this work. 93

Table 3.2 Percentage of multiple prophage integration at different APIs. 113

Table 4.1 Bacterial strains, plasmids, phages and primers used in this work. 120

Table 4.2 Sequences of the probes for detecting lambda *cII* mRNA. 122

Table 4.3 Sequences of the probes for detecting lambda *SRRz* mRNA. 123

CHAPTER I

INTRODUCTION AND LITERATURE REVIEW

Introduction

Cellular decision making is ubiquitous - a process performed by organisms of multiple levels, from metazoans to the simplest life-forms such as viruses (1, 2). It is a key step that not only determines the fate of a particular cell or organism, but also plays an important role in shaping the fitness of the species. Here we utilize one of the simplest and well-established paradigms, the bacteriophage lambda lysis-lysogeny circuit, to study the underlying mechanisms of cellular decision making. This genetic circuit consists of both negative and positive regulators, as well as effectors whose levels directly determine the decision outcome. Despite those factors, pre-existing differences in the infection process seem to also play a role in determining the cell-fate (3, 4). Recent studies have discovered and characterized some of those deterministic factors, such as host cell size, number of infecting phages, and location of infection (3, 4), which promotes a better understanding of the mechanistic details of cellular decision making. Despite those discoveries, the outcomes of this process are still unpredictable (4). The reactions that constitute this process, which might include but are not limited to DNA replication, gene expression and protein diffusion, are intrinsically noisy (2, 5, 6). Moreover, those reactions happen in a complicated environment, the bacterial cytoplasm, which is heterogeneous and can result in different strategies of intracellular phage interactions (7). Here the classical picture of the lambda lysis-lysogeny decision-

making as well as the function and regulation of players involved will be reviewed. Recent high-resolution studies on the physical properties of bacterial cytoplasm, the stochasticity of phage gene expression, and the already characterized deterministic factors that affect the phage decision-making will also be discussed, in the hope of presenting a more unifying picture of the long-standing paradigmatic lambda cell-fate selection system.

Players of the Lambda Decision Making

After the ejection and circularization of phage DNA, transcription of phage genes start immediately from promoters pR and pL, which go in opposite directions (Figure 1.1). *cro* and *N* are the first genes expressed. Transcription terminators t_{R1} and t_{L1} are located immediately downstream of *cro* and *N* genes, respectively, and terminate transcription with low levels of leakage expression allowed. Protein N modifies the RNA polymerase to allow transcription to bypass the downstream terminators. This allows expression of genes including but not limited to, *cII*, *O*, *P*, and *Q* from the pR promoter, and *cIII* and *kil* from the pL promoter (Figure 1.1). The Kil protein inhibits host cell division by inhibiting the FtsZ ring formation and causes lysis-independent cell filamentation and death (8, 9). *O* and *P* genes encode proteins essential for phage DNA replication, while *CII* and *CIII* are important for lysogenic development, and *Q* regulates the lytic gene expression (10). The function and regulation of those proteins are relatively well-characterized thanks to decades of effort, allowing a better understanding of decision making at the molecular level.

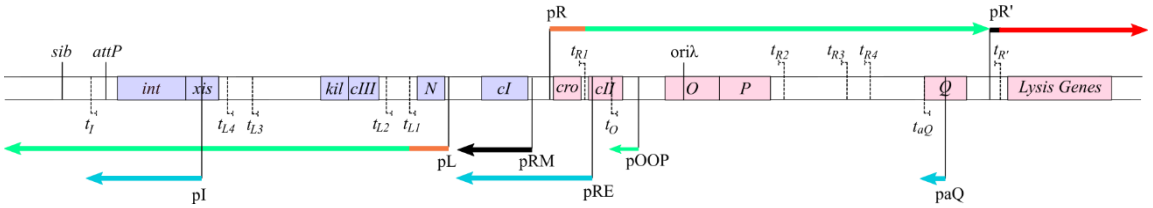

Figure 1.1 Simplified genetic map of the phage regulatory region.
Key genes involved in the lambda lysis-lysogeny decision making are shown in their map order. Genes transcribed rightwards are colored in pink, and leftwards in light purple. Dashed vertical lines represent terminators. The phage *attP* site and the location of the *sib* element are also shown above. The horizontal arrows indicate mRNA transcripts. Orange: immediate-early transcripts; Green: early transcripts. Blue: transcripts under the control of CII. The pRM transcript is shown in black. Transcription starting from pR' stops at the terminator $t_{R'}$ unless the anti-terminator Q is present to allow transcription to read through the terminator region. This figure is adapted from (11).

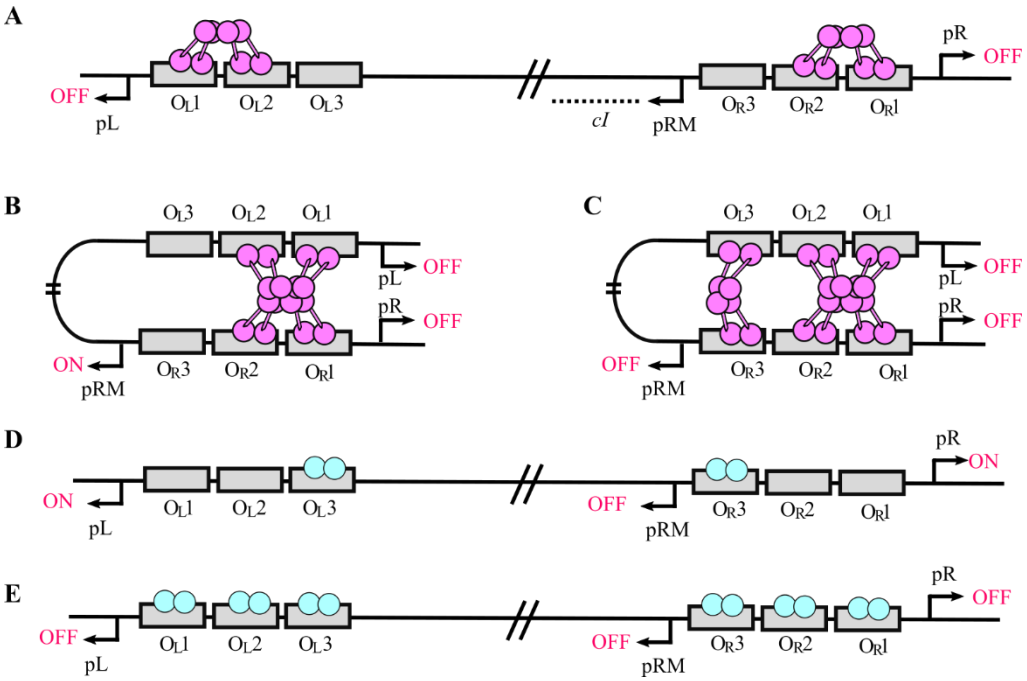

Figure 1.2 Regulation of pR, pL and pRM by CI and Cro.
(A). Binding of CI repressors to $O_R1$and/or O_R2, $O_L1$and/or O_L2 represses transcription from pL and pR, respectively. Binding of CI dimers at O_R1 or O_L1 recruits CI to bind to O_R2 and O_L2, a phenomenon called cooperativity. The binding of CI dimers at O_R2 activates CI transcription from pRM. (B). The interaction between CI dimers bound at O_L1, O_L2, O_R1, and O_R2 interact with each other, to form a loop. Promoters pL and pR are both off in this configuration, while pRM is activated. (C). Cooperative CI binding at O_L3 and O_R3 allows the region to be filled at a lower CI concentration. pRM activity is inhibited. (A-C) are adapted from (12). (D). Cro dimers binding at O_R3 inhibits pRM activity. pR and pL are not affected when Cro binds to O_R3 and O_L3. (E). Cro dimers binding at O_R1 or O_R2 inhibits transcription from pR and pL promoters, as well as pRM. No cooperativity is observed between Cro dimers bound at adjacent operators.

CI and Cro

CI and Cro repress the transcription of each other by competing for operator site binding. The competition between CI and Cro has been extensively studied both experimentally and theoretically as a paradigm for bistable genetic switch (13-15). CI is a well-known repressor which functions to maintain the lysogenic state, while Cro is considered important for the lytic development due to its competition with CI.

CI is a protein of 236 AA (amino acids), which folds into two domains connected by a 38 AA polypeptide chain. The N terminal domain of CI confers its DNA binding activity, while the C terminal domain mediates the dimerization. Cro, on the other hand, is a small protein with 66 AA. Cro also functions as a dimer. The genes for CI and Cro are located in adjacent sites on the lambda genome but oriented in opposite directions and controlled by different promoters, pRM and pR, respectively (Figure 1.2A). The right operator O_R (O_R1, O_R2 and O_R3) partially overlays with pR and pRM, and their binding by regulators controls the activities of both promoters. Both CI and Cro can bind to the O_R region, but with different affinities. The CI's binding affinity order for O_R is $O_R1 > O_R2 > O_R3$, while it is the opposite for Cro. Moreover, CI has higher binding affinities to the operators compared to Cro in general. The binding of CI or Cro to O_R1 blocks the access of RNAP to the P_R promoter, therefore inhibiting Cro transcription (Figure 1.2A, B&E). On the contrary, their binding to O_R3 would result in the inhibition of transcription from pRM (Figure 1.2C&D). As O_R2 is positioned slightly closer to the pR promoter, the binding of CI or Cro to O_R2 also has inhibitory effects on pR transcription (Figure 1.2A&B). Meanwhile, CI binding to O_R2 can increase the pRM

transcription activity by roughly 10 fold as CI directly contacts the RNAP to increase the binding affinity of RNAP to the pRM promoter. At low concentrations, CI preferentially binds to O_R1 to block the synthesis of Cro. This binding also increases the binding affinity of CI to O_R2, a phenomenon termed 'cooperativity', due to the interactions between CI dimers in adjacent sites, leading to more CI synthesis (Figure 1.2A). At high concentrations, CI binds to O_R3 to repress its own expression. In fact, it has been shown that in lysogenic cells, CI can exist in different binding configurations as described above and rapidly switch between each state (16). Through the positive and negative auto-regulation, CI controls its own expression to an 'optimal' level. Cro, on the other hand, is strictly a repressor, and its overall affinities to O_R are lower compared to CI. At lower concentrations, Cro binds to O_R3 to inhibit CI transcription from pRM. When Cro reaches a higher concentration, it binds to O_R2 and O_R1 and inhibits its own transcription from pR.

Besides O_R, CI and Cro can also bind to O_L, which is located more than 2 kb away from the O_R region, to control the gene expression from pL. CI and Cro binding to the O_L region can regulate transcription from pL in the same way as pR. However, this is by no means the only function of O_L. It has been shown that the CI dimers binding at O_R1 and O_R2 can interact with the dimers binding at O_L1 and O_L2, forming a CI octamer and looping out the DNA between O_L and O_R (Figure 1.2B). Moreover, the CI dimers bound at O_R3 can interact with CI dimers at O_L3 region, similar to the cooperativity observed between CI dimers at O_R1 and O_R2, thus allowing the O_L3 region to be filled with CI at a relatively low concentration (Figure 1.2C).

Even though much focus has been placed on Cro and CI competition for decision making, more and more evidence suggests that CI is not involved in the actual decision-making process, because its expression reflects the choice that has been made. In fact, in the infection process, CI only comes into play when CII activates transcription from pRE promoter, which allows high level expression of CI (10, 17). The number of CI molecules transcribed from the pRE promoter is reported to be much higher (~7.5 fold) than that in stable lysogens which have ~100 nM of CI. This overshoot of initial CI level might allow the effective establishment of the lysogenic state, suggesting that CI is critical in the commitment stage but not the decision-making process, as a lysogenic decision has been reached when CII activates CI expression (17, 18). In contrast, Cro is one of the first two genes expressed when phage infection happens. As a weak repressor, Cro can regulate early gene transcription, therefore affecting the lytic-lysogenic decision-making process. It has been shown that lack of Cro would result in failure to form plaques as well as higher lysogenization frequencies (19, 20), indicating that overall, Cro functions to repress the phage lysogenization and to allow lytic development. However, whether Cro performs those functions by competing with CI or through other means such as regulation of early genes remains to be studied.

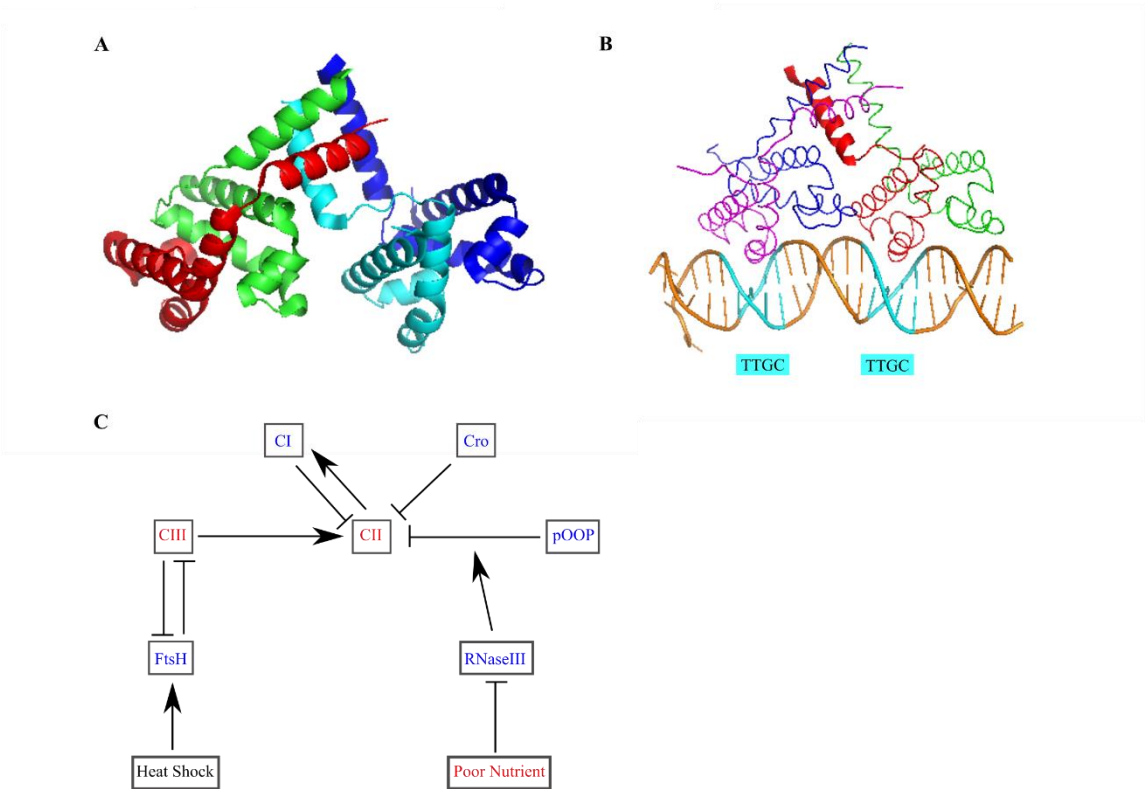

Figure 1.3 Structure and regulation of CII.
(A). Crystal structure of CII. CII forms tetramers. Image was adapted from (21). PBD ID: 1xwr. (B). Structure of CII bound to target DNA. The TTGC motifs are colored cyan. Image was adapted from (22). PBD ID: 1zs4 (C). CII level is regulated by multiple factors. At the RNA level, *cII* transcription from pR is repressed by Cro and CI. Transcript pOOP can also decrease *cII* mRNA level in an RNaseIII dependent manner, while under poor nutrient conditions, RNaseIII level is lower. At the protein level, CII is regulated by FtsH through degradation. CIII protects CII from degradation by competitive binding to FtsH. FtsH is under the control of heat shock promoters (23), therefore more FtsH will be expressed under heat shock conditions. Nevertheless, the number of FtsH proteins available for CII degradation is hard to predict under this condition, as FtsH might also be sequestered for other processes such as stress response.

CII and CIII

CII is a key protein in the lysis-lysogeny decision-making process of lambda. It functions by activating three promoters: pRE for repressor CI synthesis, pI for the expression of integrase, and paQ to inhibit *Q* expression (10, 14). CII activates the promoters by binding as a tetramer to two direct repeats flanking the -35 element. The crystal structure of CII reveals that each CII monomer is comprised of four helices (h1-4). The three helices (h1-3) at the N terminal confer the DNA binding activity as well as mediating the dimerization of CII (Figure 1.3A). The tetramerization of CII is mediated by the interaction between the h4 of each CII in the dimers (Figure 1.3A). On the promoters, two CII dimers bind to the TTGC motifs located on each side of the -35 element, respectively, forming a tetramer to activate the transcription (Figure 1.3B) (21, 22).

cII gene expression is tightly regulated both at the mRNA level and the protein level (Figure 1.3C). Being part of the pR transcript, *cII* transcription is regulated by both Cro and CI, as has been discussed above. Moreover, the *cII* gene expression is also in part regulated by the antisense RNA transcribed from promoter pOOP. This promoter is located in the immediate downstream of the *cII* gene (Figure 1.1), and transcribes an ~77-nt RNA, of which 55 nt are antisense to that of the *cII*-coding region. This OOP antisense RNA is shown to inhibit CII expression by destabilizing the *cII* mRNA in an RNase III-dependent manner (24, 25). When the OOP RNA is overproduced from plasmids, the phages form clear plaques, indicating the lack of CII for phage lysogenization (26).

The protein level of CII is tightly controlled by FtsH mediated degradation. The half-life of CII is reported to depend critically on its initial level, which is only ~1.5 min at low concentrations compared to ~22 min at high concentrations (27). The host protease FtsH (also known as HflB, for high-frequency lysogenization) is responsible for CII degradation (28, 29). The intracellular level of FtsH is limited, estimated to be ~400 molecules per cell (30). It is therefore possible that the limited concentration of FtsH is the reason for the concentration dependent stability of CII, since FtsH may be saturated at high CII levels. FtsH dependent proteolysis is processive. It typically starts by recognizing a specific region on the substrate and continues to degrade the entire protein (31, 32). For CII, degradation starts at the C-terminal region and eventually small peptides ranging from 4 to 26 residues long are generated (33, 34).

The DNA sequence of *cII* predicts a polypeptide consisting of 97 AA (35, 36). However, the first two amino acids are removed from the mature, active protein (36, 37). This maturation process has also been shown to affect the intracellular level or stability of CII. In a *cII* mutant carrying a *CII* gene where the second amino acid Val has been mutated to Ala, only the terminal N-formylmethionine is removed, and the protein is shown to be more stable (36, 38). As a result, phages carrying this mutation exhibit a much higher lysogenization frequency compared to that of WT (36, 38).

During the early gene period of the lambda infection process, another protein, CIII, is also expressed from the pL promoter (Figure 1.1). CIII is a 54-AA protein which forms oligomers and competes with CII for FtsH binding. CIII protects CII from degradation by FtsH (18, 39), however, CIII can also be degraded by FtsH (39, 40).

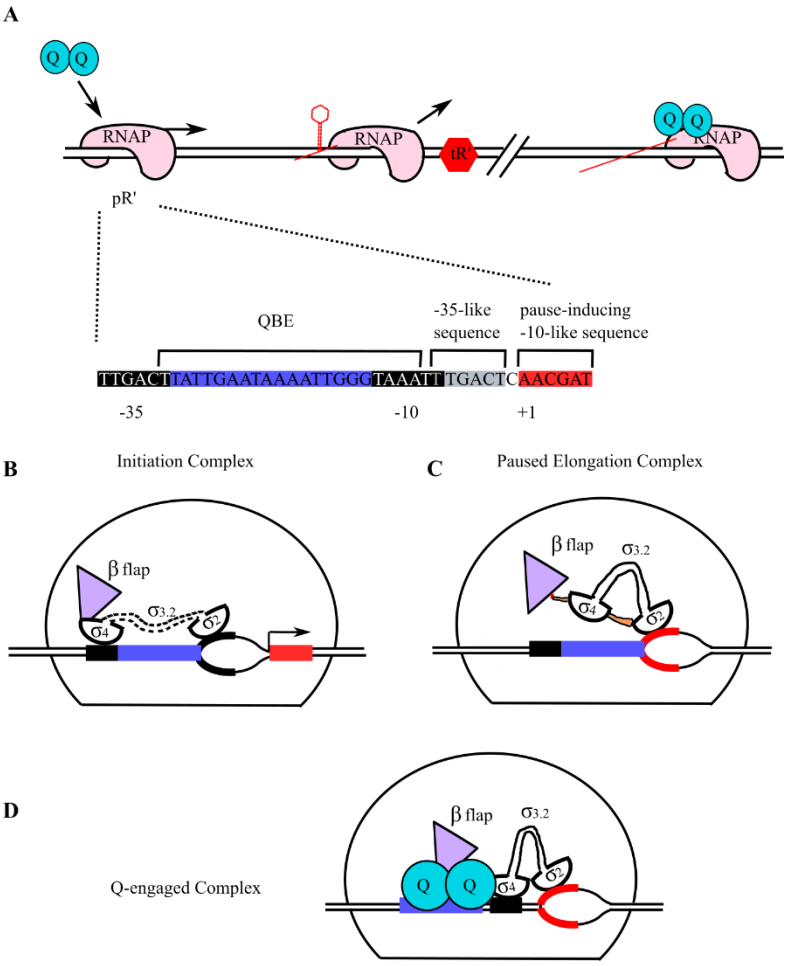

Figure 1.4 Q regulates transcription from pR'.
(A). Q is required for transcription from pR' to pass through the downstream terminators. The detail sequence information for pR' region is shown. QBE lies in between the -35 and -10 elements. The -10-like sequence located at the +1 location induces transcription pause. The -35-like element TTGACT is bound by σ4 subunit to stabilize the RNAP when Q is bound to the paused elongation complex. Overall, transcription stops when it reaches the pause-inducing -10-like elements. The binding of Q allows transcription to bypass the downstream terminators to generate a transcript that is at least 25 kb long. (B) Initiation complex. The σ2 and σ4 subunit bind to the -10 and -35 elements, respectively. The σ4 subunit also interacts with the β flap domain of the RNAP holoenzyme. The linker σ3.2 is located in the nascent RNA exit channel. (C). Transcription pauses when it reaches the pause-inducing -10-like element. The nascent RNA chain displaces the σ3.2 from the RNA exit channel and σ4 from the β flap domain. (D). Dimers of Q bind to the paused elongation complex through QBE, and interact with both β flap domain and σ4. The binding of σ4 to the -35-like sequence is stabilized, and transcription can continue. This figure is adapted from (41) and (42).

Q

There are three stages of transcription: initiation, elongation and termination. The RNA polymerase initiates transcription at the promoter region, elongates the nascent RNA chain and eventually releases the complete messenger RNA when it encounters a terminator. The transcription termination and anti-termination system is one of the strategies utilized by living organisms to regulate gene expression. The Q-mediated anti-termination of the bacteriophage lambda late gene expression is among one of the most studied systems (43). Q is a protein of 207 amino acids, and it functions as a dimer. It functions by staying as a stable component of the transcription elongation complex, allowing the transcription to bypass downstream terminators (Figure 1.4A) (44). The crystal structure of Q has recently been reported (42), which has shed more light on its mechanism of action.

The bacterial RNAP holoenzyme consists of the core enzyme ($\alpha_2\beta\beta'\omega$) and the σ factor that confers promoter-specificity of transcription. All primary σ factors share four regions of conserved sequences (σ1-4). Regions 2 and 4 are independently folded DNA binding domains that specifically recognize and bind to the promoter -10 and -35 regions, respectively, to form the initiation complex. Binding of region 4 to the -35 element also requires interaction between region 4 and the β flap domain of the β subunit (45). Notably, in the transcription initiation complex formed at pR', the σ factor region 3.2, which is a flexible linker, is located at the RNA exit channel (Figure 1.4B) (46, 47). As transcription progresses and RNAP moves along the DNA template, region 2 eventually reaches and binds to the pause-inducing -10-like sequence, which is located at

the +1 position of the pR' transcript (Figure 1.4C) (44). The nascent RNA chain leads to the displacement of region 3.2 from the exit channel and also destabilizes the interaction between region 4 and the β flap domain (Figure 1.4C). Those events together cause the pause of transcription from pR' and the formation of the paused elongation complex (Figure 1.4C) (46, 47).

The involvement of Q in anti-termination requires several conditions. First, for Q to engage in the paused initiation complex, the nascent RNA chain mediated destabilization of the σ region 4/β flap interaction is required (41). Other factors required for Q function include a Q binding element (QBE) and a TTGACT motif. The QBE is located in between the -35 and -10 elements, while the TTGACT motif is located just one bp upstream of the pause inducing -10-like sequence. The dimers of Q bound at QBE also interact with the region 4 and the β flap domain of RNAP (48). Binding of Q to the σ factor region 4 stabilizes the binding of region 4 to the TTGACT motif, which resembles to -35 element (49). The Q dimer, through its interaction with the β flap domain and region 4, becomes a stable component of the elongation complex, allowing the RNAP to pass through downstream terminators and transcribe at least 25 kb of the phage late genes (Figure 1.4D) (41, 50, 51). The last gene on the pR' transcript is *stf*, which encodes the phage side tail fiber. However, whether transcription stops after *stf* or not is still unknown. It is possible that the RNAP may fall off the DNA template or that Q may disassociate from the complex after travelling for a long distance, causing transcription to stop.

An interesting observation of Q is that it seems to function in a "partially *cis*-acting" manner (52). In an experiment assaying the endolysin (product of phage late gene *R*, under the control of pR' promoter) production after co-infection with two phages: $Q^{+}R^{-}$ and $Q^{-}R^{+}$ at high APIs (average phage input, 7 for each phage), only a very low level of endolysin activity was detected, indicating that Q functions preferentially on the genome from which it has been synthesized (52). Since the action site for Q, the pR' promoter, is located immediately downstream of the *Q* gene (Figure 1.1), it is possible that Q protein is synthesized from an mRNA transcribed in close proximity to the *Q* gene, causing the preference of Q protein to bind to its DNA template which is close by and resulting in the *cis*-acting phenomenon. Another possibility is that that many Q proteins might become "lost" when Q protein diffuses to find another genome and might engage in non-specific interactions with a number of DNA sites that are not its targets (52). Nevertheless, direct evidence is still lacking on the mechanism of cis-acting by Q, and further examination of this system at higher resolutions is required.

Research also suggests that Q anti-termination activity does not correlate with its protein level. In fact, the activity of Q is only detected after its protein level reaches a certain threshold (17). The mechanism for this threshold effect is still unknown. As Q needs to search for and interact with both the QBE and the RNAP in a specific conformation in the paused initiation complex, it is possible that this process is time consuming or not very efficient. Alternatively, the efficiency of Q dimerization process can also be limited (17). Nevertheless, as Q functions as a 'gate' to the expression of late genes for the development of the lytic pathway, the high threshold value of Q can

prevent the expression of destructive genes and allow normal development of the lysogenic pathway.

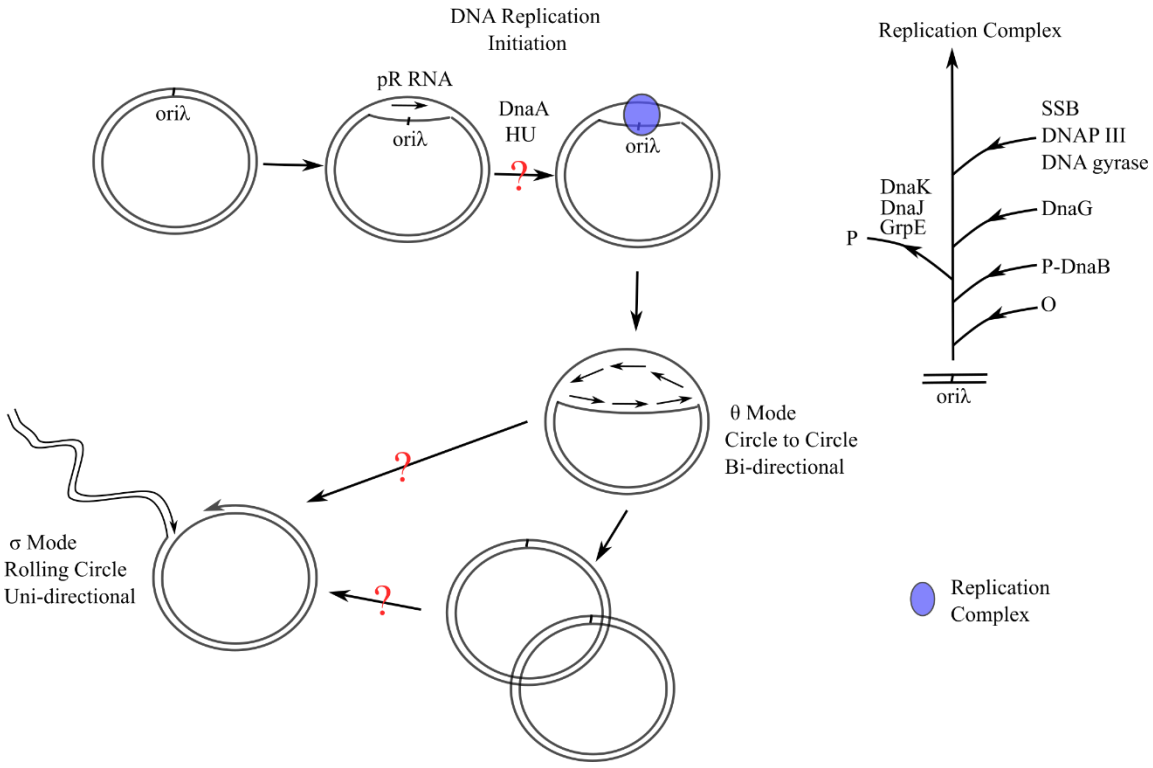

Figure 1.5 A schematic for phage DNA replication.
The phage DNA replication starts from the oriλ region. Transcription activation from pR promoter is required for initiation of DNA replication. DnaA and HU may also be involved in the initiation process, although further research is needed to confirm their involvement. A brief outline of the assembly of DNA replication complex is shown on the right. Initially, O binds to oriλ to form the O-some. P in association with DnaB are then recruited to the O-some. In order to release the function of DnaB, DnaK, DnaJ and GrpE reorganize the complex to allow P to leave the complex. Primase DnaG then binds to the complex, and subsequently factors such as SSB, DNA gyrase and DNA polymerase III are also recruited to the complex, to form the replication complex. Early on, DNA replication proceeds bi-directionally in the θ mode, which generates DNA in circles. Later on, DNA replication switches to rolling circle, where concatemeric phage DNAs are produced. The factors triggering the switch remain to be investigated.

Phage DNA replication

The phage DNA replication process requires several host factors as well as the phage encoded O and P proteins. Both *O* and *P* genes are located on the pR transcript and are expressed together with the early lysis-lysogeny determining genes such as *cII* and *Q*. Therefore DNA replication may happen when a lysis-lysogeny decision is being formulated, and may affect the decision outcomes. In fact, it has been suggested that the lack of DNA replication significantly decreases the frequency of lysogeny, while also altering the lysogenic response to API (53), yet the reason remains unknown. Here the detailed mechanism of phage DNA replication will be reviewed, in hope to shed more light on its possible effects on the decision-making process.

The origin of phage DNA replication, oriλ, is located inside the *O* gene (Figure 1.1), which encodes the DNA replication initiator (54). Similar to the *E. coli* DNA replication initiator DnaA, the O protein recognizes oriλ, recruits and organizes the components in the replication complex for DNA replication initiation (55). Genetic and biochemical evidence have suggested that O protein binds to oriλ by its N terminal domain, forming the O-some, while its C terminal domain can bind to phage P protein (56, 57). P protein then recruits the host factors required for DNA replication to the O-some by binding to the bacterial helicase DnaB (57). The binding affinity of P-DnaB *in vitro* is significantly higher compared to that between DnaB and the DnaC of *E. coli*, such that P can effectively redirect the host factors for the replication of phage DNA (58). On the other hand, *in vitro* experiments also show that P is capable of inhibiting the binding of DnaA to the *E. coli* oriC and ATP, and may therefore inhibit the initiation of

host DNA replication (59). In those experiments, when oriC DNA is added to the reaction mixture with pre-incubated purified P and DnaA proteins, the binding of oriC to DnaA is inhibited and this inhibition increases with the amount of P (59). However, whether P is capable of inhibiting DnaA function *in vivo* remains to be further investigated. Nevertheless, due to the binding activity of O and P, the complex of P in association with DnaB was then recruited to the O-some, to form the complex oriλ-O-P-DnaB (Figure 1.5) (57). The presence of P in this large complex inhibits the activity of DnaB, and the host chaperones DnaJ, DnaK and GrpE are required for the rearrangement of the complex in order for P to disassociate (Figure 1.5) (60). The helicase activity of DnaB is then liberated to unwind the DNA template, and the bacterial primase DnaG recognizes the single-stranded DNA-DnaB complex to synthesize RNA primers (Figure 1.5) (61). Using the RNA primers, DNA polymerase III holoenzyme subsequently extends and synthesizes the DNA.

Even though O is well-known as the initiator, its binding to oriλ is not the only factor required to trigger the initiation of lambda DNA replication. Research has shown that transcriptional activation of the oriλ from pR is necessary for DNA replication initiation (62), which indicates that Cro and CI can also regulate DNA replication initiation by inhibiting the pR promoter. The strict requirement of pR transcription activation for DNA replication initiation seems to depend on the presence of a histone-like *E. coli* protein, HU (63). *In vitro* reconstruction of the phage DNA replication system shows that, with a minimum of nine proteins added (O, P, DnaB helicase, DnaG primase, single-strand DNA binding protein, DNA polymerase III holoenzyme, DNA

gyrase, DnaJ, and DnaK), phage DNA replication can happen and does not depend on pR transcription activity (63). However, when HU is added, pR transcription activation becomes essential for DNA replication again (63). The histone-like protein HU is a DNA binding protein that was shown to also participate in the initiation of *E. coli* DNA replication. It assists the action of DnaA in the unwinding of the *oriC* DNA (64). However, the role of HU in mediating the transcription activation dependence of phage DNA replication initiation remains unknown. Meanwhile, evidence also suggests that the initiation of phage DNA replication may require the function of a host protein, DnaA as well (65, 66). DnaA is the initiator for *E. coli* DNA replication with two main functions. The first is to recognize the *E. coli oriC*, and to organize the assembly of the replication complex. The second is its regulatory role in the activation of *oriC* and initiation of DNA replication by activating transcription starting from promoters in or around *oriC* (55). It has been suggested that the lambda O protein is equivalent to DnaA only in the first aspect, and DnaA seems to fulfill the second role for phage DNA replication, as DnaA-binding DnaA-boxes are also found between the lambda pR promoter and the *O* gene (65). Altogether, the initiation of phage DNA replication involves the transcription activation of pR promoter, and the possible role of DnaA in this process requires further investigation.

Phage DNA replication happens in two different modes, the θ mode at the early infection stage, and the σ mode at the later stage (Figure 1.5) (67). In the θ mode, replication proceeds bi-directionally from the origin of replication and generates progeny DNAs in the circular form. The number of DNA molecules per cell doubles every 2-3

min in the θ mode (68). However, θ replication can only last for a short time, and the replication is then switched into the σ mode, albeit not with 100% efficiency (69). In fact, only ~3 out of 50 phage DNAs per cell generated by θ replication are able to switch in σ mode replication (69). σ replication, also called rolling circle replication, produces concatemeric DNAs ranging from 2~8 unit length long (67). Those concatemeric DNAs are further cut into units with cohesive ends and each unit is packaged into the proheads of progeny phages (69).

The factors triggering the switch from θ to σ mode of replication is still under investigation. The lambda O protein is unstable and can be degraded by the host ClpP/ClpX proteases. However, the O proteins bound in the replication complex are rather stable and not accessible by the protease (70). Therefore the abundance of O is unlikely to be the limiting factor for the DNA replication initiation and to trigger the switch from the θ mode to σ mode replication (71). It has been suggested that transcriptional activation of oriλ by pR may be involved in the switch. It was proposed that the depletion of DnaA by the rapidly replicating phage DNA may trigger the switch from bidirectional θ replication to unidirectional θ replication, and later to the σ mode replication (71). However, more experiments are still needed to investigate the possible roles of DnaA in this process.

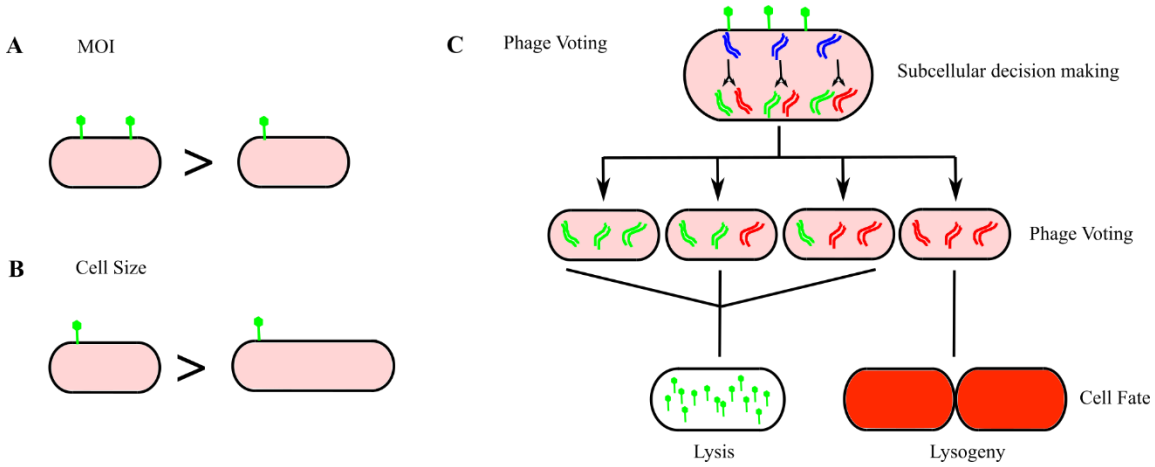

Figure 1.6 The effect of MOI, cell size, and phage voting on lambda lysis-lysogeny decision making.
(A). The effect of MOI on lambda lysogenization. More infecting phages lead to higher frequencies of lysogeny. (B). Cell size effect on lambda lysogenization. Smaller host cell size leads to higher frequencies of lysogeny. (C). A schematic showing phage voting. Cell outcome is determined by each individual phages infecting the same cell. Only a unanimous vote towards lysogeny by all infecting phages can lead to cell lysogeny. This figure is adapted from (4).

Deterministic Factors Affecting the Lysis-Lysogeny Decision Making

Despite the unpredictable nature of cellular decision-making, higher resolution studies on the lambda lysis-lysogeny decision-making system has revealed some previously hidden deterministic factors affecting this process, arguing for the growing need for quantitative methods to be applied. Pre-existing difference for each infection, such as cell size and number of infecting phages, might affect the decision outcomes (3, 4), and failure in characterizing those factors may render the decision-making 'probabilistic' or 'noisy' as was assumed. If one can characterize all the influencing factors, a deterministic decision is possible to be reached where the cell fate can be accurately predicted using the known parameters (3). Here we will review some of the already characterized factors that affect the decision making of lambda.

Multiplicity of infection (MOI), cell size and phage voting

The number of infecting phages, or the MOI, is the first factor known to affect the lysis-lysogeny decision making of lambda (Figure 1.6A). In a series of works by Kourilsky (53, 72, 73), it was shown that the lysogenization frequency of lambda increases as the API increases (53). The lysogenization frequency of WT phage as a function of API follows the Poisson distribution of $n \geq 2$, indicating that it requires two or more phages on average to lysogenize a cell.

Cell size is another deterministic factor that affects the decision making (3). By infecting different groups of cells that were fractionated based on the cell volume, researchers found that the group of cells with small volumes shows a much higher lysogenization frequency compared to the group with large cells. This suggests that cell

size inversely correlates with the lysogenization frequency of phage lambda (Figure 1.6B).

Recent development of fluorescent phage labeling technique has allowed the direct observation and counting of phage particles under the fluorescence microscope (4, 74). With live-cell imaging, the progression of the decision followed by infection can be studied in more detail (4). In this study, the impact of MOI and cell size on the lysis-lysogeny decision-making process was reaffirmed. However, when the percentage of lysogeny is plotted as a function of viral concentration (MOI divided by cell size), the data do not collapse into a single curve, indicating that MOI and cell size do not simply affect the decision making by changing the overall viral concentration. Instead, it seems that for each MOI, the lysogeny frequency each follows a different curve. This leads to the hypothesis that the unit of decision making is probably the individual phages infecting the cell rather than the cell entity as was assumed. In this case, the fate of the infected cell is collectively determined by the decision of all infecting phages. In fact, the data suggest that each phage can 'vote' towards the cell fate, as if they have their own 'identity', and that a lysogenic establishment requires unanimous voting towards the lysogenic pathway (Figure 1.6C) (4, 75). By considering the decision making at the single-phage level, the level of noisiness is further reduced compared to the single-cell and population level, suggesting that higher resolution characterization of the cellular events can reveal more deterministic factors involved in decision making to explain away some randomness in this process.

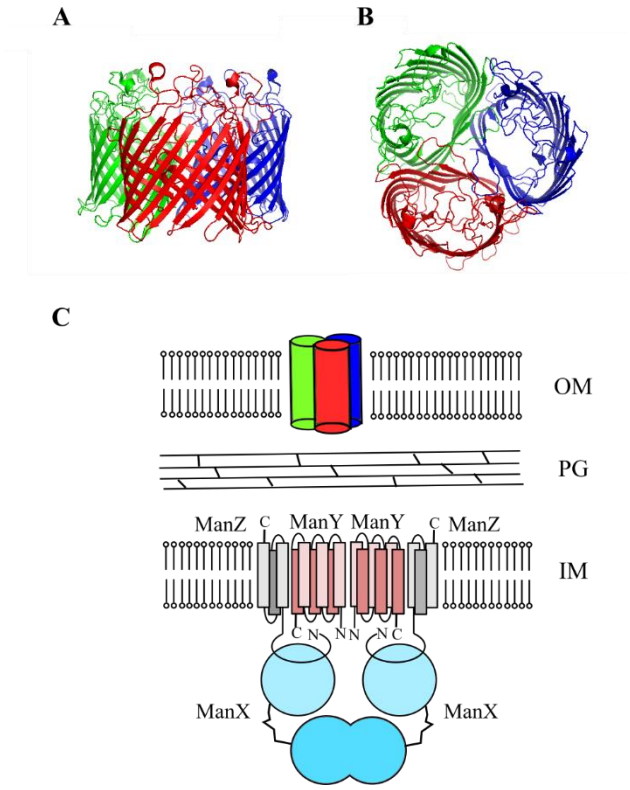

Figure 1.7 LamB and ManY.
(A) Side view and (B) top view of the LamB protein. LamB forms trimers. Each monomer forms a wide channel with a diameter of about 2.5 nm. (C). The location of LamB and ManY. ManY is located in the inner membrane, while LamB is located in the outer membrane. This figure is adapted in part from (76) and (77).

Position of phage infection

One interesting feature of phage infection is that phages seem to bind to the polar region of the host cells preferentially (4, 78), although the mechanism still remains to be investigated. The phage adsorption occurs first through the binding of the phage tail tip protein gpJ to the receptor LamB, the maltose porin (Figure 1.7A&B) (79, 80). Labeling the receptors with quantum dots reveals that LamB is well-distributed on the cell surface, exhibiting helical distributions (81). The initial phage-cell interaction happens at random locations and the binding between gpJ and LamB is reversible, which allows the phage particles to translocate along the cell surface. Eventually the phage encounters a 'spot' where the binding becomes irreversible and DNA ejection is triggered (81). It seems that this favorite 'spot' for DNA ejection is at the cell pole, but what triggers the transition remains unknown.

The ejection of phage DNA was reported to depend on an inner membrane protein, ManY (82, 83), although recent work also suggests that this dependence may not be as significant as once thought (84). ManY is the IIC component of the mannose specific phosphotransferase system (PTS), and is predicted to have six membrane-spanning segments with the N- and C-termini on the cytoplasmic side (Figure 1.7C) (85). Exogenous expression of GFP-ManY protein fusion in a ManY deleted strain shows that GFP-ManY preferentially localize to the cell poles, correlating with the location preference of phage attachment site (78). However, the deletion of ManY does not alter the location preference of phages (78).

Overall, current knowledge of the phage infection process includes the phage-cell interaction happening at the outer membrane, and the ejection of DNA which may depend on an inner membrane protein, but how the phage DNA gets across both the inner membrane, the peptidoglycan layer and outer membrane remains mysterious. Early studies showed that phages can eject DNA into liposomes with LamB within 1 min (86), suggesting that the phage-LamB interaction is enough for the triggering and completion of DNA delivery across one lipid bilayer. It is therefore possible that ManY facilitates the translocation of phage DNA through the peptidoglycan layer and the inner membrane to some extent. In fact, studies using lambda phages with smaller genome size showed that DNA ejection depends more critically on ManY compared to phages with full-size genome (84). As phages with shorter genomes have less force associated with the release of DNA from the compacted capsid, it is possible that the delivery of DNA needs more help from ManY. Further investigation on the intermediate steps are required for a more complete understanding of the phage infection process.

Although the molecular basis is unknown, the effect of phage infection location preference on the infection outcome may be nontrivial. In fact, phage infections from the non-polar region lead to a higher failure rate (4). One possible explanation for this observation is that unsuccessful DNA ejection is more likely in non-polar regions due to the low abundance of ManY, although failure in phage developments is also possible even when the DNA is successfully ejected. FtsH, the membrane associated protease that degrades CII, is shown to locate primarily in the polar region of the cell (78) and may

affect the local CII abundance. Whether the DNA entry site would affect the initial CII accumulation to result in different decision behaviors or not remains to be investigated.

Overall, researches performed at higher resolutions allow more detailed understanding of the lambda infection and decision-making process. Those works suggest that pre-existing differences in the infection, either in the cellular state, the number of infecting phages, and the position of phage infection can explain away some of the randomness in the phenotype, and reduce the 'noise' of the cellular decision making. However, the characterization of those factors do not account for all the noisiness of this system (4), and whether this is due to our inability to capture all pre-existing differences or is actually partially due to the stochastic features of cellular processes remains to be further addressed.

Stochastic Factors Affecting the Lysis-Lysogeny Decision Making

Cellular decision making is a stochastic process. The environment that the cell or the entity resides in may change in unpredicted manners to trigger different cellular responses. At the molecule level, the series of biochemical events involved in decision making is also inherently noisy. For phage lambda, despite the efforts to characterize the deterministic factors that contribute to its cellular decision making, the cell-fate decision remains noisy. It is therefore necessary to investigate how noisiness arises and how it can contribute to the decision outcomes. Here three possible factors that might lead to the noisy phenotypes will be reviewed. The first is stochastic gene expression that underlies every biochemical reaction, and the second is the heterogeneous bacterial

cytoplasm in which the decision making happens. Last but not least, the contribution from the variability in the timing of infection will also be reviewed.

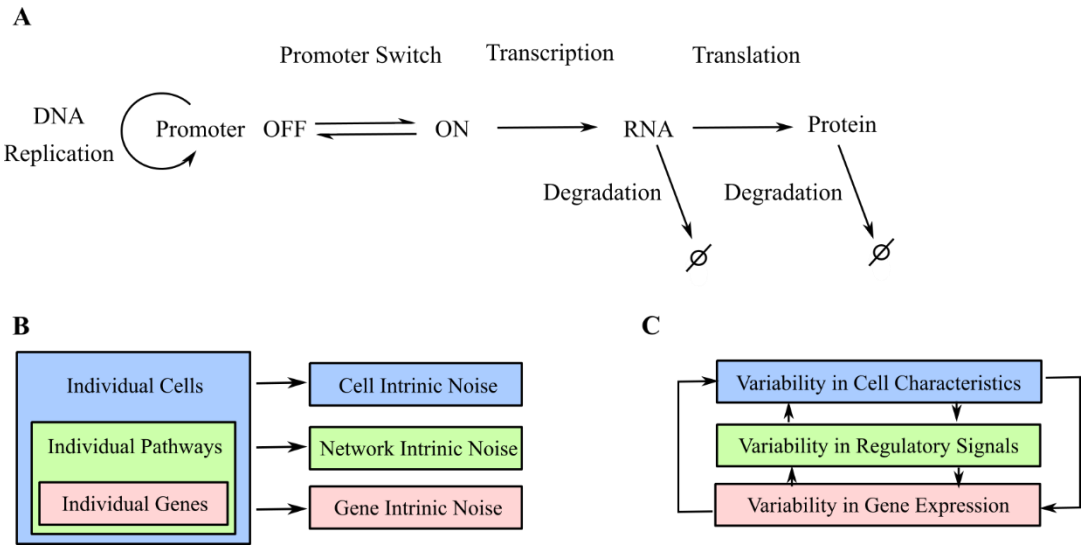

Figure 1.8 Noise at different levels.
(A). The flow of genetic information. RNA is transcribed from the DNA template when the promoter is in the ON state. The information is further passed down to proteins through translation. DNA replication results in more promoters and transcription templates. During the gene expression process, the promoters can randomly switch on and off, leading to transcriptional 'bursting' at the RNA level. The RNA can also be degraded or translated into proteins in a stochastic manner, leading to translational 'bursting'. The noise arising during this process are termed gene intrinsic noise. (B). Intrinsic noise at different levels. At the single-gene, pathway and cell level, noise can be generated. (C). Noise at different levels can affect each other.

Stochastic gene expression

Noise pervades all domains of life. Cell-to-cell variability has both been observed experimentally and tested theoretically. In 1957, Novick and Weiner showed that the β-galactosidase production in individual cells shows 'all' or 'nothing' phenotypes after inducer is added (87). Increasing the concentration of inducers increases the percentage of cells with protein expression rather than increasing the expression level of each cell proportionally (87). Similar phenomenon is also observed for protein production from the *araBAD* promoter when arabinose is used for induction (88). Later on, theoretical work showed that the randomness of cellular events can be of great biological significance (89). Fluctuations in protein production rate were predicted to be able to give rise to phenotypic variance for the lambda lysis-lysogeny decision-making network (89). More recently, single-cell analysis reveals that cell-to-cell variability can arise from different sources of noise, extrinsic noise and intrinsic noise (90). Extrinsic noise possibly results from global fluctuations in factors such as the concentration of ribosome or RNA polymerase, and can therefore act on cellular processes in a correlated manner. On the other hand, intrinsic noise comes from the inherent stochasticity of each reaction and thus acts independently on each process in an uncorrelated way (Figure 1.8). The origin of the intrinsic noise was later found to partially result from the 'bursty' protein production behavior (91-94). Using single-molecule techniques, researchers observed that translation happens in a 'bursty' manner, where variable number of proteins are produced from the mRNA before the mRNA is degraded (91, 94). Moreover, by tracking mRNA production in real time in single cells

using the MS2-GFP method (95-97), researchers found that mRNAs are also produced in bursts, a phenomenon referred to as 'transcriptional bursting' (98). The promoters controlling the mRNA expression can also randomly switch on and off, due to reasons such as the stochastic binding or falling off of regulators. During each ON period, variable number of mRNAs can be produced, leading to the mRNA 'bursting' phenomenon (98). In fact, it was recently shown that promoters can rapidly switch between different states (16). By quantifying the activity of the paradigmatic lambda promoter-pRM at the mRNA level as well as the protein level of its regulator, CI, the researchers showed that the pRM promoter can not only switch between the ON and OFF states, but also between different ON states where different configurations of CI binding are present (16). The questions then arise: how is the noise at the individual-gene-expression level passed down through the intricate biological networks to exert its effects on the terminal outcomes (Figure 1.8)? More specifically, how do living organisms control or take advantage of noise to perform their tasks such as cellular decision making?

Strategies such as feedback loops and redundancy are often utilized by gene regulatory networks to control the gene expression noise, and to ensure a more 'deterministic' outcome, as reliability is important for many cellular processes (99). Negative feedback, where the protein negatively regulates its own production, is a common type of regulation in gene networks, and has been shown to exhibit noise-reduction functions (5, 100, 101). In an engineered network with negative feedback, gene expression variability is shown to be lower compared to when negative feedback is

absent (101). Negative feedback is also predicted to be able to increase the frequency of fluctuations, which can minimize the effects of fluctuations on downstream processes as a 'slow' downstream process can only sense a time-average signal (102). Redundancy refers to multiple copies of genes that do not necessarily share the same DNA sequences but perform the same functions. Redundancy can increase the dynamic stability of the gene network (103). One example is haploinsufficiency, a phenotype associated with the inactivation of a single allele in a diploid organism. Haploinsufficiency could be related to the higher variability of gene transcription from a single gene copy. In diploid cells, expression from two copies of genes can buffer out the noise and have higher frequencies of maintaining the abundance of the gene product above a certain threshold (104, 105).

Despite the effort of cells to attenuate noise to achieve reliable, ordered outcomes, they can also take advantage of the noise to allow a certain level of randomness in the output in order to differentiate into different pathways. Positive feedback is a commonly used mechanism for cells with bistable switches (106-109). In a network with positive feedback, gene expression noise can be amplified to fraction the cells into distinct subpopulations, where a group of cells can show high expression of certain genes while others show low expression.

The first example of noise utilization for phenotypic diversification is demonstrated mathematically (89), which shows that the lysis-lysogeny decision-making by phage lambda takes advantage of the fluctuations in protein production rate to randomly bifurcate into distinct pathways. Following that, a series of works have been

reported to promote the understanding of how noise can give rise to the phage bifurcation (110). However, those works most often focused on the CI-Cro mutual regulation, and recent experimental work has provided evidence that CI might not be involved the actual decision making process, but rather to enforce and maintain the choice established by CII (17). Moreover, other cellular processes, such as the replication of phage DNA, are also stochastic in nature and might have tremendous effects on decision-making as well. Experimentation and theoretical examinations of those factors are needed to have a more comprehensive understanding of the lambda decision-making system.

Heterogeneity of the bacterial cytoplasm

More and more research focuses on the physical properties of the bacterial cytoplasm, yet how the phage components, such as DNA, RNA and proteins, behave in the cytoplasm remains poorly understood. As phage decision making is affected by intracellular factors such as protein concentration and phage-phage interactions (111), studying the intracellular dynamics of those components could promote the understanding of the developmental strategies by lambda.

Both normal and anomalous diffusion have been reported for particles residing in the bacterial cytoplasm (112, 113), indicating complex properties of the cytoplasm. Recently, a more systematic research has been reported (7), which provides a more unifying picture on how the cytoplasm exerts its effects on the motion of different particles. The cytoplasm is found to possess glass-like properties, and affects the motion of particles in a size-dependent manner (7). Particles below the size scale (~30 nm) show

normal diffusion as if in a simple fluid, while particles with larger sizes exhibit anomalous diffusion with non-Gaussian distribution of displacements (7). Dynamic heterogeneity is also observed, where particles can show both slow and fast motions, even in the same cell (7).

The characteristics of cytoplasm are found to be similar to colloidal glass, and this is likely due to the extreme crowding by macromolecules (114). The bacterial cytoplasm is an aqueous environment hosting particles whose size ranges from 0.1 nm to several thousand nanometers. Solvents such as ions and H_2O are small in size and particles residing within them can exhibit Brownian motion (112). However, the cytoplasm is extremely crowded, with macromolecular concentration estimated to be ~0.3 to 0.4 g/ml and taking up 20-40% of the total volume (115, 116). Those macromolecules, or crowders, can either be mobile or fixed in a network to result in the reduction of the total available solvent volume and the slowdown of the motion of particles travelling in them (117-119). This volume exclusion effect can sometimes lead to the increase of local molecular concentrations, and cause a phenotypic change at the cellular level. For example, recent research showed that as the crowder concentration increases, the diffusion coefficient of RNA and proteins significantly decreases. Microenvironments can form, where the local mRNA production rate exceeds the diffusion rate, causing a heterogeneous distribution of mRNA (120). In silico studies have further shown that spatial fluctuations of transcription factors can drastically increase the noise in gene expression (121). Whether the physical properties of bacterial cytoplasm affect the diffusion of phage genomes and their relevant gene products

remains to be investigated, and whether macromolecular crowding has any effects on the lysis-lysogeny decision making of lambda awaits further investigation. In the following sections, the current knowledge of the physical properties of phage DNA, RNA and proteins will be reviewed.

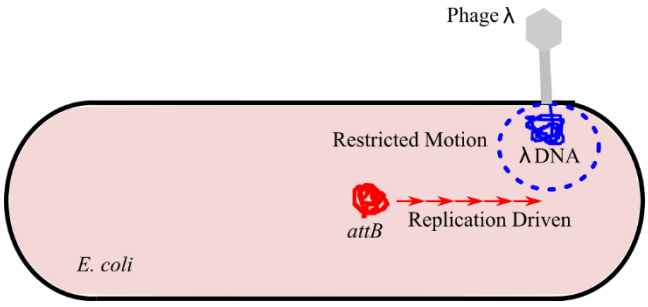

Figure 1.9 Replication driven DNA integration.
After being ejected into the cytoplasm, phage DNA primarily locates near the site of ejection and exhibits restricted motion. The *attB* locus on the *E. coli* genome overall moves towards the phage DNA, a process driven by chromosome replication, to facilitate DNA integration and cell lysogenization. This figure is generated based on (122).

DNA

Recent development of fluorescence labeling techniques has allowed the tracking of lambda DNA in live *E. coli* cells (122, 123). One recent effort to track the lambda DNA in live *E. coli* cells (122) utilizes one of the FROS (fluorescent repressor operator systems) techniques – the ParB/*parS* system (124-127). Inserting multiple repeats of the *parS* sequence on the lambda genome near the phage integration site, the *attP* locus, allows the observation of DNA movement when parB-mCherry fusion proteins are expressed from a plasmid. Using this method, lambda DNA was shown to exhibit confined diffusion and reside within a small area from its ejection site (122). One possible explanation, raised by the authors, is that the phage DNAs could be associated with the bacterial membrane and remain tethered there throughout the infection process. Some evidence can be collected from the literature to support this hypothesis (128). In those experiments, the lysate of the phage infected cells are sedimented through sucrose gradients, after which the free DNAs are found on the top. The presence of phage DNAs at the bottom in the rapid sedimenting complex (RSC) would therefore indicate their association with the materials in the RSC. The RSC materials were determined to be cell membrane as they break up when treated with detergents and other membrane-disrupting agents (128). Moreover, those researches mostly focused on the attachment of the parental DNA, and what happens to the progeny DNAs is largely unknown. Nevertheless, certain phage activities seem to be required for the membrane association, although phage DNA replication is not required (129-136). It seems that either the N protein itself, or the genes activated by N are responsible for the membrane association,

even though this was proposed at a time that the role and mechanism of N function is not clear yet (129, 130, 133, 134, 136, 137). It is now clear that N functions as an anti-terminator for the transcription of genes for homologous recombination, site-specific recombination, DNA replication, cellular division inhibition, CII, CIII, Q, and some other genes termed ‘non-essential’ for their lack of clear impacts on the lytic and lysogenic development of phages (11). Whether or not any of these components could mediate the phage DNA-membrane association remains to be investigated. Of all the possible lambda encoded proteins, only RexB, gpI, holin, anti-holin, and spanin are predicted to have transmembrane domains. RexB is expressed together with CI in the lysogenic pathway for the exclusion of other bacterial virus (138). Holin, anti-holin and spanin are lysis proteins expressed during lytic development. It is therefore unlikely that those proteins are responsible for the phage DNA-membrane association phenomenon observed early after infection. The other candidate, gpI, is a tail tip protein. While it is possible that gpI can translocate together with the phage DNA to the cell membrane during the DNA ejection process to mediate phage DNA-membrane association, experimental verification is lacking. In fact, whether gpI is present in the mature phage particle or not still remains to be studied (139, 140). Nevertheless, researches also suggest that the first round of phage DNA replication might occur at the cell membrane (141, 142), and may also interact with the bacterial DNA (68). Overall, those observations are all based on experiments that show co-sedimentation of phage DNAs with the bacterial membranes or chromosome, from which interaction of DNA and those

components are inferred. Whether or not this reflects the true intracellular behavior of phage DNA remains to be further investigated.

Despite the unknown mechanism of confined phage DNA motion, simultaneous labeling of the *attB* site on the *E. coli* chromosome allows Tal et al. to observe the phage DNA integration in real time (122). During the integration process, *attB* moves towards the phage DNA to facilitate the integration (Figure 1.9) (122). A replication driven mechanism was then proposed - the *E. coli* DNA is driven by replication to move towards the relatively confined phage DNA. This is supported by the observation that when the *attB* locus is moved towards the terminus, the lysogenization frequency is much lower compared to its native locus (122). This demonstrates how the intracellular dynamics of different components could potentially exert significant effects on the lysis-lysogeny decision-making of phage lambda. Nevertheless, questions on the molecular mechanisms of phage DNA dynamics and their contributions to the noisy decision phenotypes still remain and call for experiments with less perturbation of the system and finer observations of the DNA behaviors together with the resulting cell fates.

RNA and protein

Gene expression allows the information to be passed down from DNA to RNA and protein. The localization and cellular dynamics of the components along the path of gene expression, i.e., RNA or protein, might play important roles in determining the future of living organisms. In fact, even the bacterial cell, once thought as a bag of well-mixed enzymes, is found to have very well-organized protein localizations (143). Homologs of the cytoskeleton proteins in eukaryotic cells are found in bacteria, and they

regulate the cellular development of bacteria cells in a sophisticated way (144). This finding has also inspired investigations on the cellular organization of RNAs and proteins, which is partially accredited by the development of techniques to label and track single RNA and protein molecules *in vivo* (145).

In eukaryotic cells, the nucleus is separated from the rest of the cytoplasm by the nucleus membrane. Transcription happens within the nucleus, and mRNAs are subsequently translocated to the cytoplasm where ribosomes are found. Bacterial cells, however, lack membrane structures to separate the chromosome from the remaining space. It is generally accepted that in bacteria the transcription and translation processes are coupled, whereby multiple ribosomes may bind to the RNA and actively translate the information into proteins while the RNA is being transcribed from its DNA template (146, 147). If true, this process can result in a large complex, which can slow down RNA translocation. Recently, this transcription-translation coupled mechanism is being reevaluated, thanks to the development of modern techniques to allow direct visualization of those processes in more detail (145). Observing the *E. coli* DNA at high spatial and temporal resolutions reveals that the chromosome is a dynamic helical ellipsoid that occupies the majority of the cellular space but excluding the polar region, especially the old pole (148). While most of the RNA polymerases co-localize with their templates, the nucleoid, the ribosomes are not (149, 150). In fact, the majority of ribosomes are found to be separated from the nucleoid (149, 150). These observations raise questions such as, to what extent is the transcription coupled to translation; and how is the RNA translocated to the ribosome rich regions to be translated.

The *in vivo* dynamics of RNA molecules can be followed in real time using an MS2-GFP based system (96, 97, 151, 152). In this system, the target RNA is engineered to have 96 repeats of MS2-binding sequence that can be specifically bound by MS2-GFP, MS2 coat protein fused to the Green Fluorescent Protein (GFP) (97). Utilizing this method, the RNAs were shown to often exhibit localized motion without leaving their restricted area, possibly because they are tethered to the DNA template during or after transcription (97). Other groups have also reported that the RNA transcripts may stay near their transcription sites and exhibit limited dispersion (153). In the same report using the MS2-GFP system, motion spanning the whole cell is also observed for some RNAs where the RNAs seem to be able to diffuse freely in the cytoplasm and traverse the whole cell within a short time, indicating great heterogeneity in RNA dynamics (97). Some mRNAs are also found to localize to particular subcellular domains where their protein products function (154). Overall, different intracellular RNA behaviors are observed and this might reflect the diversity of RNA translocation mechanisms.

The location of RNA and proteins from phage lambda in their native context has rarely been reported. Where phage RNA and proteins locate inside the cell, and whether they show restricted motions or free diffusion remain to be studied. The dynamics of those gene products can have significant impacts on the lysis-lysogeny decision, especially in the case where multiple phages are infecting. A well-mixed pool of RNA and proteins inside the cell would promote sharing of resources and products between different phage DNAs, while localized and restricted motion can lead to the formation of microenvironments for individual phages and allow them to develop freely on their own.

Research (4, 111, 155) suggests that it is probably a combination of both mechanisms that determines the cellular decision making of phage lambda. On one hand, the frequency of each individual phage to 'vote' for lysogeny depends critically on the overall intracellular viral concentration, indicating that the presence of other phages contributes to the vote by each phage (4). On the other hand, it seems that the phages infecting the same cell are able to 'vote' differently towards lytic or lysogenic pathway, suggesting that they can maintain their 'identity' to some degree (4, 111, 155). In fact, phage 'voting' seems to happen at the individual DNA level, as the replicated DNAs from the same infecting phage can also make different decisions (111, 155). Complex intracellular phage-phage interactions also exist, as different infecting phages can cooperate with each other during the lysogenization process, and compete during the lytic development (111), possibly through sharing or sequestering some gene products. The factors that lead to the maintenance of phage 'identity' and the extent of 'sharing' remain to be characterized.

As proteins are the main factors that perform the functions and determine the distinct cellular phenotypes observed in the lysis-lysogeny pathways, examination of the protein location and diffusion behavior can provide more direct inference on how the physical properties of the cytoplasm affects the decision making. Techniques such as immunofluorescence, which detects proteins through specific antibodies, allow the observation of intracellular protein level and localization, although concerns have also been raised that those labeling/imaging techniques might alter the native localization of

the proteins to result in falsely positive data. Nevertheless, the exact localization of the phage RNAs and the proteins remains to be further explored.

Heterogeneity in the timing of phage DNA ejection

The phage infection process begins with the adsorption of phage particles onto the cell surface, followed by the ejection of DNA into the cytoplasm and the expression of phage genes. Not only the location, as has been discussed, but also the timing and kinetics of DNA ejection might have potential effects on the lysis-lysogeny decision making. In the case where multiple phages are infecting, differences in the DNA arrival time between different phages can cause variations in both the timing and level of gene expression from each infecting phage, leading to distinct decision-making behaviors. Under extreme conditions, when the second phage DNA arrives in a cell that has already established the lysogenic pathway by the first infecting phage, the second phage may remain silent. Although in this case, the DNA of the second phage might still have a chance to be integrated into the host chromosome if there is still integrase present, to result in a polylysogen. Moreover, it has been reported that for lytic cells that are initially infected by two or more phages, the second phage to arrive can be dominated by the first phage, where the first phage gains much greater advantages in progeny production (111). Under these circumstances, the observed lysis-lysogeny decision-making outcomes can be very different compared to when both DNAs arrive simultaneously. In cells where resources are limited, especially, the difference might be greater, as the early ejected DNA are more likely to capture and utilize more of the

resource while the others fail (111). It is therefore of great importance to assess the timing of the phage DNA ejection when examining the lysis-lysogeny decisions.

In vitro DNA ejection experiments show that lambda DNA ejection is a fast process, which takes only ~1.5 seconds (156). However, *in vivo* studies reveal that ejecting the whole DNA takes an average of 5 minutes, with great cell-to-cell variability (157). In this study, membrane impermeable dye SYTOX orange is used to stain the phage DNA and the ejection of DNA is inferred when the dye is translocated into the cell. Using this method, the kinetics of DNA ejection are found to vary drastically for each individual. Sometimes the DNA ejection can be finished in one step without interruptions, while in other cases pauses in ejection are observed, with waiting times as long as 5 minutes (157). While *in vivo* experiments are sometimes expected to reflect the true nature of the biological processes, in this case, the utilization of dyes to stain the DNA might cause some unwanted perturbations of the DNA ejection process. For example, the binding of SYTOX orange may interrupt with the ejection process if the channel to deliver DNA is already limited in size. Whether and how the great variability in the DNA ejection timing and kinetics contribute to the noisiness of the phage decision making remain to be investigated.

Last but not least, studies on phage DNA ejection have mostly focused on the "so-called" wild type laboratory strain – λpapa, which lacks the side tail fibers (158). λpapa is in fact a mutant strain with a single nucleotide deletion in the gene coding for the side tail fibers – the *stf* gene, which results in a truncated protein (158). The true 'mother' strain, λUr, exhibits faster adsorption compared to λpapa (159). The side tail

fibers of λUr may also facilitate the DNA ejection process by providing stronger binding of the phage particle to the cell surface and may secure the particles in the docking position. Nevertheless, whether having side tail fibers would affect the decision-making outcome or not awaits further investigation.

The Thesis Overview

For a better understanding of the lambda lysis-lysogeny decision making, a more complete and unifying picture is presented based on literature reviews. The key players involved in this process, including their regulation and mechanism of action, are discussed in detail. Moreover, a potential impact factor, the phage DNA replication, is also introduced. Besides the well-known players, the lambda decision making is also affected by both stochastic and deterministic factors. The previously characterized deterministic factors have been presented and discussed here, as well as the current understanding of the stochastic factors, which include but are not limited to: 1) stochastic gene expression, 2) the heterogeneous cellular environment and the complex dynamics of phage components, and 3) the variability in the timing of phage infection.

In the next few chapters, the research that has been conducted as well as the findings will be presented and discussed. In chapter II, the physical dynamics of phage DNA *in vivo* will be examined, and their correlation with the final cell-fate decision will be determined. A novel phage DNA labeling technique is developed to allow the tracking of single phage DNA molecules in real time, and complex behaviors of the DNA motion is discovered. In chapter III, evidence is obtained for different phage decisions in a single cell through the simultaneous tracking of the phage DNA

integration events and the lysis-lysogeny decision. A previously uncharacterized event, where phage DNA integration happens even in cells going into the lytic pathway, is discovered and its evolutional impacts are discussed. In chapter IV, the role of DNA replication in the decision-making process is investigated. Through single-molecule quantifications of phage gene activity, the impact of DNA replication is uncovered. The role of stochastic gene expression in phage decision making is also investigated through mathematical simulations. Lastly, conclusions from this work are summarized in Chapter V.

CHAPTER II

PHAGE DNA DYNAMICS IN CELLS WITH DIFFERENT FATES*

Introduction

Bacteriophage (or simply phage) lambda is one of the best well-studied systems due to its relatively simple genetic regulatory circuitry and its important feature serving as the simplest paradigm of cell fate decisions (13, 160). Upon infection by phage lambda, bacterium *E. coli* enters one of two alternate pathways: lytic (virulent) or lysogenic (dormant). In the lytic pathway, around 100 new viruses are produced inside the cell, and then released to the environment following cell lysis (cell death). In the lysogenic pathway, the virus's DNA is integrated into *E. coli*'s genome, in which the virus remains as dormant state inside the cell, and the cell keeps its growth. Although this lysogenic state is extremely stable, it may be switched to the lytic state when the cell undergoes DNA damage by inducing agents such as UV. The lytic pathway, lysogenic pathway and lysogenic induction serve as important model systems for understanding developmental pathways and the switch between two pathways (14).

The lysis/lysogeny decision-making process has been well studied at the level of cell culture (10, 14, 53, 73, 160, 161) and, more recently, at higher resolution (3, 4, 89, 110, 162). The nutritional condition of the cell is an important factor to influence cell

---

* Reprinted from *Biophysical Journal*, 108(8), Qiuyan Shao, Alex Hawkins, and Lanying Zeng, "Phage DNA Dynamics in Cells with Different Fates", Pages No. 2048-60, Copyright 2015, with permission from Elsevier.

lysis/lysogeny since host factors regulate the expression of viral key genes for lysis/lysogeny (28, 53, 73). In the 1970s, by the use of bulk assay, multiplicity of infection (MOI: infecting phage per cell) has been identified as an important factor in the lysis/lysogeny decision. Through the quantification of cell lysogeny as a function of average phage input (API or <MOI>: averaged infecting phage per cell) and assuming the adsorption of phage particles to the *E. coli* surface follows a Poisson distribution, the authors concluded cell lysogenization requires 2 or more wild type phages when cells are grown in rich medium (53). Recently, by the use of single-cell methods, cell length (size) has been established as another important factor in the lysis/lysogeny decision where smaller cells tend to lysogenize more frequently (3, 4). More intriguingly, quantitative data at the single-cell/single-virus level suggested that individual viruses make individual decisions inside the cell, and then cooperate in a way such that only a unanimous vote by all the infecting viruses can lead to cell lysogeny (4). Following that, based on the experiment data of (4), a theoretical group proposed an alternative scenario in which the resulted cell fate could be due to partial gene dosage compensation (162). The quantitative understanding of the lysis/lysogeny decision-making process thus far is still incomplete. In order to fully unravel the decision-making process, still greater resolution is needed.

A few studies have shown that when phage lambda is mixed with *E. coli*, phage lambda prefers to attach to cellular poles or midcell ("future pole"), presumably for lambda DNA ejection into the host (4, 78, 81). Following that the ejected lambda DNA serves as the blueprint for the viral gene expression eventually leading to different cell

fates. It appears that the preferred DNA ejection site only influences the rate of successful ejection, and once the phage DNA is successfully ejected into *E. coli* cytoplasm the lysogenization frequency remains the same (4). Now we would like to probe this system in more detail by following the DNA movement inside the cell, and ask whether phage DNA movement has any correlation with cell fates and what kind of motion phage DNA exhibits in cells at different developmental stages when cells undergo different cell fates. This may help uncover the mechanism of the lysis/lysogeny decision making at the subcellular level. Many lines of work have shown that it is not a "well-mixed soup" in bacteria, instead, macromolecules undergoes spatiotemporal organization (163). For example, different proteins involved in cell division such as FtsZ is localized at midcell when cells are about to divide (144), MinCDE family oscillates between cell poles (164) as well as different chromosome loci are localized differently inside the cell in *E. coli* (165). The local environment the phage DNA is surrounded by may have a significant influence on the stochastic gene expression leading to different cell fates (4).

In this study, we first report a new plasmid-based method for labeling phage lambda to count the infecting phage in order for the quantitative study under the fluorescence microscope. We then describe a new technique with the use of fluorescently fused *E. coli* SeqA protein to monitor the intracellular motion of lambda phage DNA in living cells. Using this new system, we characterize the motion of lambda DNA particles at different stages of the infection cycle. We find that lambda DNA particles exhibit subdiffusive behavior like the large particles reported in the literature.

At the early stage of the infection cycle, lambda DNA moves similarly in all cells no matter the cell chooses the lytic or lysogenic pathway, which suggests that the lambda DNA movement does not affect the cell lysis/lysogeny decision. In contrast, lambda DNA movement varies after the cell commits to one pathway or the other.

Materials and Methods

Bacterial strains, plasmids, phages and primers

Strains, plasmids, phages and primers used are described in Table 2.1.

*Construction of the plasmid pACYC177-PLate*D-eyfp*

The construction of the plasmid is as follows: *D-eyfp* was first amplified from λeyfp (74) using primers PLZ1lambda1 and PLZ1lambda3back, and cloned between *EcoRI* and *BamHI* restriction sites. This *D-eyfp* replaced gene *D* in pPLate**D* plasmid (4) resulting in a plasmid pPLate**D-eyfp* with the origin of replication of pBR322, denoted pBR322-PLate**D-eyfp*. The fragment PLate**D-eyfp* was digested with enzymes *BamHI* and *HindIII*, and ligated to pACYC177 or pACYC184 vectors resulting in the plasmid pACYC177-PLate**D-eyfp* or pACYC184-PLate**D-eyfp* with the origin of replication of p15A. To produce fluorescent gpD-mosaic phages, lysogens harboring the *D-eyfp* plasmid was heat induced followed by a series of phage purification steps (4). The fluorescent gpD-mosaic phages λ_{LZ7}, λ_{LZ3} and λ_{LZ6} were produced from W3350(λ_{IG2903})[pACYC177-PLate**D-eyfp*], W3350(λ_{IG2903})[pBR322-PLate**D-eyfp*] and W3350(λ_{IG2903})[pACYC184 -PLate**D-eyfp*], and λ_{LZ220} (see next section for details) and λ_{LZ221} were produced from MG1655(λ_{LZ613})[pACYC177-PLate**D-eyfp*][pGG503] and BA15(λ_{LZ613})[pACYC177-PLate**D-eyfp*] respectively.

Table 2.1 Bacterial strains, plasmids, phages, and primers used in this work.

Strain name	Relevant genotype	Source/reference
Bacterial strains		
MG1655	*sup*^{0}	Lab collection
W3350	*sup*^{0}	Lab collection
LE392	*supE, supF*	Lab collection
BA15	*MG1655, dam*$^-$	M. Radman
LZ204	*MG1655, dam*$^-$*, seqA-ecfp, cm*^{R}	This work
LZ208	LZ204[pP_{RE}-*mCherry*]	This work
Phage strains		
λ_{LZ613}	Parental, *cI*$_{857}$ *bor::kan*^{R}	This work
λ_{LZ220}	Fully methylated, gpD-mosaic, *cI*$_{857}$ *bor::kan*^{R}	This work
λ_{LZ221}	Unmethylated, gpD-mosaic, *cI*$_{857}$ *bor::kan*^{R}	This work
λ_{IG2903}	*b::kan*^{R} *cI*$_{857}$	(4)
λ_{LZ7}	gpD-mosaic, *b::kan*^{R} *cI*$_{857}$	This work
λ_{LZ3}	gpD-mosaic, *b::kan*^{R} *cI*$_{857}$	This work
λ_{LZ6}	gpD-mosaic, *b::kan*^{R} *cI*$_{857}$	This work
Plasmids		
pP_{RE}-*mCherry*	mCherry under the control of P_{RE}, *amp*^{R}	(4)
pPLate**D*	gpD under the control of λ late promoter, *amp*^{R}	(4)
pACYC177-PLate**D-eyfp*	gpD-EYFP under the control of λ late promoter, *amp*^{R}	This work
pGG503	Dam under the native promoter, *tet*^{R}	(166)
Primers		
PLZ1lambda1	5’-GCTGAAAAATTCAGTGTAAGGGATGTTTATGACG	This work
PLZ1lambda3 back	5’-GAAGGGGATCCTTACTTGTACAGCTC	This work
SA6for	5’-TCCCCGCGGAACGTTGCAGACAAAGGACAAAG	(167)
SA7back	5’-ACATGCATGCCAATACGCTTCCAGTATTC	(167)
ECFP forward 1	5’-ATCTGCTAGCGTGAGCAAGGGCGAGG	This work
ECFP reverse 1	5'- AGATGGATCCTCATTACTTGTACAGCTCGTCCATGC	This work
pSeqA-CFP, Cm forward 1	5'-TTGCGTCACCTGCTATCGTCG	This work
pSeqA-CFP, Cm reverse 1	5'-GGACAGGGCGTGAGTATCTTTACC	This work

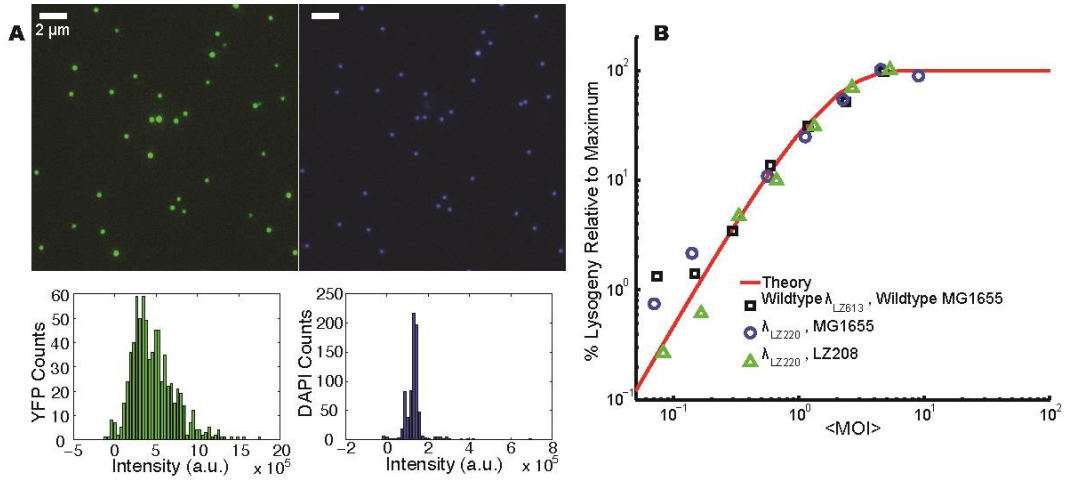

Figure 2.1 Fluorescently labeled phage and the control lysogenization experiment in bulk.

(A) Fluorescence and DNA packaging efficiency of the fully methylated fluorescent phage (λ_{LZ220}). DAPI (4',6-diamidino-2-phenylindole) was used to label the phage genome. Top two panels: YFP and DAPI signals from the phages under the fluorescence microscope. YFP and DAPI signals colocalize very well, and individual phages are easily distinguishable. Only ~1% of the fluorescent phage particles examined (7 out of 680) lacked the DAPI signal (indicating that these particles did not successfully package the viral DNA or had already ejected their DNA elsewhere), and ~1% (8 out of 680) lacked the YFP signal which could be due to the undetectable YFP signal or this phage had moved its location during imaging. Bottom two panels: intensity histograms of the YFP and DAPI signals. (B) Fully methylated fluorescent phage λ_{LZ220} shows the same lysogenization response to MOI in *dam*$^-$ *E. coli* LZ208 and (the normal *dam*$^+$ strain, MG1655) as the wild type phage λ_{LZ613} in MG1655. Symbols are the experimental measurements, and the red line shows the theoretical prediction, the $n \geq 2$ Poisson distribution (53).

Fully methylated fluorescent phages

The parental phage λ_{LZ613} was created by crossing λ *cI*857 with plasmid pER157 (168) (gift of Ryland Young, Texas A&M University) to replace the *bor* region with the Kanamycin antibiotic cassette through the standard protocol (160). The *bor* gen encodes an outer membrane lipoprotein, which is not involved in lysis/lysogeny decision making (169). Under the normal *dam*$^+$ *E. coli* environment, the produced lambda phage is undermethylated (or partially methylated) due to the limited Dam methylase available. The fully methylated lambda phage can be obtained with the help of the Dam methylase overproduction plasmid pGG503 (166, 170). This pGG503 plasmid (gift of Paul Modrich, Duke University; Martin Marinus, University of Massachusetts Medical School) was then transformed into the phage lysogen MG1655(λ_{LZ613})[pACYC177-PLate**D-eyfp*]. Stable fluorescent mosaic phage λ_{LZ220} was produced and purified as described (4, 75). Briefly, 500 ml of phage lysogen is grown in LB supplemented with 0.5 μg/ml thiamine HCl to $OD_{600} \approx 0.6$ followed by heat induction to produce crude lysate. The crude lysate is then precipitated by PEG, ultracentrifuged in CsCl step gradient and equilibrium gradient, and dialyzed against SM buffer (100 mM NaCl, 10 mM $MgSO_4$, 0.01% Gelatin, 50 mM Tris-Cl, pH 7.5). We stained the fully methylated fluorescent phage (λ_{LZ220}) with DAPI (4',6-diamidino-2-phenylindole, Sigma-Aldrich, St. Louis, MO) to test DNA packaging efficiency. 10 μl of phage (~$2x10^9$ pfu/ml) were mixed with 10 μl DAPI (10 μg/ml) and incubated at room temperature for 10 min or on ice for 30 min. 1 μl of phage-DAPI mixture was applied on a coverslip (No.1.5, Fisher Scientific, Waltham, MA), and 1.5% PBS-agarose slab was overlaid on the sample. The

sample was imaged under the fluorescence microscope with 5 *z*-axis (vertical) slices taken at 200 nm intervals, using 100 ms exposure in the YFP and DAPI channels (see microscopy details in section **Microscopy and Imaging**). Typical images are seen in Figure 2.1A. Only ~1% of the fluorescent phage particles examined (7 out of 680) lacked the DAPI signal (indicating that these particles did not successfully package the viral DNA or had already ejected their DNA elsewhere), and ~1% (8 out of 680) lacked the YFP signal which could be due to the undetectable YFP signal or this phage had moved its location during imaging. Figure 2.1A demonstrates the co-localization and uniformity of YFP and DAPI signals from each phage. Individual phages can be easily distinguished under the microscope.

Construction of the SeqA-ECFP

Our approach is based on a method developed by Babic and coworkers (167), which has been used to directly visualize horizontal gene transfer in *E. coli*. Starting with pSeqA-C (gift of Miroslav Radman, Universite Paris Desartes Faculte de Medecine), as described by Babic *et al.* (167), a 700 bp region on the 3' end of *seqA* was amplified from MG1655 chromosomal DNA using primers SA6for and SA7back and cloned between *SacII* and *SphI* restriction sites of pSeqA-C downstream of the cm^R. This homology region allows later integration into the *E. coli* chromosome. The resulting plasmid is pSeqA-C3H. An *ecfp* insert was amplified from plasmid pPROTet.E-*ecfp* (gift of Christopher Rao, University of Illinois at Urbana-Champaign) using primers ECFP forward 1 and ECFP reverse 1 with restriction sites *NheI* and *BamHI* added to the ends. pSeqA-C3H was digested with *NheI* and *BamHI* (excising the *yfp* region), and the

vector was extracted. The insert was also digested with *NheI* and *BamHI*, ligated with the vector, and transformed to select for chloramphenicol resistance (cm^R). The resulting plasmid, pSeqA-CFP, contains *seqA-ecfp* and the 3H homology region, with a cm^R cassette located in between. This whole region (~3 kb) was amplified using primers pSeqA-CFP, Cm forward 1 and pSeqA-CFP, Cm reverse 1. This resulting fragment was integrated into the dam^- strain BA15 (gift of Miroslav Radman, Universite Paris Desartes Faculte de Medecine) resulting in the host strain LZ204 using Wanner gene replacement method (171).

Fully methylated fluorescent phage shows the same lysogenic response in different hosts in bulk

Through our bulk experiments (the same experimental procedure as in (4)), we show that in different host strains (dam^-, LZ208 and wild type dam^+, MG1655), fully methylated fluorescent mosaic phage λ_{LZ220} behaves like wild type phage in wild type cells by exhibiting the same lysogenic response as a function of MOI (shown in Figure 2.1B).

Microscopy and imaging

An overnight culture of LZ208 was diluted 1:100 in M9 minimal medium (11.3 g/L M9 salts, 1 mM $MgSO_4$, 0.5 μg/ml thiamine HCl, 0.1% casamino acids, 100 μM $CaCl_2$, and 0.4% maltose) and grown to $OD_{600} \approx 0.4$ at 37 ºC. Cells were concentrated and resuspended into ice-cold M9 to $OD_{600} \approx 4$. λ_{LZ220} phages were added to reach an MOI of ~ 1, followed by incubation on ice for 30 min and additional 5 min incubation at 35 ºC to trigger phage DNA ejection (4, 53, 78, 172). The phage-cell mixture was

diluted 1:10 into M9 and 1 µl of the diluted phage-cell mixture was placed on a thin 1.5% or 2% M9 agarose slab (~1 mm thick). After 1 min, a coverslip (No.1.5, Fisher Scientific) was gently overlaid and the sample was imaged under the fluorescence microscope at 30 ^{o}C by a cage incubator (in vivo scientific). Microscopy was performed on an inverted epifluorescence microscope (Nikon Ti-E) using a 100x objective (Plan Fluo, numerical aperture 1.40, oil immersion) and standard filter sets. Images were acquired using a cooled EMCCD camera (iXon3 897, Andor). Acquisition was performed using Nikon Elements software (Nikon).

To localize all phages surrounding the cells, a series of 15 *z*-axis (vertical) images at spacing of 200 nm were taken through the YFP channel using 100 ms exposure each. To obtain more data in each time-lapse movie, cells were imaged at multiple stage positions (typically 8) in each experiment. During the time-lapse movie, the sample was imaged in phase contrast (100 ms exposure, for cell recognition), YFP (100 ms exposure, for phage detection), CFP (30 ms exposure, for phage DNA detection inside the cell) and mCherry (100 ms exposure, for detection of the P_{RE} transcriptional reporter signal) channels. The time-lapse movies were taken either continuously or at time intervals of 200 ms, 500 ms, 1 s, 5 s, 10 s and 20 s for around 30 frames till the sample was photobleached. These were short movies in order to characterize phage DNA diffusion. We also took long movies at a time interval of 5 min until the cell fate was visible (~4 hours). For long time-lapse movies, with time, as infections led to one of the possible pathways, lytic cells were identified by SeqA-CFP foci and cell lysis. Lysogenic cells were identified by SeqA-CFP foci and the increased mCherry

fluorescence indicating P_{RE} activity followed by cell division. Typical time-lapse movies for lytic and lysogenic cells are shown in Movie S1 and S2 respectively, and a few snapshots are shown in Figure 2.2B. In order to ensure our imaging condition does not affect the lysis/lysogeny decision making (e.g. the leaking UV could induce the lysogen), we performed time-lapse movies of phage lysogen growth with the same imaging parameters and the lysogen grew normally.

All data analysis was performed in Matlab (The MathWorks). Cell recognition in the phase-contrast channel was performed using the Schnitzcell routine (gift of Michael Elowitz, California Institute of Technology), cell lineage tracking was done by a home-made script, and spot recognition was similar to Spatzcells (173). We performed short movies with 30 time frames at the time intervals of 30 ms (continuous streaming, 2 experiments, 8 cells), 200 ms (3 experiments, 4 cells), 1 s (5 experiments, 12 cells), 2 s (6 experiments 9 cells), 5 s (9 experiments, 16 cells), 10 s (6 experiments, 11 cells), and 20 s (3 experiments, 6 cells). For long movies, we performed a total of 13 experiments (lasting around 4 hours at the time interval of 5 minutes) in which we measured the fates of 326 cells infected by 413 phages.

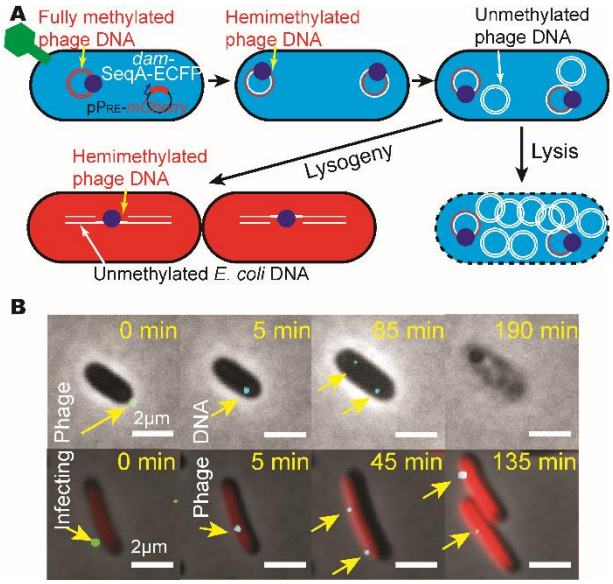

Figure 2.2 Assaying the phage infection process.
(A) Representative schematic of phage DNA labeled by SeqA-ECFP protein. The initial SeqA-ECFP focus corresponds to the ejected phage DNA. Two foci will appear when the phage DNA replicates to two hemimethylated phage DNAs. These two foci will remain for the infection cycle. The cell also harbors pP_{RE}-mCherry plasmid. Red fluorescence (mCherry) will accumulate if the cell follows the lysogenic pathway. (B) Overlay images from a time-lapse movie to follow phage DNA inside the cell for a lytic cell (top panel) and a lysogenic cell (bottom panel). At 0 min, the spot (appear as green, pointed by yellow arrows) on the cell surface shows the infecting phage. At 5 min, the SeqA-ECFP focus (appear as cyan, pointed by yellow arrows) appears representing the ejected phage DNA. Two foci appear at a later time (lytic cell at 85 min and lysogenic cell at 45 min). Following that the lytic cell lyses and the lysogenic cell divides with each daughter having 1 focus.

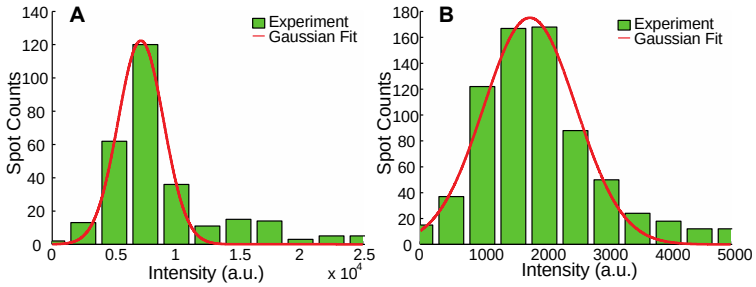

Figure 2.3 Histograms of phage intensity.
Green bars are the experimental data, and red curve is a Gaussian fit. The spot intensity is well fitted by a Gaussian distribution. (A) λ_{LZ1} with a Gaussian mean of 7136. (B) λ_{LZ2} with a Gaussian mean of 1767, which is about ¼ of that of λ_{LZ1}.

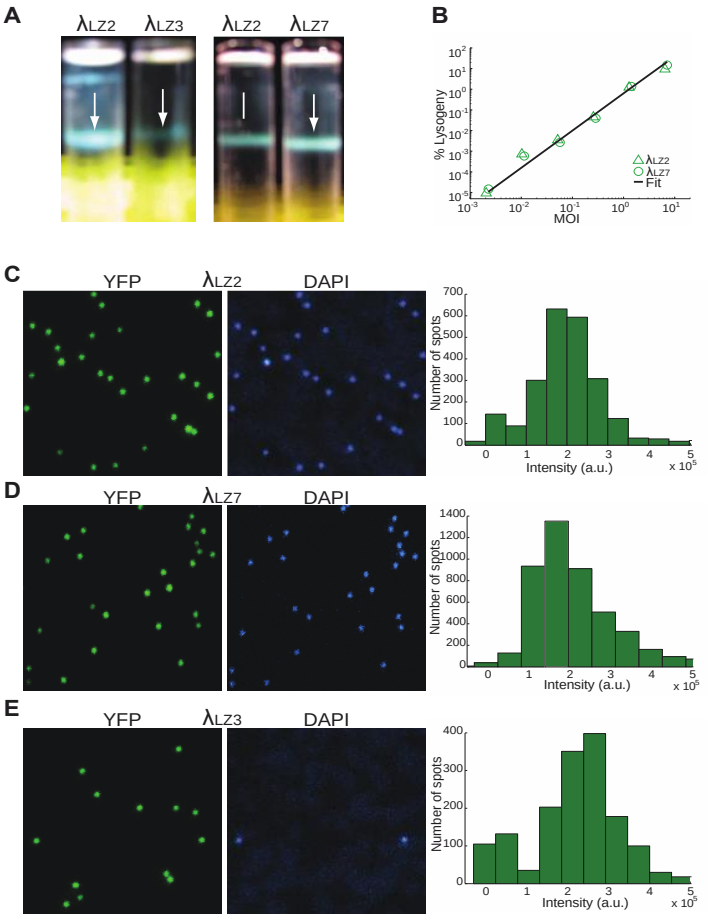

Figure 2.4 Phage bands after ultracentrifuge and the DNA packaging efficiency test of the fluorescent phages.

(**A**) Phage bands after ultracentrifuge through CsCl equilibrium gradients. Arrows point to the phage bands, containing ~ 10^{12} pfu phage particles. The fluorescent gpD-mosaic phage (λ_{LZ3}) is slightly lighter than the fluorescent gpD-mosaic phage (λ_{LZ2}), which indicates the ratio of gpD-EYFP over gpD proteins of λ_{LZ3} is higher than that of λ_{LZ2}. The fluorescent gpD-mosaic phage (λ_{LZ7}) is slightly heavier than the fluorescent gpD-mosaic phage (λ_{LZ2}), which indicates the ratio of gpD-EYFP over gpD proteins of λ_{LZ7} is lower than that of λ_{LZ2}. (**B**) Bulk assay of lysogenization probability as a function of MOI. Δ: fluorescent gpD-mosaic (λ_{LZ2}); ○: fluorescent gpD-mosaic (λ_{LZ7}). Line: theoretical prediction based on the single-cell lysogenization response combined with a Poisson collision statistics between individual bacteria and phages. The experimental data was shifted to accommodate for the imperfect adsorption and infection efficiencies. The fluorescent gpD-mosaic λ_{LZ7} phage exhibits the same MOI-response as λ_{LZ2}.

Figure 2.4 continued.
(**C**), (**D**) and (**E**) Fluorescence and DNA packaging efficiency of the fluorescent gpD-mosaic phage (λ_{LZ2}, λ_{LZ7} and λ_{LZ3}). DAPI (4',6-diamidino-2-phenylindole) was used to label the phage genome. Left two panels: YFP and DAPI signals from the phages under the fluorescence microscope. Individual phages are easily distinguishable. YFP and DAPI signals co-localize very well for λ_{LZ2} (~0.5%, 12 out of 2300 YFP spots lack of DAPI signal, 0%, 0 out of 2300 DAPI signal lack of YFP) (**C**) and λ_{LZ7} (~0.4%, 15 out of 3800 YFP spots lack of DAPI signal, 0%, 0 out of 3800 DAPI signal lack of YFP) (**D**). Many YFP signals lack DAPI signals for λ_{LZ3} (~27%, 567 out of 2103 YFP spots lack of DAPI signal, 0%, 0 out of 2103 DAPI signal lack of YFP) (**E**). Right panel: the intensity histogram of the YFP signals (on average of $2x10^5$, $1.8x10^5$ and $2.5x10^5$ for λ_{LZ2}, λ_{LZ7} and λ_{LZ3} respectively).

Results

A plasmid-based approach for the construction of stable, well-behaved and fluorescent phage lambda

To obtain a quantitative picture of the dynamics in the lambda system, one would like to follow the viral life cycle under the microscope in real-time, at the resolution of individual phages and cells. There are certain different ways to label phage particles fluorescently (3, 4, 74, 78, 122, 157, 174), and the key issue is to ensure the labeled phages functional and well-behaved for the examination of viral life cycle. Recently, we have constructed two fluorescent phages λ_{LZ1} and λ_{LZ2} based on λeyfp (4, 74). Fluorescent gpD-mosaic λ_{LZ2} was created by co-expression of fluorescent gpD-EYFP encoded by the *eyfp* gene fused lambda *D* gene in the lysogen of λ_{LZ1} and wild type gpD from a plasmid under the control of λ late promoter. We have tested the candidacy of fluorescent phages (fluorescent gpD-EYFP λ_{LZ1} and gpD-mosaic λ_{LZ2}) to behave like

wild type for the single virus study under the microscope. Through our study, we found that gpD-EYFP λ_{LZ1} cannot survive through phage purification steps meaning that phage keeps losing its titer significantly along the way, which indicates that the capsid made with pure gpD-EYFP proteins is not stable. Additionally, other tests, including the phage morphology through electron microscopy, DNA packing efficiency through DAPI staining, and MOI-response through bulk assay, on the unpurified phage were all failed. On the other hand, fluorescent gpD-mosaic λ_{LZ2} passed all the control tests using the successfully purified stock, i.e., similar morphology as wild type, close to 100% DNA packaging efficiency within 1% accuracy and similar trend on cell lysogeny versus API as wild type through bulk assay. The number of gpD-EYFP versus wild type gpD in the capsid of fluorescent gpD-mosaic λ_{LZ2} is around 1:4 by comparing the fluorescence intensities of fluorescent gpD-EYFP λ_{LZ1} and gpD-mosaic λ_{LZ2} under the microscope (Figure 2.3). As there are about 420 copies of gpD per phage head (160), λ_{LZ1} presumably contains about 420 copies of fluorescent gpD-EYFP, therefore gpD-mosaic λ_{LZ2} contains about 100 copies of fluorescent gpD-EYFP. The appropriate ratio of these two versions of gpD is the key to the stability of the phage capsid and the brightness of the phage.

As described above the construction of fluorescent gpD-mosaic phage λ_{LZ2}, the fluorescent gpD-EYFP proteins are from the lambda lysogen DNA containing the gene *D-eyfp* and the wild type gpD proteins are from plasmid pPLate**D*. Here, in order to achieve the co-expression of wild type gpD and fluorescent gpD-EYFP proteins, we can switch the sources of the production of these two types of proteins, namely, wild type

gpD proteins from the lambda lysogen DNA and fluorescent gpD-EYFP proteins from a plasmid. This can facilitate the study of a number of phage mutants without requiring *D-eyfp* recombinant viruses of each mutant and also eliminates the possibility of perturbing phage behavior while manipulating the phage genome. The constructed plasmid, pACYC177-PLate**D-eyfp,* containing the lambda *D* gene, fused with enhanced yellow fluorescent protein (EYFP) is under the control of the lambda late promoter (see **Materials and Methods** for details). The resulting phage from lysogen W3350(λ_{IG2903})[pACYC177-PLate**D-eyfp*] is noted as fluorescent gpD-mosaic phage λ_{LZ7}. Again, to verify the validity of the fluorescent version λ_{LZ7} to behave like wild type λ_{IG2903}, we repeated the same control experiments as we verified fluorescent gpD-mosaic λ_{LZ2}, and compared it with λ_{LZ2}. λ_{LZ7} efficiently packages the viral DNA, is structurally stable, and exhibits the appropriate lysis/lysogeny decision phenotype (Figure 2.4).

Phage DNA detection

To follow phage DNA from the point of infection through the entire infection cycle, it was necessary to provide fluorescent labels for both the phage particle and its DNA. To this end, we constructed a host, LZ204, which is methylation deficient (*dam*$^-$) and constitutively expresses the fluorescent fusion, SeqA-ECFP. SeqA binds to lambda DNA in both fully methylated and hemimethylated form with the same efficiency and affinity (175, 176). The phage λ_{LZ220} was fully methylated by the production in a *dam*$^+$ host with a Dam methylase over production plasmid pGG503 (166, 170) (The fluorescent phage and bulk test are shown in Figure 2.1). The wild type phage lambda produced in a wild type cell is undermethylated (or partially methylated) owing to lack

of Dam methylase (170). In addition, the λ_{LZ220} phage is fluorescently labeled through the plasmid-based approach described above as a result of being mosaic for the gpD decoration protein. In order to monitor the lysis/lysogeny decision under the fluorescence microscope, LZ204 was transformed with the lysogenic reporter plasmid pP_{RE}-*mCherry* (4). Infections that follow the lysogenic pathway develop red fluorescence as a result of key lysogenic establishment protein CII-dependent activation of P_{RE}, whereas opposed to the overt lysis that terminates the lytic pathway (4, 17).

Prior to phage infection, the SeqA-ECFP fusion proteins exhibit uniform cytoplasmic distribution inside the *dam*$^-$ host. After fully methylated phage DNA is ejected into the cell, SeqA-ECFP would be expected to bind to the phage DNA, forming a fluorescent focus. When the phage DNA replicates in the *dam*$^-$ host, this fully methylated phage DNA would be converted into two hemimethylated duplex DNAs, and thus two fluorescent foci should be visible. As the phage DNA replicates further in the *dam*$^-$ host, the number of foci should remain at two for the rest of the infection cycle. A schematic of this experimental setup is shown in Figure 2.2. All of these expectations were fulfilled, for a total of 333 infections with the fully methylated and fluorescently labeled λ_{LZ220} phages. Images and movies of representative lytic and lysogenic infections are shown in Figure 2.2B and Movies S1 and S2. The fluorescent intensity of the first fluorescent focus, corresponding to the initial lambda DNA ejected into the cytoplasm, was shown to be mostly uniform (Figure 2.5A). Since phage particles may locate at different *z* planes, we expect a range of fluorescent intensities since we image only at the focal plane to avoid photobleaching. As expected, unmethylated phage

(λ_{LZ221}) produced in a *dam*$^-$ host generated no fluorescent foci at any time during the infection cycle.

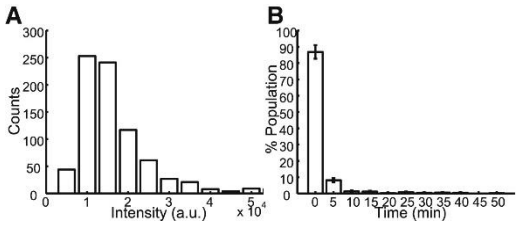

Figure 2.5 Intensity of phage DNA focus and the timing of phage DNA appearance. (A) Histogram of the fluorescence intensity of the SeqA-ECFP foci representing the phage DNA ejected into the cytoplasm. (B) Histogram of the time of the appearance of the SeqA-ECFP foci (N = 519). ~ 95% of the spots appear within 5 minutes under these experimental conditions. Data are shown as mean ± SEM (counting error).

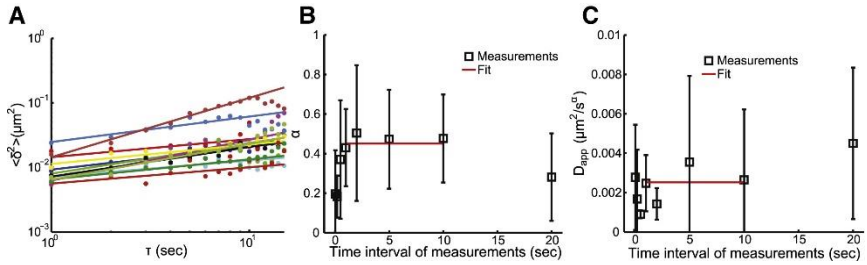

Figure 2.6 Subdiffusive motion for phage DNA particles.
(A) $\langle \delta^2 \rangle$ as a function of time interval of τ for the experiment of 1 second interval between measurements (loglog plot). Experimental data and the power fit for each trajectory are shown as markers and lines respectively. (B) The subdiffusion scaling exponent α for different time intervals between measurements. Square: experimental measurements. Red line: A fit to the measurements of 1 s, 2 s, 5 s and 10 s. (C) The apparent diffusion coefficient D_{app} for different time intervals between measurements. Symbols and red line are defined the same as in (B).

Phage DNA dynamics during the immediately early stage of phage infection in living cells

In order to examine the motion of phage DNA particles and characterize the diffusion coefficient of phage DNA inside the cell, we performed experiments with different time resolutions (time intervals of 30 ms, 200 ms, 500 ms, 1 s, 5 s, 10 s, and 20 s). Since these movies are short (typically 30 frames) and the initially ejected DNA has not yet been replicated, we normally observe 1 SeqA-ECFP focus per cell. Therefore, the phage DNA dynamics reported below is for the immediate early stage of phage infection before the cell commits to either lytic or lysogenic pathway. The phage DNA trajectories enable us to estimate the diffusion coefficient of these particles. In the literature, various tracer particles were reported to exhibit subdiffusive motion in bacteria (7, 113, 165, 177). Here, we use the following equation to extract the subdiffusivity of this two-dimensional diffusive system (165): $\langle \delta^2 \rangle = 4D_{app}\tau^{\alpha}$, where $\langle \delta^2 \rangle = \frac{1}{n}\frac{1}{m}\sum_{i=1}^{n}\sum_{j=1}^{m}[\vec{r_i}(t_j+\tau) - \vec{r_i}(t_j)]^2$ is the ensemble-averaged mean squared displacement between two time points, D_{app}: is the apparent diffusion coefficient, τ is the time interval, α is the subdiffusion scaling exponent, n is the number of trajectories, and m is the number of time points. Figure 2.6A shows $\langle \delta^2 \rangle$ as a function of τ for those 12 cells with a time interval of 1 second between measurements. Each trajectory can be fitted into a power function with $\alpha = 0.43 \pm 0.20$ (mean $\pm$ standard deviation). Deviation from the power fit at longer times might be due to the effect of averaging over a small number of position pairs and/or limited cell size (113). The average value of 0.43 is in a reasonable agreement with those reported for *E. coli* chromosome loci (165).

However, there is a great cell-cell variability reflected by the large standard deviation of 0.20 with α ranging from 0.25 to 0.92. In order to eliminate the effect of phototoxicity to cell health on particle movement, we also performed experiments with different time intervals between measurements of 30 ms, 200 ms, 500 ms, 2 s, 5 s, 10 s and 20 s. We found that the averaged α is almost constant for time intervals of 1 s, 2 s, 5 s, and 10 s (shown in Figure 2.6B) indicating that the measurements converge. The red line shows the mean of those 4 measurements of α = 0.47 (with a standard deviation of 0.03) in the figure. For time intervals less than 1 s, α is lower than 0.4. 30 ms and 200 ms intervals only have an α less than 0.20, which could be due to the phototoxicity by too frequent shining light to the sample resulting in unhealthy cells. The 20 s interval has an α less than 0.30, which might be due to the limited cell size. Nevertheless, with the subdiffusion scaling exponent of α less than 1, the phage DNA-protein complex exhibits subdiffusive motion in *E. coli* cells.

The apparent diffusion coefficient extracted from the measurements of 1 s, 2 s, 5 s and 10 s is $D_{app} = (2.5 \pm 0.9) \times 10^{-3} \mu m^2/s^{0.47}$. Here, our phage DNA-protein aggregates are expected to be large particles. There are 116 GATC sites distributed along the 48.5 kbp lambda genome for SeqA-ECFP protein to bind. It was reported that in *in vitro* experiments one SeqA tetramer binds to each of hemimethylated GATC sequences that are up to 31 bases apart on the DNA (178, 179). We estimate roughly a few tens SeqA-ECFP molecules, each a few nanometers in size, will bind on the phage genome. From this parameter and the size of the lambda genomic DNA, we estimate the phage DNA-protein complex to be on the order of a hundred nanometers (180). In the

literature, the diffusion coefficient for large protein or RNA-protein aggregates at the order of a hundred nanometers ranges widely from the order of 10^{-4} $\mu m^2/s$ to 10^{-2} $\mu m^2/s$, and the particles are reported to exhibit either subdiffusive or normal diffusion (7, 97, 113, 181). As shown in Figure 2.6C, the standard deviation for each measurement is very high, which is consistent with the literature for large particles exhibiting non-homogeneous diffusive motions inside the cell and dynamic heterogeneity within the cytoplasm of individual cells (7).

Phage DNA shows different patterns of motions during the late stage of phage infection in lytic and lysogenic cells

To examine whether phage DNA movements are correlated with cell fates, we have performed hours-long time-lapse movies (typically 4 hours at a time interval of 5 min) with the optimized microscope parameters for cell growth. We observed that initial fluorescent spots appear near the phage infection site, which is presumably the site at which the phage DNA is ejected into the cytoplasm. As shown in Figure 2.5A, the intensities of the fluorescent spots are relatively uniform, indicating a stable binding of SeqA-ECFP proteins to phage DNA. Most phages (~95±5%) eject their DNA within 5 minutes after we started the time-lapse movies (Figure 2.5B). However, ~5% of the phage particles eject the DNA after prolonged adsorption. One explanation might be cell-cell variability on phage DNA ejection *in vivo*, in which DNA ejection could finish in single step or have paused events (157), which might be a result of the absence of the side tail fibers in the laboratory lambda or λpapa (158).

From the time-lapse movies, we observed that fluorescent particles exhibit both localized motion and motion spanning the whole cell. One typical cell is shown in Figure 2.7. The initial ejected phage DNA is located around the cell polar position, and moves locally for ~ 25 min. This fluorescent focus then splits into two foci, corresponding to the two copies of replicated phage DNA particles. One of the particles remains to move locally, while the other one traverses the entire cell within 20 minutes. Subsequently, two foci move locally. This non-homogeneous motion is also observed in the studies of RNA-protein complex and large GFP-μNs particles in *E. coli (7, 97, 113)*. Therefore, one possibility of the non-homogeneous motion is due to the large particle size. Another possibility is that the motion is associated with the phage DNAs being at different stages of the infection cycle. After ejecting its DNA inside the host cell, phage DNA undergoes replications switching from θ mode to σ mode, packages into phage head for the lytic cycle or integrates into the host genome and replicates along with the host for the lysogenic cycle. We will extend the discussion in the next section and Discussion section.

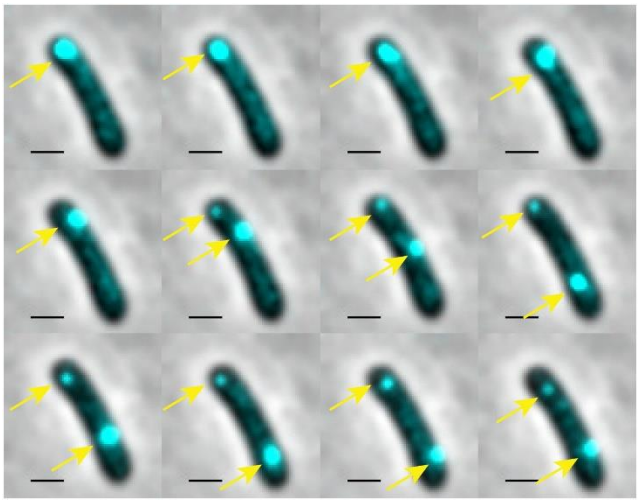

Figure 2.7 Phage DNA particles exhibit both localized motion and motion spanning the whole cell.
Images are 5 minutes apart. During the 1st 5 frames, 1 fluorescent focus representing the initial ejected DNA particle moves locally. At frame 6, 1 fluorescent focus splits into two foci representing two phage DNA particles. During frames 6-9, the top phage DNA particle moves locally, and the bottom one travels the whole cell. During frames 10-12, both phage DNA particles move locally. Scale bar = 1 μm.

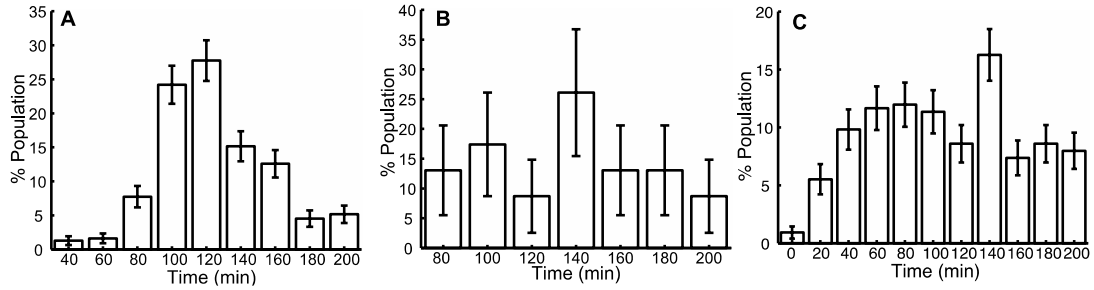

Figure 2.8 Cell division time.
(A) Histogram of the lysis time of a mean of 125 minutes (N=303 lytic cells). (B) Histogram of the lysogen division time with a mean of 140 minutes (N=35 lysogenic cells). (C) Histogram of the normal (uninfected) cells division time of 110 minutes (N=326 uninfected cells). Error bar is the counting error.

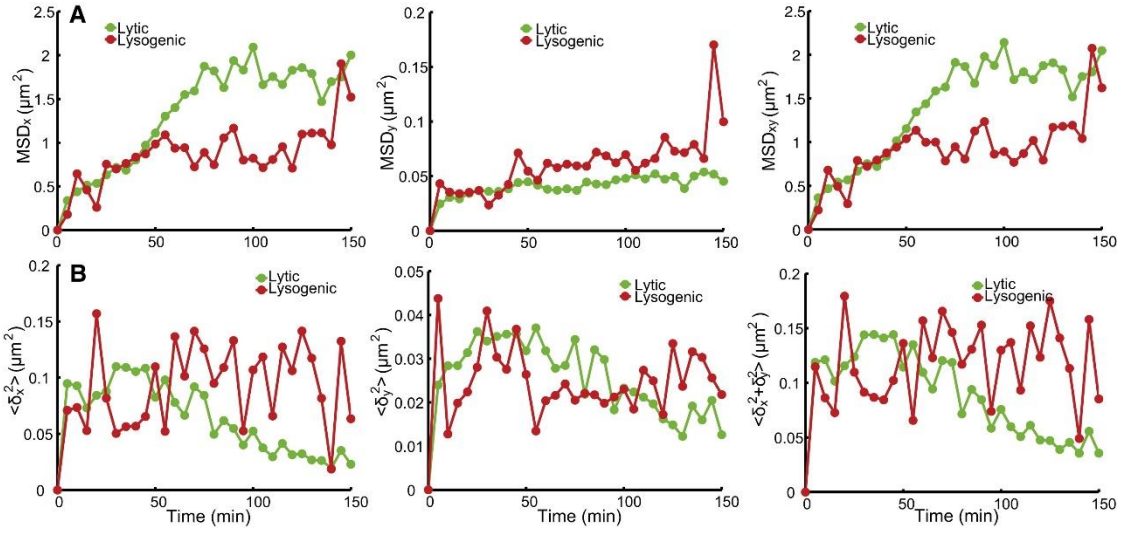

Figure 2.9 Motion of phage particles in lytic and lysogenic cells.
(A) Mean squared displacements (MSD) of phage particles in lytic and lysogenic cells as a function of time. Left, middle and right panels show the MSD in x, y and combined xy directions respectively. Within the first 50 minutes after infection, MSD_x in lytic and lysogenic cells follow a similar trend. MSD_x in lytic cells reaches a higher plateau than that in lysogenic cells after 50 minutes of infection. MSD_y in lysogenic cells reaches a slightly higher plateau except one outlier data point at 145 minutes than that in lytic cells. (B) $\langle \delta^2 \rangle$, MSD of phage particles between two adjacent time points. The movement of phage particles in lysogenic cells does not seem to change over time; while that in lytic cells slows down over time. Overall, the movement in x direction dominates, and that in y direction is limited, which might be just due to the confined space in y.

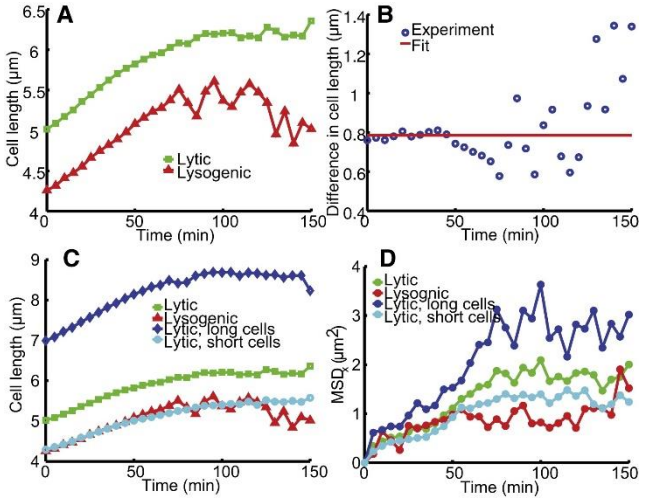

Figure 2.10 Cell size partially accounts for the MSD plateau.
(A) Cell size as a function of time. Lytic cells (green, N=303) are longer than lysogenic cells (red, N=35) throughout the entire infection cycle. (B) The cell size difference as a function of time. At the first 50 minutes, the cell size difference between lytic and lysogenic cells is almost a constant (red line). (C) Cell size as a function of time including lytic long cells (blue, N=86) and lytic short cells (cyan, N=217). Here the average cell length of lytic short cells is similar to that of lysogenic cells (red). (D) MSD in x direction as a function of time. MSD of particles in longer cells reaches a higher plateau than short cells. However, the plateau of lytic short cells (cyan) is higher than that of lysogenic cells (red with the same cell size) indicating cell size only partially accounts for the difference in MSD plateau.

Under our experimental conditions, lytic cells take about 125 minutes to lyse and lysogenic cells take about 140 minutes to divide as opposed to 110 minutes for uninfected cells (shown in Figure 2.8A, B and C, respectively). The delayed division for lysogen might be a result of Kil protein expressed in infected cells (8) . Kil is known to inhibit the expression of *ftsZ*, the key gene for cell division (182). We then track the phage DNA movement for 150 minutes to capture the entire infection cycle. In order to characterize the phage DNA motion, we plotted the mean squared displacement (MSD) as well as mean squared displacement between two time points $\langle \delta^2 \rangle$ as a function of time over the entire infection cycle. MSD is defined as $MSD(t) = \frac{1}{n}\sum_{i=1}^{n}[\vec{r_i}(t) - \vec{r_i}(0)]^2$, where $\vec{r_i}(t)$ is the coordinate of a given particle at moment t, $\vec{r_i}(0)$is the coordinate of this particle at the beginning of the trajectory, and n is a number of total trajectories. $\langle \delta^2 \rangle$ is defined as $\langle \delta^2 \rangle(t) = \frac{1}{n}\sum_{i=1}^{n}[\vec{r_i}(t+\tau) - \vec{r_i}(t)]^2$. From Figure 2.9A, during the first 50 minutes after infection, The MSDs of the labeled lambda DNA in lytic and lysogenic cells follow a similar trend along cell major axis (x direction), but ultimately reach a much higher plateau in lytic cells (1.78 μm^2 for lytic cells versus 0.92 μm^2 for lysogenic cells with a difference of 0.86 μm^2). One may ask whether the cell size contributes to the MSD difference since phage DNA particles may have more room to move in larger cells. Indeed, the average lytic cell is longer than lysogenic cells for a mean of 0.8 μm (shown in Figure 2.10A and B). To further explore this effect, we group the lytic cells into short (N=217 cells) and long (N=86 cells) cell subgroups, and make the average size of the short cells similar to that of the lysogenic cells (Figure 2.10C).

We found the plateau of MSD in x is higher for longer cells (Figure 2.10D). We also noticed that the plateau of lytic short cells (1.29 μm^2) is higher than that of lysogenic cells with the same average cell size. Therefore, the cell size only partially accounts for the plateau difference in lytic versus lysogenic cells. The other possibility of the lower plateau in lysogenic cells might be a result of confined movement of the host genome as phage DNA might have already integrated its DNA into the host and then moves along with the host *attB* locus which may only "jiggle" around (165).

Surprisingly, for lytic cells as shown in Figure 2.9B, after 50 minutes of infection, the MSD between two time points gradually decreases, suggesting that phage DNA slows down its movement. This slowed-down motion is possibly a result of a longer concatemeric λ DNA since at the later stage of phage infection cycle phage DNA replication switches from Θ-mode to σ-mode, producing concatemeric λ DNA about 2-8 times a λ monomer in length (160). It was suggested that increasing particle size leads to increasing spatial confinement in *E. coli* (7). In contrast, phage DNA in the lysogenic cells maintains a consistent rate of movement throughout the entire infection cycle. Also plotted in Figure 2.9 are the MSD along the cell minor axis (y direction), and combined x and y directions. The movement in the y direction is at least 1 order of magnitude lower, which is presumably due to the limited space available along the y axis.

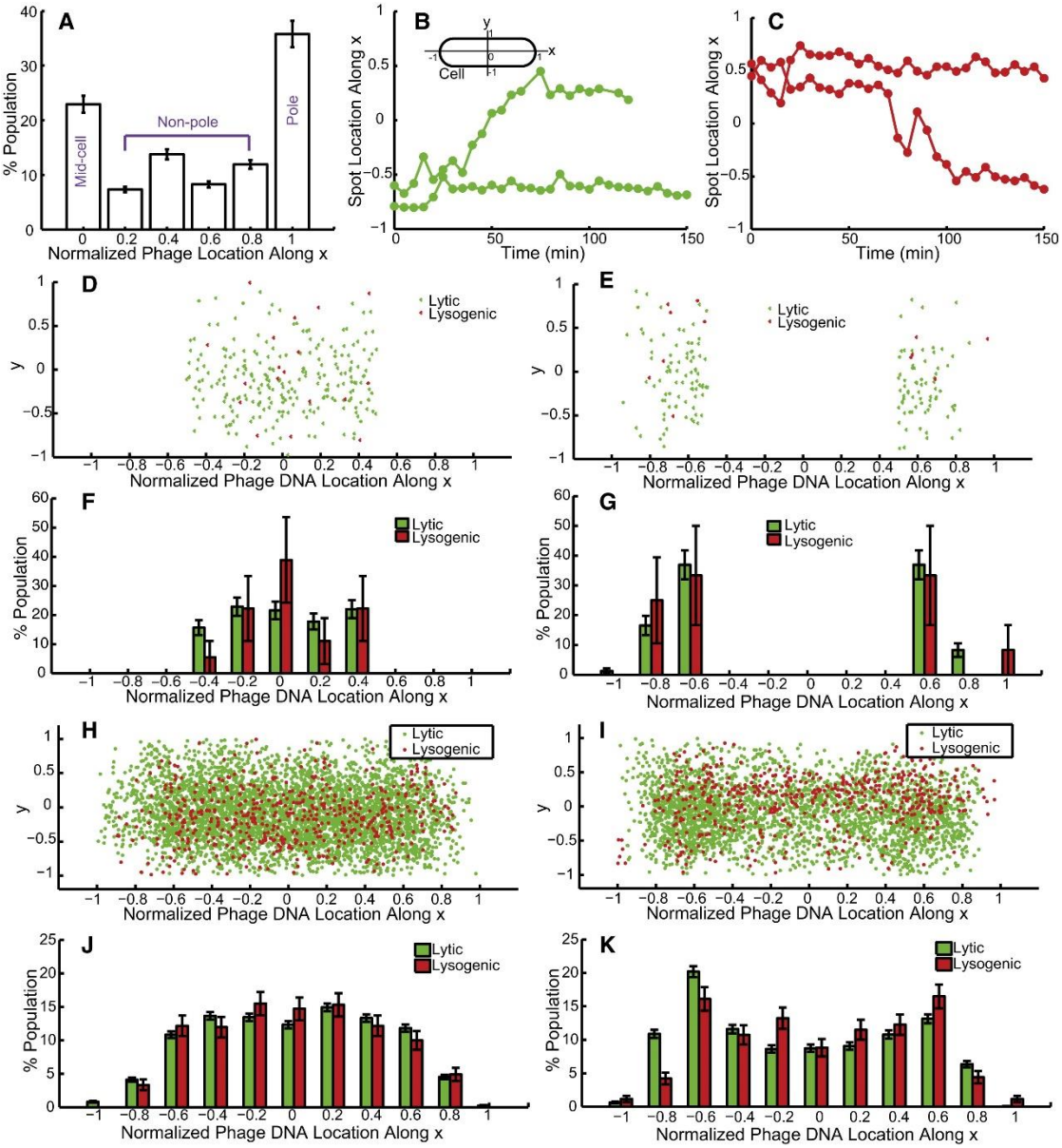

Figure 2.11 Phage and phage DNA locations.
(A) The infecting phages preferentially attach to cell poles or mid-cell for DNA ejection in agreement with previous findings. (B) and (C) Localized motion and motion spanning over the cell (localized motion + vigorously active motion + localized motion in time) are shown in lytic and lysogenic cells respectively. The definition of the cell coordinates is also shown. (D) to (G) are statistics (scatter plot and histogram) for phage DNA entry point. (H) to (K) are for all phage DNA locations over time. (D) and (F) show phage locations for cells with the phage entry point within the quarter – mid-cell region (abs(x) < 0.5). The entry point is uniformly distributed for lytic cells. However, it appears a peak at the mid-cell which might be due to low sample size.

Figure 2.11 continued.
(H) and (G) show fairly uniform distribution within the cell suggesting there are more motions spanning over the cell irrespective of lytic or lysogenic cells. Notice that the statistics at close to polar regions (-0.8, -1, 0.8 and 1) are very low which we think is a result of confined region at polar positions. (E), (G), (I) and (K) are for cell with the phage DNA entry point within the polar – quarter region (abs(x) ≥ 0.5). Phage DNAs show higher occupancies around the quarter region (-0.6 and 0.6) at the entry point (E and G), and also over time (I and K) suggesting there are more localized motions irrespective of lytic or lysogenic cells. Data are shown as mean ± SEM (based on counting error).

Phage DNA locates at similar positions for both lytic and lysogenic cells

We then set out to examine whether phage DNA has a preferred location inside the cell and whether there is any correlation among phage infection site, phage DNA location and cell fate. Under our experimental conditions, phage particles prefer to attach to mid-cell or polar positions of the cell for infection (shown in Figure 2.11A), consistent with other reports (4, 78, 81). Regarding the time-lapse movies at the single-cell/single-phage level under the fluorescence microscope, similar to what we reported in (4), there are 1) "dark" infections, where cells don't have any visible fluorescent phages attached, but cells lyse or lysogenize. Here for *dam*$^-$ cells under our experimental conditions, the "dark" infection is 32±15%, where there are 129 cells with MOI = 0 leading to lytic or lysogenic fate and 276 cells with MOI = 1, and the standard deviation is calculated from different experiments. This rate is higher than that of the wild type condition (~5%) reported in (4), which may indicate attached phages are more prone to be sheared off from the cell surface under the current condition. 2) "Failed" infections,

where cells do not undergo a lytic or lysogenic response even with adsorbed phages (4). The current condition gives 24±10% per phage, where there are 67 cells with MOI = 1 and no lytic/lysogenic fate out of 276 total cells with MOI = 1. This rate is comparable to the 23% of the wild type condition reported in (4). From our current reporter system, we observed that there is another population (2±3%, 5 out of 276 cells with MOI = 1), where there are SeqA-ECFP foci inside the cell but no detected cell lysis or lysogeny (increased mCherry expression followed by cell division), which was grouped as "failed" infections previously. This may indicate a successful phage DNA ejection that led to a dead-end developmental pathway, with neither the lytic or lysogenic pathways established. Nevertheless, to simplify our particle tracking algorithm and data analysis, we only analyze those cells with MOI = 1 (1 infecting phage per cell resulting in 1 SeqA-ECFP fluorescent focus upon phage DNA ejection) and detectable lysis/lysogeny fates, and track their phage DNA movements during the entire infection cycle.

As described in the previous section, phage DNA particles exhibit both localized motion and motion spanning the entire cell. These two distinct motions could be observed for 1 phage DNA particle at different times or different phage particles within one cell for both lytic and lysogenic cells. As shown in Figure 2.11B, the localized motion was observed for the bottom trajectory. While for the top trajectory, the phage DNA first exhibits localized motion, then moves from its polar position to mid-cell position, and finally settles down at a mid-cell position until the cell lyses. Similarly in a lysogenic cell shown in Figure 2.11C, the top trajectory exhibits the localized motion during the entire time, and the bottom one shows more "active" motion during some

period of time. It appears that these two distinct motions are not cell fate specific, rather purely due to the large phage DNA-protein complex resulting in non-homogenous motion. These distinct motions were also observed for RNA-protein complexes in *E. coli* (97).

As phage prefers polar positions for infection (Figure 2.11A), one may ask whether the non-homogenous motions are associated with the DNA ejection sites. To address this question, we grouped the phage DNA locations by the initial appearance of SeqA-ECFP foci representing the phage DNA entry point. When the entry point is within the quarter – mid-cell region (a total of 177 lytic and 20 lysogenic cells), shown in Figure 2.11D and F, phage DNA entry point is uniformly distributed in this region. When we quantify phage DNA locations over time, we found that phage DNA tends to locate uniformly inside the cell suggesting phage DNA exhibits more motions spanning the whole cell (Figure 2.11H and J). Notice that statistics at close to polar regions (-0.8, -1, 0.8 and 1) are very low which we think is a result of confined region at polar positions. Whereas when the entry point is within the quarter – polar region (a total of 126 lytic and 15 lysogenic cells), phage DNA enters around the quarter regions (Figure 2.11E and G) and clusters around the quarter regions over time (Figure 2.11J and K). This indicates that those phage DNAs may exhibit more localized motions in those areas or phage DNA tends to stay there.

In addition, as there are mixtures of phage DNA motions and different roles for phage DNAs in lytic or lysogenic cells over time, we ask whether there is any difference in the preferred position for the whole population and whether the phage DNA location

affects the cellular decision between lysis or lysogeny. In the lytic cycle, phage DNA replicates to more than 100 copies and is packaged into phage heads. In the lysogenic cycle, phage DNA is integrated into the host genome, although it is unknown that how many rounds of phage DNA replication occur before the DNA integration. Interestingly, the averaged phage DNA location over time and a histogram of phage DNA positions, shown in Figure 2.12A and B, reveal that phage DNAs, or to be more exact, the first two parental phage DNAs, spend more time around the quarter positions of the cell for both lytic (on average of 0.423 ± 0.002 (standard error), the mean is shown as a green line) and lysogenic (0.393 ± 0.007 (standard error), red line) cells, unlike the behavior of protein aggregates accumulating at polar positions (181). In the lytic cells, phage DNA presumably needs room to replicate its DNA and package into its phage head; therefore it might tend to localize at the less crowded nucleoid-free region to complete this process. In the lysogenic cells, phage DNA might replicate itself for a few rounds at the beginning of the infection cycle with the same reasoning as the lytic cells. In fact, if we examine the location over the 1st 50 minutes for lysogenic cells, the average location is 0.424 ± 0.011 (standard error) (magenta line, overlapped with the green line), the same as that of the lytic cells. At the later stage, phage DNA is integrated into the host genome at *attB* site, which is at 17 minutes on the *E. coli*, and moves along with the host genome. This may indicate *E. coli attB* site prefers the quarter positions of the cell. The mean location for 50 minutes to 150 minutes is 0.377 ± 0.008 (standard error) (magenta line). This is indeed consistent with the mean location of *E. coli attB* site for the infected cells (0.376 ± 0.020 (standard error)) by Tal and coworkers (122). As a reference, Figure

2.12C shows the histogram of phage DNA positions over the entire infection cycle along the cell minor axis, showing that phage DNA prefers the mid-cell positions, which may be due to the limited region along the minor axis.

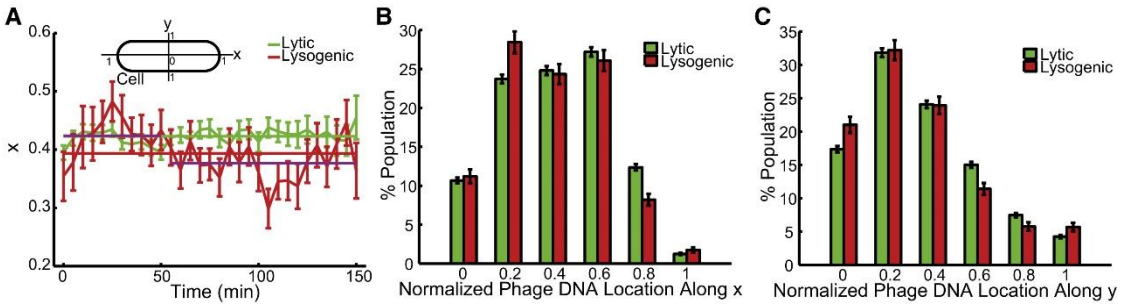

Figure 2.12 Phage DNA locations for the whole population.
(A) Time trace for average phage DNA locations along cell major axis (x) during the entire infection cycle. The solid lines show the mean location over time. Phage DNAs is preferentially located around the quarter positions of the cell for both lytic (0.42 along x axis) and lysogenic (0.39 along x axis) cells. The average values for lysogenic cells at earlier (0.42) and later stages (0.37) are shown as magenta lines. The definition of the cell coordinates is also shown. (B) and (C) Histograms of phage DNA locations over the entire infection cycle in x and y respectively. Phage DNA prefers the region around the quarter positions of the cell along the cell major axis (x) and the mid-cell positions along the cell minor axis (y) for both lytic and lysogenic cells.

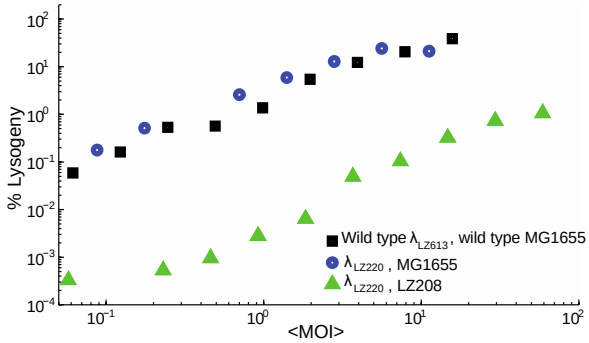

Figure 2.13 Effect of *dam*⁻ mutation and phage labeling on the lysogenization frequency.
Lysogenization frequency of fully methylated fluorescent phage λ_{LZ220} in *dam*⁻ LZ208 (green triangle) is almost 2 orders of magnitude lower than that in the normal *dam*⁺ strain, MG1655 (blue circle) which is similar to the wild type phage λ_{LZ613} in MG1655 (black square).

Discussion

In this work, we aimed at characterizing phage DNA dynamics inside the cell and correlating phage DNA movements with cell fates. We first presented a plasmid-based approach for the construction of stable, well-behaved and fluorescent phage lambda. This method allows us to label infecting phages conveniently without manipulating the phage genome to avoid any perturbation of phage behaviors. Under our experimental conditions, we showed the fluorescent phage made by gpD-EYFP plasmid pACYC177-PLate**D-eyfp* is structurally stable and bright enough to be detected under the microscope. It is worth noting that different bacterial growth rates due to different growth conditions, e.g. different growth media or temperatures, may result in different numbers of plasmids per cell (183). If one uses a different growth condition from ours to create phage stock, the ratio of gpD-EYFP protein level to wild type gpD would be

different owing to a different plasmid copy number. In order to fine-tune this ratio to a reasonable value, one may need a gpD-EYFP plasmid with a different expression level. We also created a few other gpD-EYFP plasmids with different expression levels.

We developed a new technique to label phage DNA in living *E. coli* cells. This allows us to follow phage DNA dynamics and characterize its motion through high-resolution fluorescence microscopy. Furthermore, we examined the correlation between the locations of phage DNA and the resulting cell fate. The detection of phage DNA in living *E. coli* cells takes advantage of SeqA protein binding to fully methylated or hemimethylated DNA, but not unmethylated DNA (167, 175, 176). The infecting phage is prepared to contain fully methylated phage DNA in its head. The host *E. coli* is *dam*$^-$, resulting in no methylation of *E. coli* DNA and the first two copies of replicated phage DNAs being hemimethylated upon infection by a fully methylated phage. Through the bulk assay, fully methylated fluorescent phages can still exhibit appropriate lysogenic response in *dam*$^-$ cells like wild type phage in wild type cells when the lysogenization frequency is normalized to its maximum. The normalization is a standard way to find out the characteristic feature of the system's lysogenic response (53). Note that here the absolute lysogenization frequency is about 2 orders of magnitude lower in *dam*$^-$ environment than that in wild type cells through bulk assay (shown in Figure 2.13). This drop in lysogenization frequency is probably related to the function of SeqA, which may result in a difficulty in establishing lysogens for the normal growth (i.e. normal cell division to form colonies on the plates). In a wild type *E. coli* cell, SeqA acts as a regulator for the initiation of *E. coli* replication through the binding to methylated *E. coli*

DNA (178, 184, 185). Note that as described in the Results, under the microscope, the lysogenization frequency detected by our single-cell assay is about 10% (35 lysogenic cells versus 303 lytic cells), which allowed us to perform our analysis with reasonable effort.

Lambda DNA plays different roles over time depending on the lytic or lysogenic cycle (160). Due to the cell-cell variability entering the different pathways, here we only characterized the diffusive motion by frequent imaging at the immediately early stage of phage infection cycle before the cell/phage commits to either pathway. The phage DNA could be very compact inside the cell due to the phage DNA circularization and supercoiling. We estimate the phage DNA-SeqA-ECFP protein complex to be of the order of 100 nm. In the literature, the diffusion coefficient of particles with that size ranges widely from 10^{-4} to 10^{-2} $\mu m^2/s$, and particles are reported to exhibit subdiffusive or normal diffusive motions (7, 113, 181). We found that our phage DNA-protein complex exhibits subdiffusive motion with the subdiffusion scaling exponent $\alpha = 0.47 \pm 0.03$ which is similar with those of different *E. coli* chromosome loci and RK2 plasmid (165, 177). In addition, the apparent diffusion coefficient $D_{app} = (2.5 \pm 0.9) \times 10^{-3} \mu m^2/s^{0.47}$ is also at the same order of magnitude of that of *E. coli* chromosome 84 min locus reported in (177). It is then not a surprise that $\langle \delta^2 \rangle$ is almost constant for lysogenic cells throughout the whole cycle, before and after the phage DNA is integrated into *E. coli* genome.

To address whether the location of phage DNA correlates with cell fates, we followed phage DNA during the entire infection cycle. A recent study with phage DNA

labeled by parS/ParB system revealed that phage DNA only shows confined local motion at the site of phage entry and does not carry out active search (122). The authors suggested that this confined motion was most likely because λ DNA becomes anchored to a site on the cellular membrane through which the λ DNA entered the cell. However, we observed both localized motion and "active" motion spanning the whole cell in both lytic and lysogenic cells. One may ask whether the localized motion corresponds to the ejected DNA and the "active" motion corresponds to the replicated DNAs. We observed that the "active" motion can happen right after the DNA ejection corresponding to the initial ejected DNA, which suggests λ DNA may not always attach to cell membrane. To see if different initial λ DNA location correlates with different motions, we group the cell by the λ DNA entry point. When the entry point is within the quarter – polar region, phage DNA prefers to stay around the site exhibiting localized motion, which may be attributed to the nucleoid-free feature/characteristics of those areas. At the early stage of the infection cycle, phage DNA may prefer those areas to replicate its DNA for both lytic and lysogenic cells. Later on, in lytic cells, phage DNA may prefer those areas to package into phage heads. While in lysogenic cells, phage DNA moves along with the integrated bacterial attB site located at 17 minute on the *E. coli* genome and may be located at those areas. However, when the entry point is within the mid-cell – quarter region, phage DNAs is uniformly distributed over the cell averaged over time, displaying more motions spanning the cell. It is possible that phage DNA needs to travel to areas other than entry region such as quarter position to replicate its DNA, package or integrate into the host genome etc. When we look at the whole population of phage DNA

locations, phage DNA shows a preferred location around the quarter position of the cell irrespective of lytic or lysogenic cells.

As described in this paper, our new technique allows us to track the initial copy of the ejected phage DNA and its first replicated copy, which permits us to study phage DNA dynamics. However, this technique constrains us from accessing other phage DNA copies except the first two. Therefore, complementary to our study, it would be very interesting to use other labeling schemes such as Fluorescent Repressor Operator Systems (FROS) to label all phage DNA in order to gain a full picture of the spatiotemporal dynamics of phage DNA during the entire infection cycle (186). Interestingly, we also observed some rare cases in which the number of SeqA-ECFP foci changes from 1 to 2, and then surprisingly 2 to 3 for singly infected cells. The unexpected 3 foci might indicate that the phage DNA undergoes recombination process during the infection cycle, and this is under our current exploration.

CHAPTER III

LYSIS-LYSOGENY COEXISTENCE: PROPHAGE INTEGRATION DURING LYTIC DEVELOPMENT*

Introduction

Cellular decision-making is a ubiquitous process among all organisms, from the most complicated metazoans to the simplest biological systems such as viruses, with bacteriophage lambda being one of best-studied model systems. Upon infection by bacteriophage lambda, *E. coli* cells can enter one of two distinct pathways, lysis or lysogeny; this decision-making process，celebrated as the "genetic switch" (13), has been extensively studied at the population level (10, 14, 15, 36). The lytic pathway leads to immediate and rapid phage propagation with cell death and release of hundreds of progeny, while the lysogenic pathway features continued cell growth and passive replication of phage DNA after the integration of phage DNA into the host chromosome. Historically, this "lysis versus lysogeny" decision has been considered as mutually exclusive, where lysogeny is favored in nutrient-poor environments, as low quantity and quality of host cells results in suboptimal phage propagation (53). Therefore, the lysogenic pathway provides an alternative mechanism for the virus to store its DNA until favorable environments for propagation arise in the future. The lysis-lysogenic decision-

---

* Reprinted from "Lysis-lysogeny Coexistence: Prophage Integration during Lytic Development" by Qiuyan Shao, Jimmy T. Trinh, Colby S. McIntosh, Brita Christenson, Gabor Balazsi, and Lanying Zeng, *MicrobiologyOpen* **2016** doi: 10.1002/mbo3.395, Copyright 2016 by The Authors.

making represents a diversification of evolutionary strategy for the virus, allowing it to react to and thrive in variable conditions, to maximize its own fitness.

The protein players involved in this cellular decision-making process have been well-characterized over decades (10, 14, 15), and CII, Cro and and Q are among the key proteins that determine the infection outcome, mediating either the lysogenic or lytic pathways (10). Cro facilitates the lytic pathway by being a weak repressor for phage gene expression from both pL and pR promoters (17, 20, 187, 188), while Q activates the lytic pathway after reaching a threshold, allowing for the expression of a single transcript carrying the lysis and morphogenesis genes (17, 189). Conversely, CII activation will inhibit the lytic pathway and establish the lysogenic pathway by activating transcription from three specific promoters (10, 17). Among them, the pI promoter allows the expression of the lambda integrase, Int, which catalyzes the crucial process of integrating phage DNA into the host chromosome (190, 191).

New details have emerged from higher-resolution studies of this well-established system (3, 157). Our recent study performed at the single-cell level proposed that individual phages infecting the same cell are able to "vote" for the cell's fate independently (4), which raised the possibilities that lytic and lysogenic pathways can happen simultaneously within the same cell, resulting from the different votes by multiple infecting phages. This co-existing lytic-lysogenic development may be naturally beneficial, serving as an intermediate state allowing for a faster and more sensitive commitment to lysis-lysogeny in a changing environment. Exploring this

phenomenon requires a higher resolution of study and can yield insights into the biological process of decision-making and its evolutionary strategy.

In this study, we developed an improved reporter system at the single-DNA level to allow the visualization of phage DNA integration, in addition to the progress of the lytic and lysogenic pathways. By tracking phage and host DNA movements after infection in real-time using fluorescence microscopy, and quantitatively analyzing single-molecule trajectories, we revealed new biological phenomena and further explored the possible mechanism of cellular decision-making.

Materials and Methods

Bacterial strains

Bacterial strain LZ722 was constructed by inserting a DNA array containing ~200 *tetO* repeats into strain LZ220 (123) at ~1500 bp upstream of *attB* site using lambda red recombination (171). Plasmid pFtsKi-*tetR-mCherry,* which contains the *tetR-mCherry* under the constitutive promoter FtsKi was transformed into LZ722, resulting in LZ731. For all real-time microscopy experiments, LZ731 is used as the host, while for bulk assays (lysogenization, PCR and qPCR), *E. coli* strain MG1655 is used. Unless otherwise specified, phage titration assays for determining the phage concentration was done with *E. coli* strain LE392.

Plasmid construction

To construct the plasmid pLZ729: pFtsKi-*tetR-mCherry,* plasmid pWX510 (192) was digested with HindIII and BamHI restriction enzymes to obtain sequences for *tetR-mCherry*, which was then inserted into pBR322. DNA sequences for FtsKi was PCR

amplified from pWX6 (193) using primers QS 15 and QS16 and inserted into the above plasmid between EcoRI and HindIII recognition sites, resulting in EcoRI-FtsKi-HindIII-*tetR-mCherry*-BamHI in the pBR322 backbone. When this plasmid was transformed into LZ722, the background signal (mCherry) was found to be too high, therefore we switched to another vector, pACYC177, which has a lower copy number. The piece FtsKi-HindIII-*tetR-mCherry* was PCR amplified using primers QS17 and QS18 and inserted into pACYC177 between SmaI and NheI, resulting pLZ729. The plasmid pZA32-*dam* carries the *dam* gene in between AvrII and KpnI in the pZA32 backbone, where the *dam* gene was amplified with primers QS19 and QS20 using template plasmid pGG503 (166). When phages were produced from dam^+ host cells containing this plasmid, pZA32-*dam*, the phage DNA was confirmed to be fully methylated (Figure 3.1D).

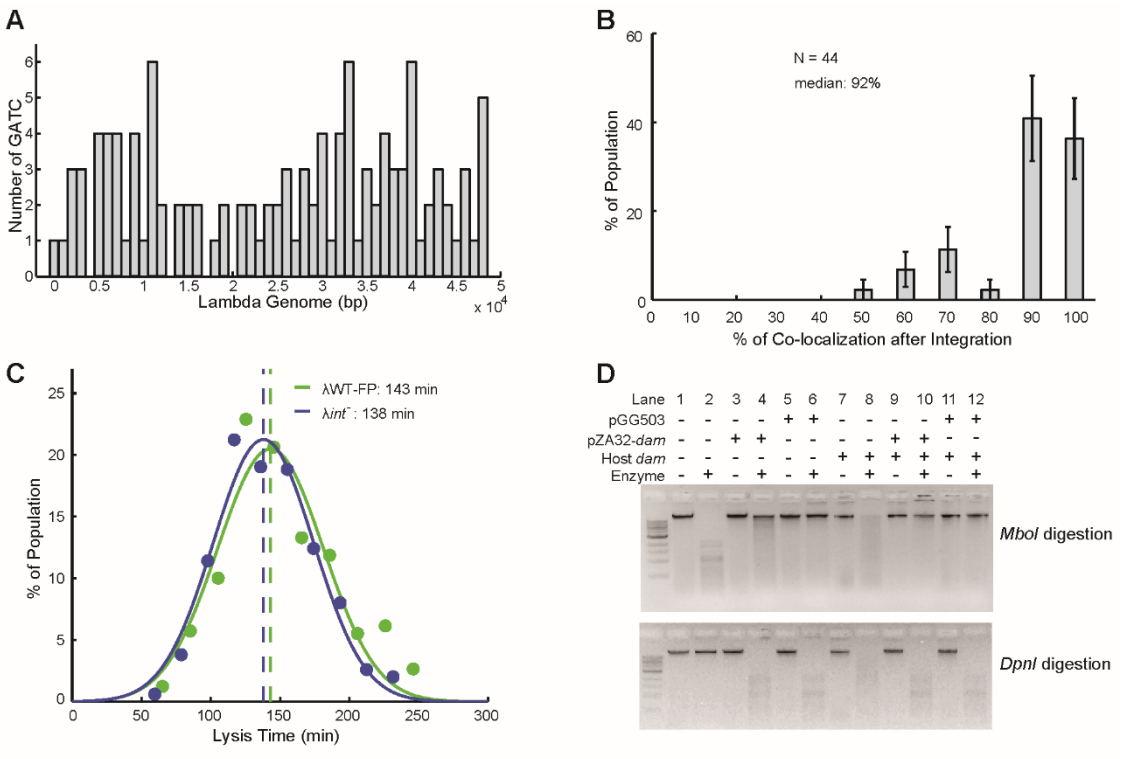

Figure 3.1 The validation of the reporter system.
(A) The distribution of SeqA binding sites on bacteriophage lambda genome. Each bar represents the number of GATC of every 1000 bp along the lambda genome. The GATC sites are fairly evenly distributed across the genome. (B) The distribution of lysogenic cells with different fraction of time of 'co-localization' within 0.5 μm after integration. The percentage of time for a cell having Dis(λ-*attB*) < 0.5 μm (indicating co-localization by our standard) after integration is calculated and the percentage distribution for all lysogenic cells (N = 44) is shown. The distribution shows that the majority of the cells have at least 90% of the time showing co-localization, i.e., Dis(λ-*attB*) < 0.5 μm after integration, indicating that the criterion for co-localization is reasonable. A low fraction of cells show lower frequency of having Dis(λ-*attB*) < 0.5 μm, which could be due to multiple integration of lambda DNA or the lost tracking of target lambda DNA/*attB* that move out of focal plane. Error bars represent ± SEM. (C) The lysis time of λWT-FP and λ*int*⁻ is similar to each other. λWT-FP: green circle, λ*int*⁻: blue circle, Gaussian fit for λWT-FP (green line) and λ*int*⁻ (blue line). The dashed vertical lines mark the center of the Gaussian fit. λWT-FP and λ*int*⁻ show a similar lysis time.

Figure 3.1 continued.
(D) Fully methylation of lambda DNA by pZA32-*dam* in *dam*$^+$ host. Genomic DNA of λWT is extracted after induction from the host as indicated (*dam*$^+$ or *dam*$^-$) with or without the corresponding plasmid, pZA32-*dam* or pGG503 as a positive control. Samples in the upper lane are digested with *MboI*, an enzyme specific for unmethylated DNA while the lower lane with *DpnI*, which digests methylated DNA. Without digestion, the lambda DNA runs as a clear band on the top of the gel (lane 1, 3, 5, 7, 9, 11), and *MboI* can fully digest the unmethylated DNA produced from *dam*$^-$ host, resulting in smears while *DpnI* can not (lane 2). When phages are induced from the *dam*$^+$ host, the lambda DNA is partially methylated, indicated by the incomplete digestion by *MboI* (lane 8). As a positive control, when the plasmid pGG503 was provided to *dam*$^+$ and/or *dam*$^-$ host, the lambda DNA is fully methylated and cannot be digested by *MboI* (lane 6, 12). With pZA32-*dam*, some of the lambda DNAs produced from the *dam*$^-$ host are still unmethylated, indicated by the noticeable smear from the top band (lane 4), however all lambda DNA obtained from the *dam*$^+$ host are fully methylated (lane 10). The results indicate that pZA32-*dam* plasmid provides enough Dam methylase in the *dam*$^+$ host background to produce fully methylated lambda DNA.

Phage strains

The phage λ *D-mTurquoise2 cI*$_{857}$ *bor::Kan*^{R} was obtained through recombination by infecting λ *Dam cI*$_{857}$ *bor::Kan*^{R} on the permissive strain LE392 bearing plasmids pBR322-*D-mTurquoise2-E*. The recombinant (λ *D-mTurquoise2 cI*$_{857}$ *bor::Kan*^{R}) was selected based on its ability to titer on non-permissive strain MG1655 and fluoresce under a fluorescence dissecting microscope. For easier selecting and counting of lysogens for λ*int*$^-$ in the lysogenization assays, λ*int*$^-$*-Kan* was constructed following the protocol as described in (123) to replace the non-essential *bor* gene region of λ*int*$^-$ with a *Kan*^{R} cassette.

Phage lysate preparation

Fully methylated mosaic phage λWT-FP was obtained by inducing a lysogen with temperature-sensitive prophage (λ *D-mTurquoise2 cI*$_{857}$ *bor::Kan*^{R}) and two plasmids, plasmid pPLate-*D* to provide wild type phage decorative capsid protein gpD (4) and plasmid pZA32-*dam* which over produces Dam methylase after 1 mM IPTG induction. Fully methylated phages λWT, λ*int*$^{-}$, λ*cII*$_{68}$ and λ*cII*$_{stable}$ were obtained by infecting host cell LE392 carrying plasmid pZA32-*dam* with the corresponding phages at 42 ^{o}C. This is important if the phage lysate will be used for quantifying the lyso-lysis using qPCR. We found that the phage lysate obtained through prophage induction contains non-negligible amount of integrated phage DNA, possibly due to insufficient induction, while the phage lysate obtained through infecting the host cells contains no integrated DNA. All phage lysates used were also purified following the protocols described in (75).

Bulk lysogenization assay

To measure the lysogenization frequency of the various phages, we followed the protocol as described in (4). For easier selection and counting of lysogens, the phage λ*int*$^{-}$*-Kan* was used instead of λ*int*$^{-}$ since *bor* gene was reported to be non-essential and would not affect the lysogenization frequency (169). All the other phages used also carried antibiotic marker by replacing the λ *bor* region. Briefly, 2 ml of the host cell MG1655 was grown in LBMM for overnight and subsequently diluted 1:1000 into 12 ml of LBMM and grown to OD_{600} ~0.4 at 37 ^{o}C, centrifuged (2000×*g* for 10 min at 4 ^{o}C) and resuspended to be ~1.5×10^{9} cells ml^{-1} in pre-chilled LBMM (LB +0.2%

maltose+10 mM $MgSO_4$). 20 μl of the resuspended cells were then infected with 20 μl of phages at different concentrations by incubation for 30 min on ice. The samples were then transferred to 35 ^oC water bath for 5 min to allow for phage DNA ejection, followed by 10 fold dilution into pre-warmed LBGM (LB+ 0.2% glucose +10 mM $MgSO_4$) and incubation with shaking at 265 rpm at 30 ^oC for 45 min. The samples were then properly diluted and plated on LB plates containing appropriate antibiotics to allow ~100 colonies on each plate.

PCR and qPCR

2 ml of host cell MG1655 was grown in LBMM overnight and was subsequently diluted 1:1000 into 100 ml of LBMM and grown to OD_{600} ~0.4 at 37 ^oC. Cells were then spun down at 2000×*g* for 10 minutes at 4 ^oC and resuspended to be ~1.5×10^9 cells ml^{-1} in pre-chilled LBMM. Infection was set up following the same protocol described in *Bulk Lysogenization Assay*, with corresponding phages at different concentrations for infections of different APIs, but with larger volumes depending on the number of samples to be taken later (100 μl of reaction per sample). For each time point, 100 μl of the reaction was added to 0.9 ml pre-warmed LBGM shaking at 265 rpm in 30^oC shaker for various times up to 120 minutes. For confirming and quantifying lyso-lysis, samples were taken at each time point and immediately filtered using 0.2 μm membrane to obtain cell-free samples. For the infection with different APIs, the samples taken at 90 min were used, and samples were diluted 10 fold into dH_2O to minimize possible PCR inhibitor effects. PCR or qPCR was performed immediately after the last sample was taken. PCR was done using primers in (194), while qPCR was done using primers QS1

and QS2 for detecting *E. coli* DNA, and primers QS3 and QS4 for detecting integration (Table 3.1). Amplification was done using SYBR Green PCR master mix (Applied Biosystems, 4309155) with 250 nM of each primer. For determining the mRNA level of *int/xis/cII*, infection was done following the same protocol but with 5× volumes for each sample. Samples were taken out at different time points: 0, 6, 12, 18, 24, 30 and 40 minutes, and immediately poured into 5 ml ice-cold methanol. Samples were then spun down at 4000×*g* for 4 minutes, at 4 ^{o}C. The cell pellet was resuspended in 1 ml of RNAprotect Bacteria Reagent (Qiagen, 76506), followed by incubation for 5 minutes at room temperature. Then the cells were spun down at 5000×*g* for 5 minutes at room temperature. After discarding the supernatant, the cells were kept at -20 ^{o}C until all samples were collected. RNA extraction was done using RNeasy Mini Kit (Qiagen, 74104), followed by DNA digestion with TURBO DNA-free kit (ambion, AM1907) for a total of 80 minutes and reverse transcription using High Capacity RNA-to-cDNA kit (Applied Biosystems, 4387406). The obtained cDNA was then quantified using SYBR Green PCR master mix. Primers QS7 and QS8 were used for quantifying *cII*, primers QS9 and QS10 for *int* and primers QS11 and QS12 for *xis*, while *ihfB* is used as a reference gene using primers QS5 and QS6 (Table 3.1).

Table 3.1 Bacterial strains, plasmids, phages, and primers used in this work.

Strain Name	Relevant Genotype	Source/Reference
Bacterial strains		
MG1655	*sup*^{0}	Lab collection
LE392	*sup*^{E}, *sup*^{F}	Lab collection
LZ722	*MG1655*, *dam*$^{-}$, *seqA-yfp*, 200×*tetO-attB*, *Cm*^{R}, *Gm*^{R}	This work
LZ731	LZ722[pFtsKi-*tetR-mCherry*]	This work
Phage strains		
λWT	Fully methylated, λ *cI*$_{857}$ *bor::Kan*^{R}	Lab collection
λWT-FP	Fully methylated, gpD-mosaic, λ *D-mTurquoise2 cI*$_{857}$ *bor::Kan*^{R}	This work
λ*int*$^{-}$	Fully methylated, λ *int(AM) cI*$_{857}$	Jeffery Gardner
λ*int*$^{-}$*-Kan*	λ *int(AM) cI*$_{857}$ *bor::Kan*^{R}	This work
λ*cII*$_{68}$	λ *cI*$_{857}$ *cII*$_{68}$ *bor::Cm*^{R}	This work
λ*cII*$_{stable}$	λ *cI*$_{857}$ *cII*$_{stable}$ *bor::Cm*^{R}	This work
Plasmids		
pFtsKi-*tetR-mCherry*	*tetR-mCherry* under constitutive promoter pFtsKi, *Amp*^{R}	This work
pPLate-*D*	gpD under the control of λ late promoter, *Amp*^{R}	This work
pZA32-*dam*	Dam under the control of PLlacO-1 promoter, *Cm*^{R}	This work
pBR322-*D-mTurquoise2-E*	*D-mTurquoise2* fusion and part of downstream gene *E*	Lab collection
Primers		
QS1	5'-GCCGACAACAAAGTCAGGTT	This work
QS2	5'-AAAAGAAGCGCAGAATTTCG	This work
QS3	5'-AGACGGGAAACTGAAAATGTG	This work
QS4	5'-CTGATAGTGACCTGTTCGTTGC	This work
QS5	5'-ACCACGTACCGGACGTAATC	This work
QS6	5'-ATCGCGCAGTTCTTTACCAG	This work
QS7	5'-GCAGATCAGCAGGTGGAAGA	This work
QS8	5'-AATCGAGCCATGTCGTCGTC	This work
QS9	5'-ATGCCCGAGAAGATGTTGAG	This work
QS10	5'-GCACGAAAAGCATCAGGTCT	This work
QS11	5'-GCCACCTGTTACTGGTCGAT	This work
QS12	5'-AACAGTTCGTCGATGGGTTC	This work
QS13	5'-GGGATCATTGGGTACTGTGG	This work
QS14	5'-TTGGGGGTGATGAGTTTACC	This work
QS15	5'-GAATTCCGCCGGTGAGCCGGTGGTTGCC	This work
QS16	5'-AAGCTTATTAGTCAAACGGCGGTGGGGCCAGCAC	This work
QS17	5'-CCCGGGGGCCCTTTCGTCTTCAAG	This work
QS18	5'-GCTAGCGGATCCTTACTTGTACAGCTCG	This work
QS19	5'-ATCACCTAGGCCTAGGGTTTCATCCGC TTCTCC	This work
QS20	5'-TGGAGGTACCGGTACCAGTCAGCATGAAGAAAAATCG	This work

Quantifying percentage of multiple prophage integration

Infection was set up as described in *Bulk Lysogenization Assay*, with the infecting phages being λWT at API of 0.1, 1 and 10. After obtaining the lysogens on the plates, 96 colonies of each infection were used to determine whether they contain single or multiple phage integration by PCR following protocols as described in (194). The percentage of cells having multiple prophage integration is then calculated based on the PCR results.

Microscopy

1 ml of host cell LZ731 was grown in M9 minimal medium (11.3 g L^{-1} M9 salts, 1 mM $MgSO_4$, 0.5 μg mL^{-1} thiamine HCl, 0.1% casamino acids, 100 μM $CaCl_2$) supplemented with 0.4% maltose (M9M) with appropriate antibiotics for overnight. 60 μl of the culture was subsequently diluted 1:100 into 6 ml M9M and grown to OD_{600} ~0.4. 1 ml of cells were then collected by centrifugation at 2000×*g* for 2 minutes at room temperature, and resuspended in 40 μl of M9M. 20 μl of phage lysate was then added to 20 μl of cells to reach an API of 0.5 - 5, followed by incubation for 30 minutes on ice and another 5 minutes at 35 ^oC water bath to allow DNA ejection. The sample was then diluted into M9M at room temperature by 10 fold. 1 μl of the diluted sample was used for imaging following protocols as described in (123) with 1.5% M9M agarose pad. Imaging was performed on an inverted microscope (Ti-E, Nikon, Tokyo, Japan) with a cage incubator (InVivo Scientific, St. Louis, MO) set at 30 ^oC. Images were taken using 100× objective (Plan Fluo, NA 1.40, oil immersion) with standard filter sets and a cooled EMCCD camera (iXon 3 897, Andor, Belfast, United Kingdom). When needed, a series

of 9 z-stack images with spacing of 300 nm in the CFP channel (200 ms exposure) was taken to capture all infecting phages in the initial frames, after which images were taken every 5 minutes through the phase-contrast, YFP, mCherry, and CFP channels (100 ms, 200 ms, 50 ms and 100 ms exposure respectively) at the focal plane to allow tracking of DNA movement and cell fate in the time-lapse movies.

Data analysis

Images were processed using MicrobeTracker (195). Briefly, cells were first outlined using MicrobeTracker, after which spots were recognized first automatically using SpotFinderZ, then manually corrected using SpotFinderM (195). Cell lineage tracking and the calculation of minimum distance between *attB* and lambda DNA, Dis(λ-*attB*), for each cell was done using custom Matlab script in our lab. The Dis(λ-*attB*) is calculated as the minimum distance between all possible pairs of lambda DNA and *attB* in each given cell at each given time point, where the distance between lambda DNA and *attB* was calculated as: $\sqrt{(x_i - m_j)^2 + (y_i - n_j)^2}$, where $i, j = 1, 2, 3$ up to the total number of lambda DNA or *attB* in each cell at each time point, and x_i, y_i are the x and y coordinates of lambda DNA, while m_j and n_j are those of *E. coli attB*.

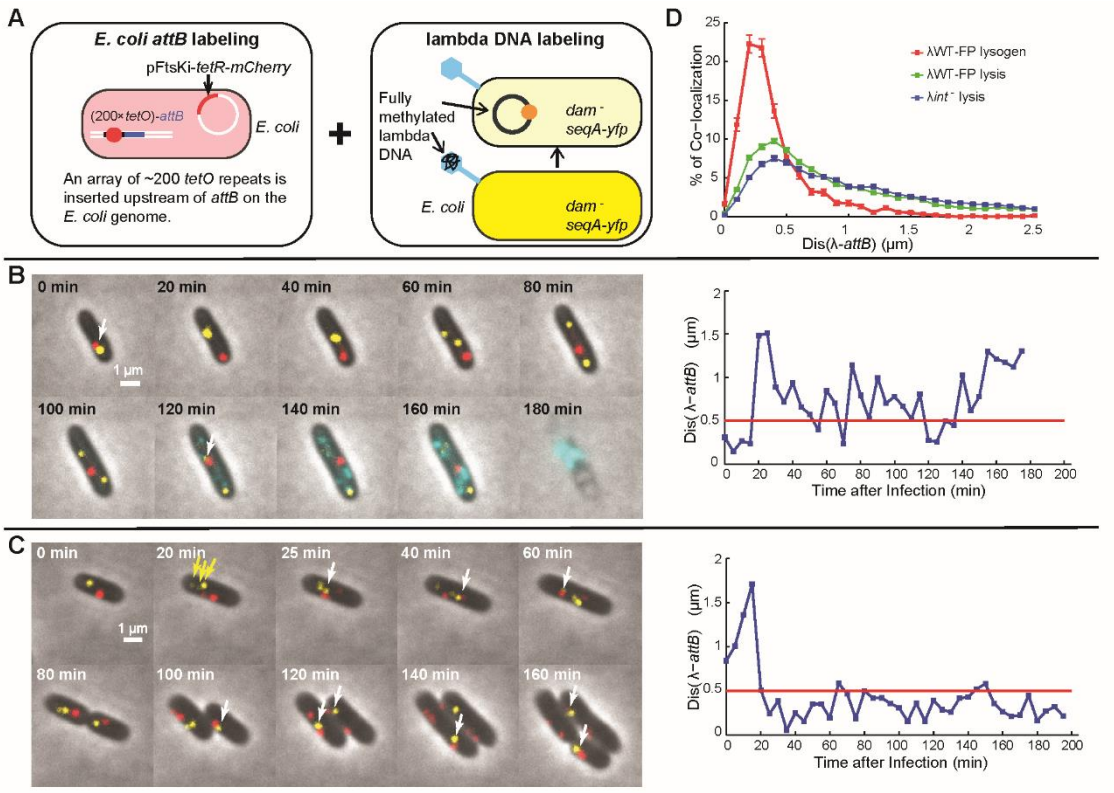

Figure 3.2 Lambda DNA and *E. coli attB* fluorescent reporters allow DNA tracking in lytic and lysogenic cells.

(A) Schematic diagram describing the reporter system. Left, the *E. coli attB* appears as a red dot reported by about 200 *tetO* repeats upstream of *attB* bound by TetR-mCherry expressed from plasmid pFtsKi-*tetR*-mCherry. Right, the DNA of a gpD-mTurquoise2 (cyan) labeled phage appears as a yellow dot when ejected into a *dam*⁻ *seqA-yfp* cell. B and C. Overlay images of representative lytic (B) and lysogenic (C) events respectively, with the corresponding right panel showing the minimum distance between *attB* and lambda DNA foci, Dis(λ-*attB*), over time (blue line) with a 0.5 μm cutoff line (red). White arrows point to the co-localized lambda DNA and *attB*. (B) The lambda DNA and *attB* do not co-localize most of the time in this lytic cell, although occasionally, i.e., at 0 min and 120 min from the selective images, co-localization apparently occurs, possibly due to random collision or imaging artifact. (C) Yellow arrows point to lambda DNA observed at 20 min. DNA co-localization (white arrows) was observed starting from 25 min in this lysogenic cell. (D) Distribution of Dis(λ-*attB*) for lytic and lysogenic cells after λWT-FP infection and lytic cells after λ*int*⁻ infection. The lysogenic cells have a higher peak at shorter distances (0 - 0.5 μm) compared to the lytic cells, while λ*int*⁻ infected lytic cells show a flatter distribution. Error bars represent ± SEM.

Results

Reporter system for phage DNA integration: E. coli attB and phage DNA labeling

In the lysogenic pathway, lambda DNA is integrated into the *E. coli* genome at the *attB* site through recombination by the phage-encoded integrase, Int, in the presence of the host factor IHF (190). To visualize this integration event, we developed a reporter system to simultaneously track the *E. coli attB* and the phage DNA. Specifically, the host cell LZ731 contains about 200 repeats of *tetO* (186) inserted upstream of *attB* on the chromosome (Figure 3.2A, left) and a plasmid pFtsKi-*tetR-mCherry,* which constitutively expresses TetR-mCherry (193), therefore the *tetO* repeats are bound by TetR-mCherry, resulting in a distinct focus (Figure 3.2A, B and C, red dots), indicating the *attB* location. The phage DNA is labeled using our previously reported method ((123), also see Figure 3.2A, right). Briefly, the phage λWT-FP was produced in a host with enhanced Dam methylase activity resulting in fully methylated phage DNA packaged in its head (see **Experimental Procedures**). The host cell LZ731 also constitutively expresses a fluorescent SeqA chimera, SeqA-YFP (167) from the chromosome, and the host DNA is not methylated owing to a *dam*$^{-}$ mutation (methylation deficient). SeqA specifically binds to fully methylated and hemi-methylated DNA, so the phage DNA appears as a YFP focus (Figure 3.2A, B and C, yellow dots) once ejected into the cell. The phage DNA reporter system allows tracking of the first two copies of each initial DNA after replication, since there are only two methylated strands of DNA. For example, in Figure 3.2B, the yellow focus splits into two at 60 min, and no new foci appear despite continued DNA replication. Cells with

more than two foci, e.g. three foci in Figure 3.2C at 20 min, indicated by yellow arrows, are presumably infected by more than one phage. The phage λWT-FP (here referred to as WT for simplicity and easier comparison with the *int* and *cII* mutants used later, and FP is used to indicate this phage is labeled with fluorescent proteins. See detailed genotype in Table 3.1) also carries a *D-mTurquoise2* marker, which encodes a chimera of the gpD decorative capsid protein fused to the mTurquoise2 fluorescent protein (196); this enables the monitoring of the lytic development by imaging cyan fluorescence (4), as observed in Figure 3.2B.

With this reporter system, the location and movement of the lambda DNA and *attB* can be tracked over time. Cells entering lytic and lysogenic pathways are expected to show no (or very short-term) co-localization and long-term co-localization respectively. In Figure 3.2B, the cell entered the lytic pathway, indicated by accumulation of gpD-mTurquoise2 (120-180 min) and cell lysis (180 min). This lytic cell occasionally showed short-term co-localization at 0 and 120 min (see also Movie S1), which could be due to random collision or just imaging artifact. In contrast, long-term co-localization was observed for cells entering the lysogenic pathway. For example, in Figure 3.2C (see also Movie S2), one pair of phage DNA and *attB* co-localized beginning at 25 min, and another pair at 40 min, showing long-term co-localization. This cell later divided and cell growth continued, indicating that the cell entered the lysogenic pathway. Occasional apparent separation of phage DNA and *attB* after long-term co-localization was also observed for lysogenic cells, for example, at 80 min in Figure 3.2C. The lambda DNA is ~48 kbp in length, and the SeqA 5'-GATC-3' binding sites are

relatively evenly distributed across the lambda genome (Figure 3.1A). Therefore, due to the uncertainty of the sites bound by SeqA-YFP on the lambda DNA and the movement of the bound unit resulting from diffusion (165), coupled with the fact that the *tetO* repeats are located ~1500 bp upstream of *attB*, the actual distance between mCherry/*attB* and YFP/lambda DNA focus is expected to vary even after integration. This is probably why the *attB* and lambda DNAs are sometimes seemingly separated while the integration appears to have already happened.

To quantitatively determine co-localization, we then calculated the minimum distance between lambda DNA and *attB*, or Dis(λ-*attB*) at each time point for each cell. For the lytic and lysogenic examples in Figure 3.2B and C, Dis(λ-*attB*) of the lytic cell was usually above 0.5 μm (Figure 3.2B), whereas in the lysogenic cells (Figure 3.2C), it generally remained below 0.5 μm after integration (here beginning at 25 min). Moreover, the distribution of Dis(λ-*attB*) across all time points during the time-lapse movies for all lysogenic (N = 44) and lytic cells (N = 515) showed that the lysogenic cells exhibited Dis(λ-*attB*) in the range of 0 to 0.5 μm much more often than lytic cells (Figure 3.2D), suggesting that 0.5 μm might be a good indicator for determining lambda/*attB* co-localization. In fact, for all lysogenic cells, after the designated integration time, we found that Dis(λ-*attB*) largely stayed below 0.5 μm over the remaining time course of the movie (Figure 3.1B); therefore we defined "spot co-localization" as having a Dis(λ-*attB*) below 0.5 μm.

Lyso-lysis: cell lysis with phage DNA integration

Interestingly and surprisingly, we observed some cells entering the lytic pathway while also showing long-term co-localization of lambda DNA and *attB*. An example is shown in Figure 3.4A (see also Movie S3) where DNA co-localization occurred from 60 min until cell lysis (130 min) suggesting that phage DNA integration might be happening. Although unexpected, this event is actually consistent with the unanimous voting model proposed recently (4), which states that each infecting phage in a cell can make a decision towards lytic or lysogenic independently. We then termed this event as "lyso-lysis".

Before quantifying DNA integration in lytic cells, we first excluded the contribution of random collision between lambda DNA and *E. coli attB* particles to the observed "co-localization". Here we used phage mutant λ*int*$^-$ as a reference/control. λ*int*$^-$ has a mutation in the integrase, which makes it defective in integration and lysogenization (Figure 3.3). As expected, the Dis(λ-*attB*) distribution for λ*int*$^-$ (N = 510) showed significantly lower frequencies at 0 - 0.5 μm (Figure 3.2D) compared to both the λWT-FP lysogenic and lytic cells. This integrase dependent activity suggested that the observed DNA co-localization are likely due to the real DNA integration with some background of random collision. To our surprise, we noticed that λ*int*$^-$ infection sometimes also led to apparent lyso-lysis events. For example, in Figure 3.4B (see also Movie S4), DNA co-localization happened at 90 min and lasted until cell lysis at 135 min after λ*int*$^-$ infection. We then compared the quantitative difference between co-localization for λWT-FP and λ*int*$^-$ infected cells. A relaxed criterion was then set up to

call out cells with apparent "integration", for both λWT-FP and λ*int*⁻ infections. As long as the Dis(λ-*attB*) is below 0.5 μm, in the last 15 minutes before lysis, the cell would be categorized as lyso-lysis. At the same time, the effective number of phages infecting the cell (or effective Multiplicity of Infection, or eMOI) can be obtained by counting the initial phage DNA number. We then obtained the frequency of lyso-lysis (calculated as number of lyso-lytic cells over total cells) at each eMOI. As expected, phage λ*int*⁻ infections led to lower percentages of lyso-lysis at all eMOIs compared to λWT-FP, although still showing a non-negligible number of apparent lyso-lysis events (Figure 3.4C). Nevertheless it suggests that lyso-lysis does exist in λWT-FP infections, although the frequency of lyso-lysis may be overestimated due to the contribution of false co-localization events reported by the system and allowed by our criterion.

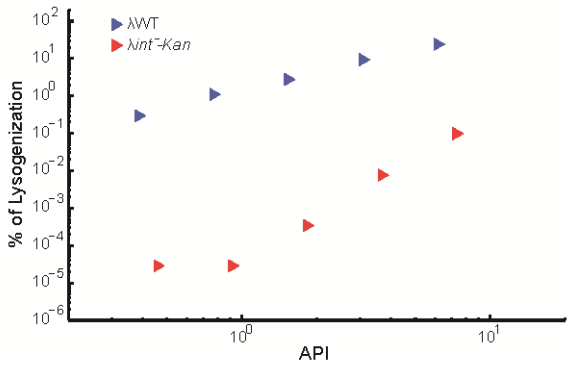

Figure 3.3 Lysogenization frequency of λ*int*⁻*-Kan* is much lower compared to λWT. The lysogenization frequency of λ*int*⁻*-Kan* (red right triangle) is at least 100 fold lower compared to λWT (blue right triangle), confirming that the lambda integrase is non-functional for λ*int*⁻*-Kan*. The lysogens obtained from λ*int*⁻*-Kan* infections are likely coming from the low level read-through of the amber codon.

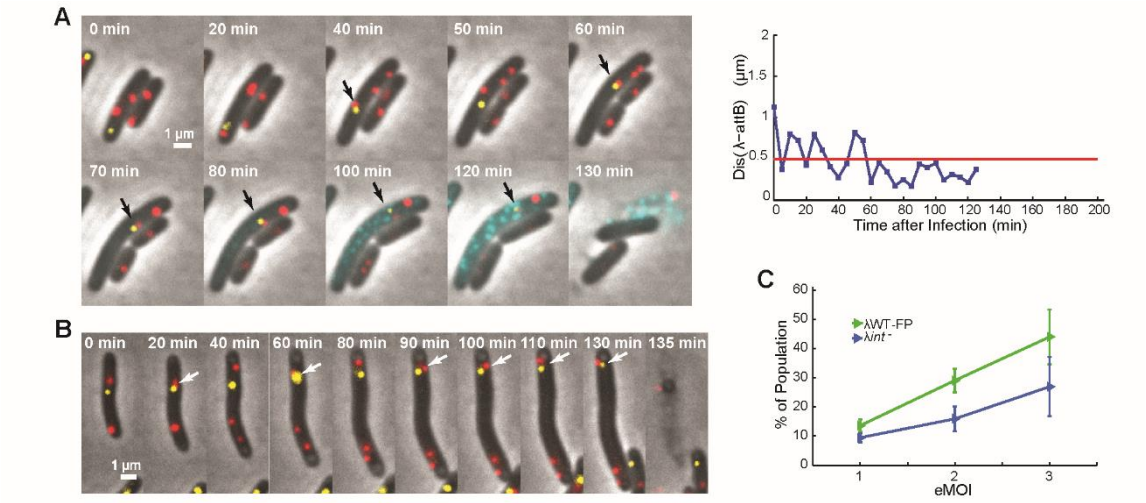

Figure 3.4 Apparent DNA integration is observed in some lytic cells.
(A) After the λWT-FP infection, a lytic cell shows a DNA integration event. DNA co-localization is observed starting from 60 min until cell lysis indicating DNA integration in lytic cells, which we name as lyso-lysis. Black arrows indicate co-localized lambda DNA and *E. coli attB* site. The right panel shows the Dis(λ-*attB*) along time. (B) Overlay images of a cell infected by λ*int*$^-$ mutant show DNA co-localization before lysis. DNA co-localization occurs at 40 min and 60 min, followed by separations right after. Starting from 90 min, lambda DNA and *attB* stay co-localized until the cell lyses at 135 min, leading to a false lyso-lysis event. White arrows indicate co-localized lambda DNA and *E. coli attB* site. (C) The percentage of lyso-lysis increases with eMOI for both λWT-FP and λ*int*$^-$, with λWT-FP showing a much higher percentage than λ*int*$^-$. Error bars represent ± SEM.

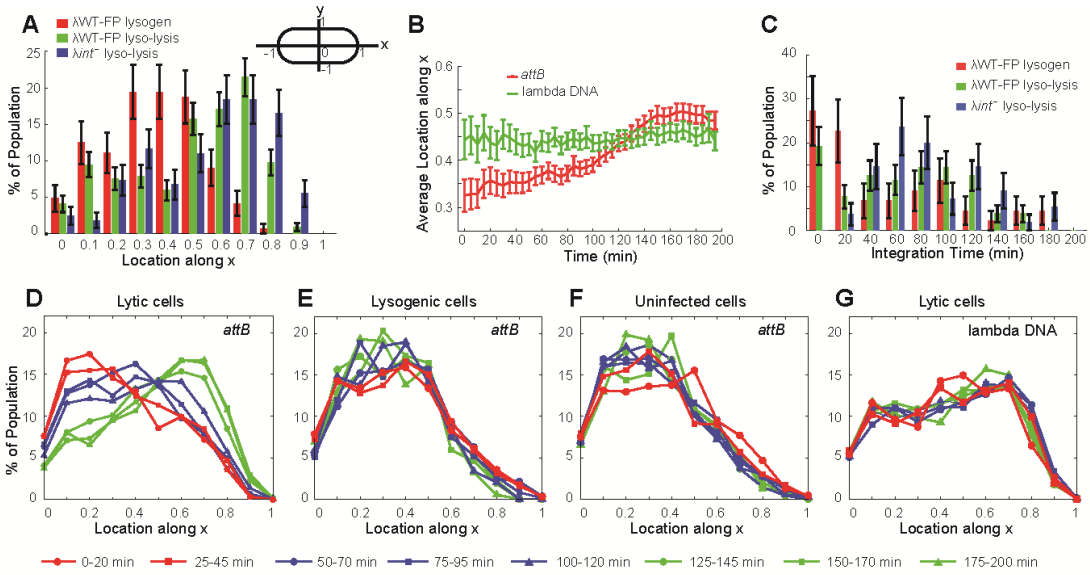

Figure 3.5 *E. coli attB* migrates to the polar region in lytic cells where lambda DNA preferentially locates.
(A) The distribution of locations for co-localization. The diagram on the top right corner specifies the coordinates of cells used. The absolute value for the location along x/y is shown in all the panels. For lyso-lytic cells, data were collected from the last 15 minutes before lysis, while for lysogenic cells, data were from the last 15 minutes of the movie (185-200 min). It shows that for lytic cells co-localization happens more often towards the cell pole, while in lysogenic cells it shows preference to the mid-quarter cell region. (B) Average *attB* and lambda DNA locations along time after infection for λWT-FP lytic cells. Lambda DNA location stays relatively unchanged at around quarter-cell region, while the location of *attB* shifts gradually from mid-quarter region towards the lambda DNA. (C) The distribution of integration times for lysogenic and lyso-lytic cells. The integration for λWT-FP lysogens happens mostly within the first 20 min with an average of 56 min. λWT-FP lyso-lytic cells integrate at an average of 68 min while the negative control, λ*int*⁻ takes 89 min on average. (D), (E) and (F) show the distribution of *attB* in lytic (D), lysogenic (E) and uninfected cells (F) along time after infection by λWT-FP. In lytic cells, *attB* migrates towards the cell pole while in lysogenic and uninfected cells, the *attB* distribution remains the same. (G) The distribution of lambda DNA along time for lytic cells after λWT-FP infection. The lambda DNA prefers the mid-polar cell region and the distribution stays the same throughout the whole lytic developmental process. Error bars represent ± SEM.

E. coli attB migrates towards the cell pole in lytic cells, leading to more co-localization with lambda DNA

To determine the quantitative differences between phage/*E. coli* DNA co-localization in lysogenic cells with true integration events and those reported lyso-lysis events for λWT-FP and λ*int*⁻ under our criterion, we analyzed the DNA trajectories of both lambda and *attB* over time. We noticed that lytic cells showed co-localization of *attB* and lambda DNA at the cell pole more often than at other positions, similar to that of lyso-lysis by λ*int*⁻ infection shown in Figure 3.4B, where both lambda DNA and *attB* migrated towards the cell pole with time and eventually co-localized near the pole. In fact, when comparing the position of co-localization between lytic cells, 15 minutes before lysis, and lysogenic cells, from 185-200 min after infection (when phage DNA has already integrated and spot tracking stops), we observed a significant difference (Figure 3.5A). Co-localization happens most frequently between mid-cell and quarter-cell positions for lysogens, while in lyso-lytic cells, the location shifts drastically towards the cell pole.

We then ask whether the spatial co-localization patterns of λWT-FP infected lytic cells result from natural preferences in *attB* and lambda DNA location during lytic development. In fact, the *attB* location distribution for lytic, lysogenic and uninfected cells showed that the *attB* position shifted gradually towards the poles in lytic cells over time (Figure 3.5D), but not in lysogenic (Figure 3.5E) or uninfected cells (Figure 3.5F). Interestingly, the phage DNA preferentially locates at the quarter-cell region, without significant changes along time in the lytic pathway (Figure 3.5G), indicating that as the

lytic cycle progresses, the *attB* moves gradually to a region where lambda DNA preferentially locates. Consistent with this hypothesis, when comparing the average lambda DNA and *attB* locations along time, it was obvious that *attB* migrated towards the lambda DNA and subsequently crossed lambda DNA traces (Figure 3.5B). Therefore, the false lyso-lysis that we detected from λ*int*⁻ and some of λWT-FP infection were likely due to *attB* and lambda DNA being in close proximity to one another, especially towards the end of the lytic cycle. If this is the case, we expect that the DNA co-localization in the false lyso-lysis events would happen later compared to the actual integration events. We then compared the apparent "integration" times (when the co-localization started) for lyso-lysis and lysogenic cells (Figure 3.5C). Integration in lysogenic cells happened mostly within 20 min after infection under our experimental conditions, which agreed with previously reported data (197), although late integration was also observed, leading to an average integration time of 56 min. Nevertheless, it was clear that integration happened later for lyso-lytic cells on average, with those from λ*int*⁻ infection showed the most significant difference with an average integration time of 89 min, while λWT-FP infection showing 68 min on average. In fact, very few lyso-lysis events from λ*int*⁻ infection showed early integration within the first 20 min, in contrast to λWT-FP lysogenic and lyso-lysis events, although the two phages shared similar lysis times (Figure 3.1C). Taken together, these findings suggest that as *attB* migrated to the cell poles, it would occupy a similar cellular region as lambda DNA, especially at later infection times, leading to the false lyso-lysis from λ*int*⁻ infection and some of the λWT-FP infections. The shift of *attB* distribution in the lytic development could simply be a

result of combination of cellular division inhibition, lack of host DNA replication and compromised length extension (see **Discussion**). The underlying mechanism remains to be investigated.

Lyso-lysis: a process regulated by CII

We designed a PCR experiment to examine whether *E. coli* genomic DNA liberated from lytic cells contains evidence of phage DNA integration as a complement to our microscopy data, as our reporter system does not specifically examine covalent DNA integration. We used primers specifically targeting the junction of *E. coli* and lambda DNA, spanning the *attL* region (Figure 3.6A, red arrows) to confirm integration (194). Phage infection was done with an API (average phage input; the ratio of phages to cells) of 1, and samples were taken every 20 minutes after infection (see **Experimental Procedures**). Samples (containing all lytic, lysogenic and uninfected cells) were then either used directly (Figure 3.6B, upper lane) as a positive control, or spun down and filtered to obtain the lysate (cell free, containing the medium and the cellular content of lysed cells) for PCR (Figure 3.6B, bottom lane). As shown, DNA integration was first observed 20 minutes after infection (Figure 3.6B, upper lane) in lysogenic and/or lyso-lytic cells, while for the cell-free lysate, integration was detected starting from 60 min after infection (Figure 3.6B, bottom lane), corresponding to the time when cells began to lyse under these conditions, to release their DNA into the environment to be detected. Therefore, this suggested that DNA integration and thus lyso-lysis happened in some lytic cells. We then further quantified the percentage of lyso-lysis (defined as number of integrated DNA over total *E. coli* DNA) in the lytic cells using qPCR with additional

primers to quantify the *E. coli* DNA number (Figure 3.6A, black arrows). Consistently, the percentage of lyso-lysis increased significantly between 60 to 90 min to 3.5% at an API of 1 (Figure 3.6C). λ*int*⁻ was used as a negative control and no DNA integration was detected, as expected (Figure 3.6C). These results further support the notion that phage DNA integration does occur in lytic cells. The number calculated here can be an underestimation since there may be multiple copies of *E. coli* DNA per cell at the time of infection, and not all copies will have phage DNA integration in lyso-lytic cells.

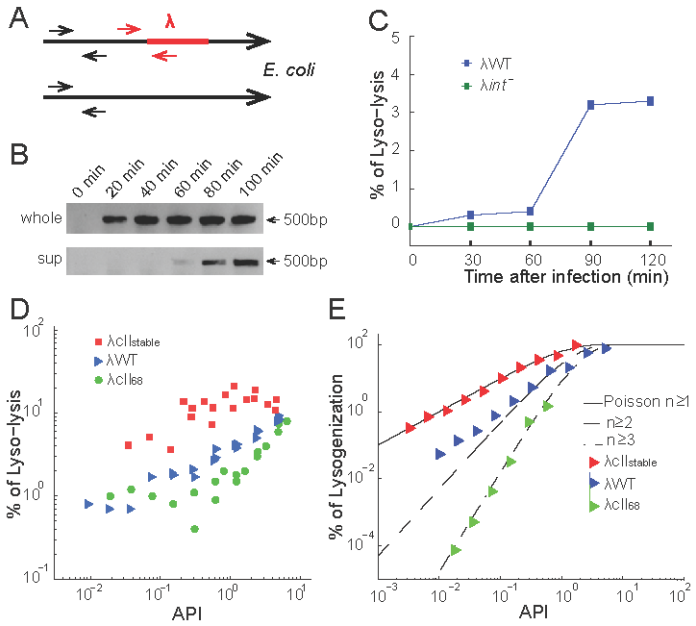

Figure 3.6 Probability of lyso-lysis increases with API and CII activity.
(A) A diagram showing the primer design for PCR and qPCR. For probing the integration using PCR, the primers span the junction between *E. coli* chromosome and lambda DNA, the integration junction, as indicated by red arrows, amplifying 500 bp in length. For qPCR, a different set of primers with the similar design is used. Another pair of primers is used for quantifying the *E. coli* DNA number, as indicated by black arrows.

Figure 3.6 continued.
(B) PCR shows lyso-lysis events. *E. coli* was infected by λWT with an API of 1, and samples were taken every 20 minutes after infection for PCR. PCR was done either using the sample directly (upper lane, labeled as "whole") for detecting DNA integration from the whole sample, or using filtered supernatant to detect DNA integration in the lysed content (lower lane, "sup"). The 500 bp band indicating DNA integration shows up after 20 min in the "whole" sample as expected, and after 60 min in the "sup" sample indicating the lyso-lysis events. (C) The lyso-lysis frequency of λWT and λ*int*$^-$ along time by qPCR at an API of 1. λWT: blue, λ*int*$^-$: green. No amplification of DNA integration is detected for λ*int*$^-$ infection throughout the whole infection process (0-150 min). For λWT infection, the frequency of lyso-lysis increases with time, with 60-90 min showing a drastic increase, corresponding to the time for cell lysis and releases of DNA for detection. (D) Lyso-lysis is regulated by CII and has increased probability as API increases. Combined data of three qPCR experiments were shown. The frequency of lyso-lysis for all three phages including λcII_{68}, λWT and λcII_{stable} increases with API and the effective CII level inside the cell. The frequency of lyso-lysis follows the trend of λcII_{68} < λWT < λcII_{stable}, which is equivalent to their relative CII activities, suggesting that the process is regulated by CII. (E). The lysogenization frequency of λcII_{68}, λWT and λcII_{stable} follows different trends. The data for each phage is shifted with respect to API to compare with the Poisson distribution. λcII_{stable} (red right triangle) follows Poisson distribution of $n \geq 1$ (black solid line), while λWT (blue right triangle) follows $n \geq 2$ (black dashed line) and λcII_{68} (green right triangle) follows $n \geq 3$ (black dash dotted line), suggesting that the cell needs 1, 2 or 3 of the corresponding phages to lysogenize.

We further explored the molecular mechanism underlying this lyso-lysis phenomenon. CII promotes the expression of *int* from pI promoter in addition to activating the transcription of repressor CI from the pRE promoter for establishing the lysogenic pathway and inhibiting lytic gene expression through the anti-sense transcript from paQ (10). It is therefore possible that transient CII activation of pI without activation of pRE or paQ leads to the lyso-lysis that we observe, without producing enough CI and antisense Q transcript to establish a stable lysogen. Lyso-lysis may therefore be enhanced through common factors that lead to increased CII activity, such

as higher APIs. Indeed, we found that as API increased, the percentage of lyso-lysis increased for λWT infection (Figure 3.6D), similar to that of lysogenization (4, 53). Since the CII activity correlates with its protein level (17), more CII might lead to more Int expression and thus more lyso-lysis. We then compared the percentage of lyso-lysis of λWT to two phage mutants, λcII_{68} and λcII_{stable}. λcII_{68} carries a mutation which makes CII unable to dimerize to function (21, 35), and λcII_{stable} is less susceptible to FtsH degradation and is more stable (38). Therefore the average CII activity after infection with the same API is: λcII_{68} < λWT < λcII_{stable}. As expected, the frequency of lyso-lysis followed the same trend: λcII_{68} < λWT < λcII_{stable} (Figure 3.6D). Another interesting phenomenon was that the slope of lyso-lysis frequency as a function API (at log-log scale) is inversely related to the effective CII levels, showing the trend: λcII_{68} > λWT > λcII_{stable}, which is the same as that of the lysogenization frequency for these phages (Figure 3.6E). Altogether, this suggests that similar to the lysogenic pathway, lyso-lysis is also regulated by the CII activity.

Discussion

Cellular decision-making is an important process for the fitness and survival of all organisms, and has recently attracted numerous studies (1). Temperate phages, one of the simplest biological systems display lysis-lysogeny decision-making after infecting the host bacterium. Classically, these decisions have been described as leading to incompatible outcomes, despite that early after infection, to proceed down one pathway without going at least part way down the other is impossible since early genes favoring lytic and lysogenic pathways are expressed from the same promoters, making the two

pathways interconnected (36). In this work, by specifically labeling the lambda DNA and *E. coli attB* locus to allow for the direct visualization of prophage integration, we found that some lytic cells also have lambda DNA integration, previously thought to be present only in the lysogenic pathway. This finding offers a new perspective to the fundamental process of cellular decision-making by bacteriophage lambda that phages can not only concurrently develop two distinct pathways in the early infection period but are also able to reach both outcomes in the late developmental stage.

Our recent model proposed that phages infecting the same *E. coli* cell can make individual votes to determine the cell's outcome, and unanimous voting by all infecting phages is a requirement for lysogeny (4). This means that for those cells infected with more than one phage, it is possible that some phages vote lysogenic and the others lytic, leading to cell lysis, and observations of lyso-lysis support this model. However, our data also suggests that lyso-lysis exists even with one single phage infection (Figure 3.4C, 3.6D), which is counterintuitive according to this unanimous voting model. It may be possible that phage voting occurs at the level of single phage DNA, where DNA replication early after infection provides additional deciding-units, which can then decide different fates to result in lyso-lysis. This scenario is in fact supported by our observation that 71% (235 out of 330 eMOI = 1 infections) of the very first two copies of replicated DNAs separate from each other and move to different locations inside the cell. Moreover, the key protein for lytic development, Q, has been reported to function largely *in cis* (52), suggesting that the localization of Q might be restricted. Therefore, if enough physical separation of the DNA happens early before a decision is reached, each

DNA might maintain its individuality and be able to make a different decision since one phage DNA committing to the lytic pathway would not be expected to force other DNAs to vote lytic due to the restricted localization of Q.

From the perspective of phage gene expression and regulation, it is also possible that lyso-lysis is simply a result of Int expression due to low levels of CII activity during the lytic process. The phage DNA integration is a highly regulated event, depending both on the integrase level as well as its competitor, the excisionase, Xis, which can alter the direction of recombination towards excision (190, 191, 198). During early infection, *int* is expressed from the pL promoter together with *xis* in the same transcript (10), however, the *int* mRNA level is lower compared to *xis* (Figure 3.7, first 5 min), due to retroregulation of *int* by the downstream DNA element *sib* (199). DNA integration is therefore unlikely to happen during the very early infection period. Later, for cells committing to the lysogenic pathway, *int/xis* expression from pL will be shut down by CI, while the pI promoter is activated by CII, allowing only *int* to be expressed (10), resulting in DNA integration. During lyso-lysis, Int must also be expressed to reach sufficient levels for integration. It is possible that a low level of CII is present to promote Int expression from the pI promoter. If so, the level might be too low to either affect other phage DNA or activate pRE to commit to lysogeny, allowing lysis to proceed. In fact, the *int* mRNA level after λ*cII*$_{68}$ infection is substantial (Figure 3.7). Since λ*cII*$_{68}$ infection leads to >99% of lytic cells especially at a low APIs (Figure 3.6E), it appears that lytic cells have significant CII protein. This relatively high level of *int* mRNA level is most likely due to the high copy number of phage DNA templates available in lytic

cells, as phage DNA replicates to such an extent that not all DNA can be packaged to produce viable phages. This means that there is an excess of unused lambda DNAs in lytic cells, and integration might be a good strategy for cells to utilize the free lambda DNA as a backup, should lysis unexpectedly fail.

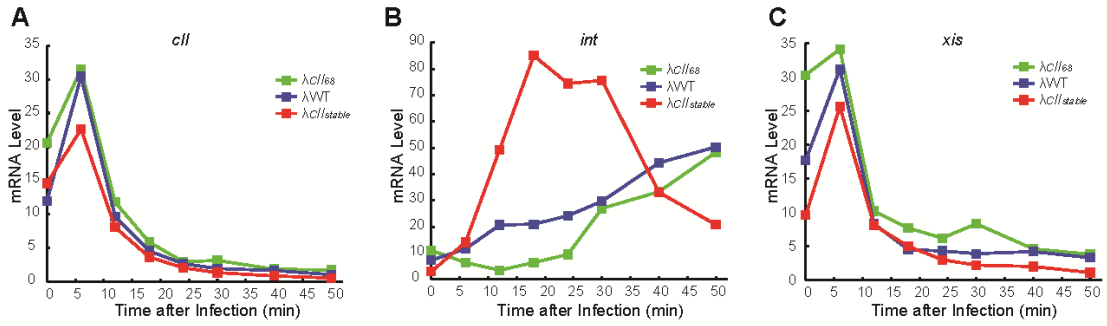

Figure 3.7 The *cII*, *int* and *xis* mRNA levels along time for cells infected by λ*cII*$_{68}$, λWT and λ*cII*$_{stable}$.
The mRNA level is normalized to that of reference gene *ihfB*. λ*cII*$_{68}$: green, λWT: blue and λ*cII*$_{stable}$: red. (A) The *cII* mRNA level for cells infected by different phages shows the same trend, where *cII* reaches a peak at around 6 min after infection and subsequently decreases, likely due to degradation by RNase and inhibition of transcription by CI or Cro. The λ*cII*$_{stable}$ infection shows a lower peak, which is most likely due to the earlier establishment of lysogenic and therefore an earlier peak that we didn't detect due to the limited time resolution. At the time of taking the 6 min sample, the *cII* level for λ*cII*$_{stable}$ is most likely already at its decreasing phase. (B) The *int* mRNA level is low early after infection due to degradation by RNase, and subsequently increases, possibly due to the activation of transcription from pI promoter by CII. λ*cII*$_{stable}$ infection leads to earlier and higher level expression of *int* compared to λWT and λ*cII*$_{68}$. (C) The *xis* mRNA level. Cells infected by different phages show the same trend of *xis* mRNA level after infection along time. The *xis* mRNA level increases and reaches a peak at around 6 min after infection, and subsequently drops due to degradation and inhibition of transcription from pL promoter by CI or Cro.

Table 3.2 Percentage of multiple prophage integration at different APIs.

API	% Multiple integration
0.1	48 ± 7
1	55 ± 7
10	70 ± 8

Lysogens were reported to have a high frequency of having multiple phage DNA integrated even at low API (Table 3.2), as reported previously (197, 200) and kinetic studies on the DNA integration process suggest multiple phage DNAs can either integrate sequentially or all at once (197, 201). Whether all the lambda DNAs inside the cell will be integrated into the genome or not and what happens to the rest of lambda DNA remain unknown. Here, our observation that some phage DNA integrated very late while the cells seemed to have entered the lysogenic pathway (Figure 3.5F) suggest that some replicated unlabeled phage DNA may integrate early while the others, i.e., the labeled DNA, diffuse throughout the cell until they are also integrated.

We observe that *attB* migrates to the cell pole in lytic cells, where phage DNA is more enriched as shown in Figure 3.5G. This movement pattern is very similar to the prophage integration in lysogenic cells (122). In our system, due to the limited number of lysogens obtained, the relatively low time resolution (5 min) and long preparation times (~10 min), most of integration happens within the first 20 min under the microscope. Therefore, we are unable to observe the detailed *attB* and phage DNA relative movements prior to integration in cells committed to lysogeny. However, for

lytic cells, it is possible that the *attB* migration leads to more occurrence of co-localization of *attB* and lambda DNA, and thus, whenever Int is present, DNA integration can happen. This *attB* migration happens without the presence of Int, which leaves the driving force unknown. Further analysis reveals that in lytic cells the *attB* number does not increase significantly (Figure 3.8C), suggesting that the lambda lytic development inhibits the host DNA replication to some extent, possibly due to the competition of limited resources by actively replicating phage DNA (58). Moreover, the length extension of lytic cells is slower compared to lysogenic cells (Figure 3.8B). Therefore, lack of cellular division, compromised host DNA replication and slower length extension might contribute together to the drastic shift of *attB* distribution after lytic development.

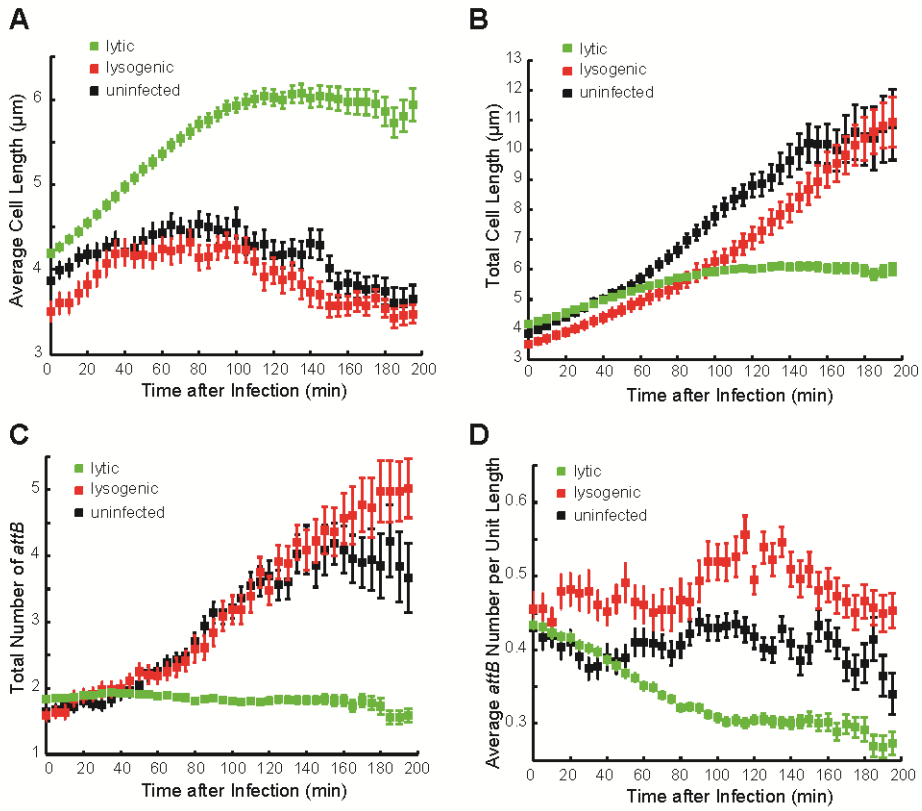

Figure 3.8 Division inhibition, compromised host DNA replication and length extension during the λWT-FP lytic development.

Lytic: green, lysogenic: red, and uninfected: black. Error bars represent ± SEM. (A) The average cell length of lytic, lysogenic and uninfected cells along time. For lysogenic cells, due to the constant cellular division, the cell length remains almost constant like uninfected cells, while the lytic cells show increase along time due to the division inhibition. (B) Total cell length per lineage of lysogenic, lytic and uninfected cells along time. For each initial cells detected, the cell lineage is determined and at each time point the total length of this lineage of cells is calculated, i.e., for a specific uninfected cell, the sum of cell length of all its progeny at a certain time point is calculated. The average of the sum length of each group of cells is then calculated and shown. It is obvious that at the beginning of infection, the length extension of lytic cells is equivalent to that of lysogenic and uninfected cells, however, after about 60 minutes the length extension slows down significantly. (C) The total number of *attB* for each cell lineage for lytic, lysogenic and uninfected cells. The *attB* number increases in lysogenic and uninfected cells along time, while it remains the same in lytic cells, indicating inhibition of host DNA replication by phages in the lytic development. **(**D**)** The average *attB* number per unit of length. Lysogenic and uninfected cells manage to keep a roughly constant number of *attB* per unit of length during growth, however, this number drops in lytic cells, most likely due to lack of host DNA replication.

CHAPTER IV

CRO AND DNA REPLICATION REGULATE STOCHASTIC CELL-FATE SELECTION BY BACTERIOPHAGE LAMBDA

Introduction

Cellular decision-making is a common process among all life forms, and a key step that organisms take to integrate the environmental signals to choose an optimal response to improve their overall fitness (1, 2). From various studies of different systems, the genetic circuits responsible for this task appear to determine the cell fate in a seemingly probabilistic way (4, 109, 202-206). This raises the question of how the components of the circuit jointly contribute to cell-fate choice. To investigate this problem, we utilize a well-established system for cellular decision-making, the paradigm of bacteriophage lambda infection, which leads to two distinct cell-fate outcomes – lysis or lysogeny. The genetic components involved in this lytic-lysogenic decision have been well characterized (10, 11, 13, 15, 67), and recent single-cell/phage level studies have revealed some previously hidden deterministic factors that contribute to the cell-fate decision (3, 4). However, these factors do not account for all of the randomness in cell-fate phenotypes (4). The processing of the genetic circuit itself may contribute to decision-making in a manner yet to be characterized. Pioneering work has been done to investigate the role of stochastic gene expression on the decision-making of phage lambda using mathematical modelling, which has provided the first evidence that fluctuations in protein production rate can partition the initially homogeneous cell

population into distinct phenotypic subpopulations in a probabilistic way (89, 207). These theoretical works have provided key advancements in the understanding of the lambda decision-making network, which exploits noise to achieve the developmental switches. However, due to the complexity of the network and limited experimental data available to provide single-cell/single-molecule level quantifications, the underlying mechanisms remain to be further investigated.

Broadly, the lambda genetic network is very well understood, owing to decades of effort by researchers. The default pathway for phage lambda infection, the lytic pathway, is executed by a series of transcriptional and translational events of the lysis and phage morphological genes, which lead to cell bursting and of the release of hundreds of phage progeny at the late stage of infection. Those events are triggered when the Q protein, an anti-terminator, reaches a threshold, allowing transcription starting from promoter pR' to bypass the terminator, tR', lying immediately downstream (10, 17, 44). The alternative lysogenic pathway culminates in the integration of phage DNA into the *E. coli* chromosome, and inhibition of gene transcription from the two major promoters pR and pL by repressor CI to establish and maintain the dormant state (10). The choice between lytic and lysogenic development is therefore shaped by the cascade of regulatory genes expressed early in the infection process, and after a decision is made, it is enforced by either the repression of phage gene expression by *cI* to establish the lysogenic pathway, or the destruction of the cell through lysis to complete the lytic pathway. With this knowledge, we can question how early gene expression

affects the decision-making circuit of lambda to allow phage infection to bifurcate probabilistically into two alternative cell-fate outcomes.

Here, we investigate the expression of the key genetic components of the lambda lytic-lysogenic decision circuit at the mRNA level using single-molecule fluorescence *in situ* hybridization (smFISH) (173, 208). By combining this approach with live-cell imaging to determine the final outcome of phage infections, our work reveals that the weak repressor Cro regulates the *cII* expression to form a heterogeneous population, where stochastic cell-fate selection into the lysogenic or lytic pathway can occur. Moreover, to carry out the phage decisions by either sufficiently expressing *cI* to establish lysogeny or the lytic cassette to conclude the lytic pathway, multiple copies of phage DNA are required, which emphasizes the critical role of DNA replication in cell-fate bifurcation.

Materials and Methods

Plasmid, bacterial and phage strains

For a list of the plasmids, bacterial and phages strains used in this work and the detail genotypes, see Table 4.1.

The fluorescent λ*P*$^{-}$ phage bearing double reporters λ_{LZ1460} were constructed by crossing the WT phage λ_{LZ1367} (111) with plasmid pBR322-*Pam80*. This plasmid carries a fragment of the lambda genome which covers part of the *P* gene, with the CAG encoding Q at the 69 AA position mutated to an amber stop codon TAG, corresponding to the *Pam80* mutation. λ_{LZ1367} was titered on LE392 carrying plasmid pBR322-*Pam80* to produce confluent plates with connecting plaques. The phages collected from this

plate were then used to screen for the recombinant strain λ*D-mTurquoise2 cI*$_{857}$*-mKO2 P*$^{-}$ *bor::Kan*^{R} (λ_{LZ1460}). The amber mutation in the *P* gene allows the phages to propagate on suppressor strain LE392 but not on non-suppressor strain MG1655. Therefore, a mixture of LE392 and MG1655 cells at exponential phase are used for tittering and the phages that form turbid plaques are then selected and further confirmed by sequencing to be λ_{LZ1460}.

The EYFP labeled fluorescent WT phage (λ_{LZ641}) are obtained by crossing phage λeyfp (λ*cI*$_{857}$ *D-eyfp Sam7*) (74) with a plasmid pER157 (168), which contains WT *S* gene and *bor::Kan*^{R}. The resulting lysate were then screened for the ability to grow on Kanamycin plates after lysogenization on to non-suppressor strain MG1655. The resulting lysogens were then further tested for its ability to lyse after induction, to result in phage λ_{LZ641} (λ*cI*$_{857}$ *D-eyfp bor::Kan*^{R}). The EYFP labeled λ*P*$^{-}$ phage (λ_{LZ646}) were obtained by crossing phage λ_{LZ641} with another phage λ *cI*$_{857}$ *P*$^{-}$ *bor::Kan*^{R}, and screened for smaller plaques on LE392 as fluorescently labeled phages are unstable and usually form smaller plaques compared to non-fluorescent phages. Those fluorescent phages are further tested for *P*$^{-}$ by its inability to form plaques on MG1655 and confirmed by sequencing.

Table 4.1 Bacterial strains, plasmids, phages and primers used in this work.

Bacterial strains, plasmids, phages, and primers		
Strain Name	Relevant Genotype	Source/Reference
Bacterial strains		
MG1655	*sup*^{0}	Lab collection
LE392	*sup*^{E}, *sup*^{F}	Lab collection
Phage strains		
λWT	λ *cI*$_{857}$ *bor::Kan*^{R}	Lab collection
λ*P*$^{-}$	λ *cI*$_{857}$ *P*$^{-}$ *bor::Kan*^{R}	Ryland Young
λ$_{LZ1367}$	λ *cI*$_{857}$*-mKO2 D-mTurquoise2 bor::Cm*^{R}	Lab collection
λ$_{LZ1460}$	λ *cI*$_{857}$*-mKO2 P*$^{-}$ *D-mTurquoise2 bor::Cm*^{R}	This work
λ$_{LZ641}$	λ *cI*$_{857}$ *D-eyfp bor::Kan*^{R}	This work
λ$_{LZ646}$	λ *cI*$_{857}$ *P*$^{-}$ *D-eyfp bor::Kan*^{R}	This work
-	λ *cI*$_{857}$ *cro*$^{-}$	Donald Court
-	λ *cI*$_{857}$ *cro*$^{-}$ *P*$^{-}$	Donald Court
λ*cro*$^{-}$	λ *cI*$_{857}$ *cro*$^{-}$ *bor::Kan*^{R}	This work
λ*cro*$^{-}$*P*$^{-}$	λ *cI*$_{857}$ *cro*$^{-}$ *P*$^{-}$ *bor::Kan*^{R}	This work
Plasmids		
pRE-*mCherry*	*mCherry* under the control of λ pRE promoter, *Amp*^{R}	(17)
pBR322-pPLate**D*	gpD under the control of λ late promoter, *Amp*^{R} , for producing the mosaic λ$_{LZ641}$ and λ$_{LZ646}$	(4)
pACYC177-pPLate*D	gpD under the control of λ late promoter, *Amp*^{R}, for producing the mosaic WT and *P*$^{-}$ phage with double reporters	Lab Collection
pER157	For recombination, *bor::Kan*^{R}	(168)
pBR322-*Pam80*	For recombination to make *P*$^{-}$ phages	This work
Primers		
ihfB-forward	5'-ACCACGTACCGGACGTAATC	(155)
ihfB-reverse	5'-ATCGCGCAGTTCTTTACCAG	(155)
cII-forward	5'-GCAGATCAGCAGGTGGAAGA	(155)
cII-reverse	5'-AATCGAGCCATGTCGTCGTC	(155)
E-for	5'- CTGGGTGAACAACTGAACCG	This work
E-rev	5'- ATCCGTGTCATCAAGCTCCT	This work
dxs-for	5'- CGAGAAACTGGCGATCCTTA	(209)
dxs-rev	5'- CTTCATCAAGCGGTTTCACA	(209)

As the fluorescently labeled phages are unstable, we then transform plasmid pLate*D into the lysogens before induction, to create stable mosaic phages containing a mixture of wild type gpD and gpD-EYFP. The phages are then purified following protocols described in (4) and used for live-cell imaging.

RNA smFISH

pR (*cII*) and *SRRz* probes are designed, synthesized and labeled with Cy5 (GE Healthcare Life Sciences, #PA15000) and AlexaFluor488 (ThermoFisher, #A20000), respectively, following protocols described (173). The sequence of the probes can be found in Table 4.2 and 4.3. The *cI* probes reported by (210) are used, and ordered pre-labeled with TAMRA from Biosearch Technologies.

To detect the mRNA level after infection, non-suppressor strain MG1655 was used as the host for infection. The overnight culture MG1655 was diluted 1:1000 into fresh LBMM (LB supplemented with 0.2% maltose and 10 mM $MgSO_4$) and grown at 37 ^oC with shaking at 265 rpm until reaching OD_{600} of ~0.4. The cells were then collected by centrifugation at 2000 ×g for 15 min and re-suspended in 1/10 volume of pre-chilled LBMM. For each sample to be collected, 1 ml of concentrated cells were used for infection. Appropriate amount of phages (usually ~1×10^{10} pfu/ml) were added to reach API of 0.1-0.2 and mixed well. For negative control, add the same volume of SM buffer (phage buffer, 100 mM NaCl, 10 mM $MgSO_4$, 0.01% gelatin, 50 mM Tris-Cl, pH 7.5) to the sample. Incubate the samples on ice for 30 min to allow phage adsorption, then transfer to 35 ^oC water bath and incubate for 5 min to allow phage DNA ejection. After this step, transfer 750 μl of each sample to 7 ml of pre-warmed LBGM (LB

supplemented with 0.2% glucose and 10 mM $MgSO_4$) and incubate in 30 ^oC water bath with mild shaking at 225 rpm. At the specific time point, pour the sample into a 50 ml tube with 860 µl of 37% formaldehyde (final concentration 3.7%) to allow quick fixation, and incubate for 30 min at room temperature using a nutator. The samples were then treated following protocols described (173).

Table 4.2 Sequences of the probes for detecting lambda *cII* mRNA.

Lambda *cII* probes, 5'-3'			
*cII*_1	CGTTTGTTTGCACGAACCAT	*cII*_25	CCACAGAAAGGTCGTTTTCT
*cII*_2	TCTCGATTCGTAGAGCCTCG	*cII*_26	TGAATTGCAGCATCCGGTTT
*cII*_3	GCGATTTTGTTAAGCAACGC	*cII*_27	ATGTCAAACATCCACTCTGC
*cII*_4	TGTCTTCTCAGTTCCAAGCA	*cII*_28	TGATGGTGCGATAGTCTTCA
*cII*_5	GCTGATCTGCGACTTATCAA	*cII*_29	CATCAGGCGGATATCGTTAG
*cII*_6	AGAACTTTGGAATCCAGTCC	*cII*_30	TTACCGGACCAGAAGTTGTC
*cII*_7	CCCATTCAAGAACAGCAAGC	*cII*_31	TCCACTTATCGCGGAGTTTG
*cII*_8	AATCGAGCCATGTCGTCGTC	*cII*_32	TTTGGTTTGCTGGCTGTCAC
*cII*_9	AATCGCAGCAACTTGTCGCG	*cII*_33	ATAGATCCACCCCGTAAATC
*cII*_10	CCGGGCGTTTTTTATTGGTG	*cII*_34	TCTGCTCACGGTCAAAGTTA
*cII*_11	GATTTGTTCAGAACGCTCGG	*cII*_35	CTTTTCGTCGTACTGTTCCG
*cII*_12	AATGACCTCAGAACTCCATC	*cII*_36	GAACACACCGTTGATGATCT
*cII*_13	TGACTCCTGTTGATAGATCC	*cII*_37	TTCGTTCTGGTCACGGTTAG
*cII*_14	ATCGAGATCTGCCACATTAC	*cII*_38	TTTTCCCGAAAAGCCAGAAC
*cII*_15	TTGATAGTCTGGCGTAACCA	*cII*_39	CGTTAACCTGTTCCATCGTG
*cII*_16	GAATAAGCCTCAAGCAGCAT	*cII*_40	AGAAATGGTCGATTCTGCCG
*cII*_17	AACTGTCGCTTGGTCAGATC	*cII*_41	ATATCAACCAGCTCGCTGAC
*cII*_18	CAGAATGGCAAGCAGCACTT	*cII*_42	CTTCCGGCAATACTCGTAAA
*cII*_19	ATCGGTGATTCTGTCCATTG	*cII*_43	AGTAGTGCGCGTTTGATTTC
*cII*_20	TTGCACCGTTTGACAGGTAA	*cII*_44	CTGATACAGGTTGGTAACCA
*cII*_21	GACGAGTTCTAACTTGGCTT	*cII*_45	GTAATTCCGCATCAGTAAGC
*cII*_22	TTTTGAGGGATGCACCATTC	*cII*_46	CTCACCACGGTTAATTCTCG
*cII*_23	CTCGTTTTAGGGGATTTTCC	*cII*_47	GTGCACGATTTAGAGGTCTA
*cII*_24	ATTCGCCAGAATTCTCTGAC	*cII*_48	CATACACTTGCTCCTTTCAG

Table 4.3 Sequences of the probes for detecting lambda *SRRz* mRNA.

Lambda *SRRz* probes, 5'-3'			
SRRz _1	CGGTATTCGCTTAATTCAGC	*SRRz* _24	GGGTGATCGGAGTAATCAGT
*SRRz*_2	TGTACGCATTTGGTGATCCG	*SRRz* _25	GTTTAGCGTGACAAGTTTGC
SRRz _3	CAGTTTGGGTTGTGCTGTTG	*SRRz* _26	CGCCTGTTGATTTGAGTTTT
SRRz _4	AATTCAGGACAGACAGTGGC	*SRRz* _27	GAGAAGTCTTTCAGGCCAAG
SRRz _5	CCGCAGCGTAACTATTACTA	*SRRz* _28	GCTCCTTAATCTGCTGCAAT
SRRz _6	CTTTCACGAAGGTCATGTGT	*SRRz* _29	TCAATCATAGGTAAAGCGCC
SRRz _7	CAAAACGGCAGGAGGTTGTT	*SRRz* _30	GATTGCCTGACGGATATCAC
SRRz _8	TTTGTTCGTGACCGATATGC	*SRRz* _31	GCAGTGAAGCCCAGATATTG
SRRz _9	CAGGCTACTGTGTTTAGTAA	*SRRz* _32	ATCAGGCTGTCAGCCTTATG
SRRz _10	GGTCGATTACTGATAGAACA	*SRRz* _33	GCCCGCTTCTTTGAATTTTG
SRRz _11	TGGCATCTTCATGTCTTACC	*SRRz* _34	TACATCAATCTCTCTGACCG
SRRz _12	CGGCCAACAGGTCATGTTTT	*SRRz* _35	AGATAATCGCGGTGACTCTG
SRRz _13	TTGCAAACGCAAGGATTGCC	*SRRz* _36	GGCAGACGATGATGCAGATA
SRRz _14	TTTTTGTAAACGCACCGCCA	*SRRz* _37	ACGGTAATGATTAACAGCCC
SRRz _15	CACATCGTTGCGTCGATTAC	*SRRz* _38	CTGGGCTTTGTAGGTAATGG
SRRz _16	AATGAACCAGGCGATAATGG	*SRRz* _39	TCAGTTCTCTGGCATTTTTG
SRRz _17	TAAGCGAGATTGCTACTTAG	*SRRz* _40	ATGTCAGTAATTGCCGCGTT
SRRz _18	GCCGATAAACACGCTCGTTA	*SRRz* _41	CTTCGTGTATTTTGCATCGA
SRRz _19	CAATCGAGTCAGTACCGATG	*SRRz* _42	TCAGCTTTAGCATCAGCTAA
SRRz _20	GCGAAGCGTTTGATAAGCGA	*SRRz* _43	AACATCATCACGCAGAGCAT
SRRz _21	TTCTACTCCGGCTTTTTTAG	*SRRz* _44	TTTGATGTGCAACCGACGAC
SRRz _22	TCTGACGTCCGTTATCAGTT	*SRRz* _45	TTCACGCACTGACTGACAGA
SRRz _23	ATAGCTCTCCGCCTACAATG	*SRRz* _46	GAGGGTGAAATAATCCCGTT

qPCR for quantifying phage DNA and RNA level

Phage infections are set up following the same procedure as is for RNA smFISH. At each time point, samples were taken and qRT-PCR to detect the *cI* and *cII* mRNA level was performed following our previously established protocols described in (155). The *ihfB* mRNA level were used as a reference to allow the comparison of *cI* and *cII* mRNA levels over time. To detect the phage DNA number, the samples were taken following the same procedures, followed by DNA extraction using UltraClean Microbial DNA Isolation Kit (MO BIO Laboratories, #12224-50). The DNAs were then diluted and used for qPCR using primers targeting the phage genome. The *E. coli* DNA number was used as a reference using primers targeting the *dxs* gene (209).

Microscopy

To image the smFISH samples, upon the suspension of the cells in 2×SSC, 1 μl of the sample is placed on a cover slip and topped with a piece of 1.5% agarose pad (prepared with 1×PBS). The sample was then imaged immediately on an inverted microscope (Ti-E, Nikon, Tokyo, Japan). Images were taken using 100× objective (Plan Fluo, NA 1.40, oil immersion) with standard filter sets and a cooled EMCCD camera (iXon 3 897, Andor, Belfast, United Kingdom). A series of 5 z-stack images with spacing of 300 nm in the Cy5 (for *cII*, 200 ms exposure), Cy3 (for *cI*, 200 ms exposure) or YFP (for *SRRz*, 200 ms exposure) channel was taken, while one image was taken at the focal plan for the phase-contrast (100 ms exposure) and DAPI (30 ms exposure) channel.

The real-time live-cell imaging of the double reporter λWT and λ*P*$^-$ phage infection are performed as described (111). Briefly, overnight MG1655 cells grown in M9M (M9 supplemented with 0.4% maltose) were diluted 1:100 into fresh M9M medium and grown to OD_{600}~0.4. The cells were then harvested and concentrated by 10 fold by resuspending in 1/10 volume of M9M. The cells were then infected with phages at different APIs, following an incubation on ice for 30 min, and 5 min in a 35 ^oC water bath. The cells were then diluted and placed on cover slip, and topped with 1.5% agarose pad made with M9M. The imaging process were done following protocols described in (111).

The real-time live-cell imaging of the EYFP labeled λWT and λ*P*$^-$ phages were done following protocols as described in (75). Briefly, overnight MG1655[pRE-*mCherry*] cells grown in LBMM were diluted 1:1000 into fresh LBMM medium until OD_{600}~0.4. The cells were then harvested by centrifugation and resuspended in 1/10 volume of fresh LBMM. The infections were done following the same protocols, and the samples were imaged using 1.5% agarose pad made with LBM (LB supplemented with 10 mM $MgSO_4$) (75). To observe the phages infecting each cell at the beginning of the infection, a series of 9 z-stack images with spacing of 300 nm in the YFP (400 ms exposure) were taken, while images were also taken at the focal plane in the phase contrast (100 ms exposure) and the mCherry channel (100 ms exposure). After that, time-lapse movies were set up to track the progression of phage infection by taking images every 5 min in the phase contrast (100 ms exposure), YFP (100 ms exposure) and mCherry (100 ms exposure) channels, for a total length of 4 hrs.

mRNA number quantification

Microscopic images were first processed using Schitzcell, where the individual cells are recognized and segmented. The total cell fluorescence intensity are calculated by summing up the intensities inside the cells and subtracting the background, and the average intensity of the cell are calculated by dividing the total intensity by the cell size. At 0 min after infection, a small fraction of cells shows low levels of *cII* mRNA expression, typically presenting in a single focus distinctive from the negative samples without phage infection. The total fluorescence intensity of those cells and the cells from the negative samples are used to fit into a multi-Gaussian function, respectively (Figure 4.1), and the difference between them are designated as the intensity for a single *cII* mRNA. The same calculation method are applied for calculating the single mRNA intensity of *cI* and *SRRz*, where the cells with low expression of *cI* and *SRRz*, typically at 6 min and 12 min, respectively, are used. Once the single mRNA intensity is obtained, the number of mRNA in each cell is calculated by (T-m*S)/A, where T is the total intensity of the cell, m is the median of the average intensity of the cells from the negative sample, S is the size of the cell, and A is the intensity of one mRNA calculated as described above.

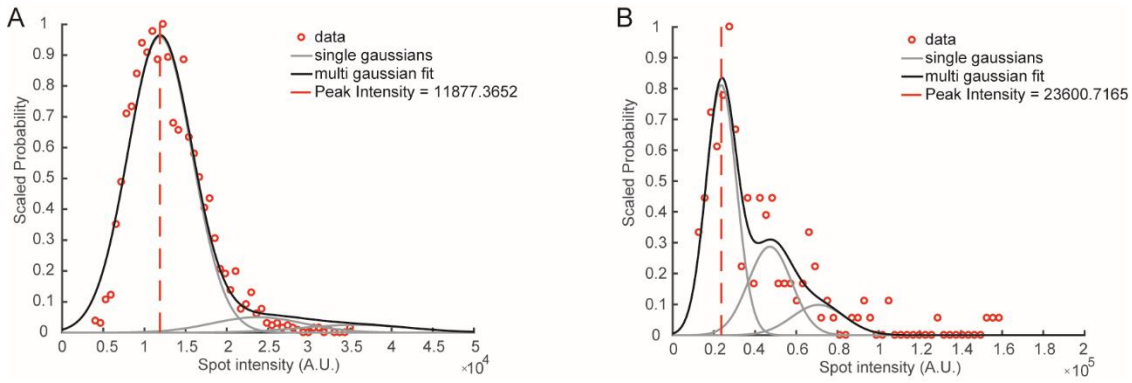

Figure 4.1 Calculation of single mRNA intensity for *cII*.
(A) Distribution of the fluorescence intensity of cells in the negative sample. The total cell fluorescence in the *cII* channel (Cy5) was used to fit into a multi-Gaussian function. The negative samples have a peak intensity of ~11877 A.U.. (B) The fluorescence intensity of cells in the 0 min infection sample that had distinct foci were used to fit into a multi-Gaussian function, and the peak intensity was shown to be ~23600 A.U.. The single mRNA intensity was then approximated by subtracting 11877 A.U. calculated in (A) from the 23600 calculated here.

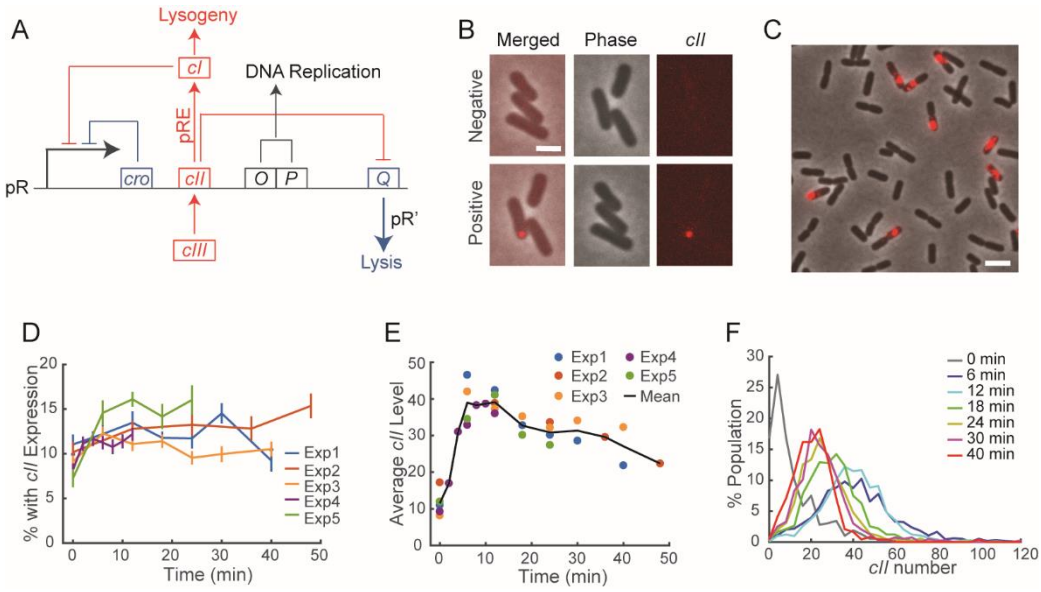

Figure 4.2 The simplified genetic diagram of lambda lysis-lysogenic decision making and the characterization of *cII* mRNA expression.
(A) The transcript under the pR promoter includes the *cro*, *cII*, *O*, *P*, and *Q* genes. Cro and CI both repress the pR promoter. O and P are required for DNA replication. CII activates the expression of CI from pRE promoter while represses Q from paQ promoter. CIII is transcribed from the pL promoter and it promotes the stability of CII. Protein Q allows transcription of the lysis and morphogenesis genes from pR'. (B) Selected images showing cells from the negative and positive samples. Top: Cells without phage infection. None of the cells in the negative sample show *cII* signal. Bottom: Cells from samples with λWT infection at 0 min. One of the cells shows a distinct focus, while the other two cells do not show any focus, either because they have not started the mRNA expression, or they are not infected. (C) Selected images showing *cII* mRNA expression at 6 min. *cII* mRNA shows up in clusters instead of punctate foci. (D) The percentage of cells showing *cII* expression. Data from different experiments were shown in different colors. The percentage of cells with *cII* expression reaches a plateau after 2 min of infection as shown by experiment #4 (labeled as Exp4), where samples were taken every 2 min. Overall, within 9-17% of the cells show *cII* expression, consistent with an API of 0.1-0.2. (E) Average *cII* levels over time after λWT infection. Data from different experiments were shown with colored dots and the mean was shown with a black curve. Only cells with *cII* expression were included in the calculation. Expression of *cII* reaches a peak at around 6-12 min after infection and subsequently drops. (F) The distribution of single-cell *cII* levels over time after λWT infection. Data from experiment #1, #3 and #5 in (E) where samples were taken at the same time points were combined and shown. The *cII* mRNA distributions at 6 and 12 min are similar to each other and gradually shift to the lower end after 18 min. The error bars denote the standard error of the mean. The scale bar represents 2 μm.

Results

Single-molecule characterization of pR transcription activity after phage infection

The pR transcript includes genes such as *cII*, the key lysogenic factor, and *Q*, the activator for the expression of genes in the lytic pathway (Figure 4.2A). Therefore, we quantified the level of pR transcription at the single-cell level using smFISH, by targeting the *cII* gene region, as an initial step to uncover the molecular mechanism of the decision-making process. In these experiments, we control the MOI (multiplicity of infection) by infecting with an API (average phage input, calculated as PFU/CFU or plaque forming units/colony forming units) of 0.1-0.2, which results in a cell population where 9-17% of cells are infected and the majority of them (90-95%) being MOI=1 infections (Figure 4.2D). This is to minimize the effect of different MOIs, which is an important factor affecting the lysogenization frequency (53), to focus on the cell-fate decisions with only one infecting phage. At 0 min after λWT phage infection, a low fraction of cells show one distinct *cII* focus (Figure 4.2B), which likely corresponds to one single mRNA. At later time points, i.e., 6 min as shown in Figure 4.2C, most of the *cII* mRNAs appear in clusters instead of punctate foci, indicating a high local concentration of *cII* mRNA. This highly localized mRNA distribution might suggest compartmentalization for phage progression within the cell. The percentage of cells showing the *cII* transcription quickly reaches a plateau of 9-17% within the first 2 minutes of infection, indicating that gene expression closely follows phage infection (Figure 4.2D). The mRNA numbers were then quantified (Figure 4.1, see details at Materials and Methods) and validated by comparing the average *cII* mRNA number per

cell obtained by smFISH to that of qRT-PCR (Figure 4.3). Overall, the average *cII* mRNA level quickly peaks at ~6 to 12 min after infection, and subsequently drops (Figure 4.2E), probably reflecting the repression of pR either by CI or Cro. Moreover, *cII* mRNA numbers show a wide distribution among different cells at different time points. At 6-12 min, the *cII* mRNA number ranges between 0-120 molecules per cell with a peak at ~40 (Figure 4.2F), indicating noisy gene expression from the pR promoter. Afterwards, the distribution of *cII* gradually shifts to the lower end and stabilizes after 24 min with a peak of ~20 molecules per cell (Figure 4.2F).

Lytic-lysogenic bifurcation requires negative regulation by Cro

Because CII concentration is a primary determinant of the lytic-lysogenic decision, we next focused on studying its regulation by other genes and its correlations with decision-making during lambda infection. As shown in Figure 4.2A, the pR promoter is regulated by CI and Cro. *Cro* is the first gene to be expressed from pR during infection, and its competition with CI constitutes the bistable genetic switch (13, 187, 211, 212). In the decision-making process, however, Cro does not compete with CI until CII activates *cI* expression from the pRE promoter, after a decision is made (17). Nevertheless, Cro is important for lytic development in the infection process, as infections by λ*cro*$^{-}$, a *cro* mutant phage, leads to very low progeny production (Figure 4.4) and much higher lysogenization frequencies compared to λWT (Figure 4.5) (19, 20). We then investigate how Cro regulates early gene transcription to result in different decision-making phenotypes by comparing the *cII* transcription of λ*cro*$^{-}$ to λWT. As Cro is a negative regulator, the average *cII* mRNA level in the λ*cro*$^{-}$ infection is much higher

than λWT at 6-24 min after infection (Figure 4.6A). At 6 min, some of the λ*cro*$^-$ infected cells show higher *cII* expression than λWT, as indicated by the single cell *cII* distribution (Figure 4.6B). The *cII* expression in the λ*cro*$^-$ strain keeps increasing through 18 min, showing an average of ~100 molecules per cell and a broad distribution ranging from 1-250 (Figure 4.6B-E). After 24 min, the *cII* level drops rapidly (Figure 4.6A and F), and by 40 min, the *cII* level reaches ~20 molecules per cell, which is even lower than λWT (Figure 4.6A and H). The lower *cII* levels for λ*cro*$^-$ at later time points may result from more CI inhibition as λ*cro*$^-$ lysogenizes more often.

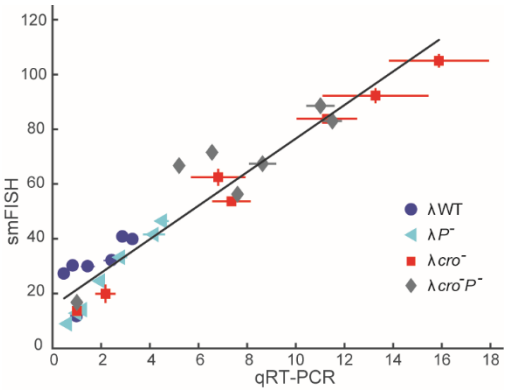

Figure 4.3 Comparison of average cII mRNA level by qRT-PCR and smFISH. For smFISH, only the cells with fluorescent *cII* signal were analyzed, and the average mRNA numbers at different time points for different phages were shown. For qRT-PCR, the average *cII* mRNA numbers were calculated using *ihfB* gene expression as a reference, and further normalized to the number obtained at 0 min. The correlation coefficient is ~0.96, indicating good agreement between smFISH and qRT-PCR data. Error bar denotes the standard error of the mean.

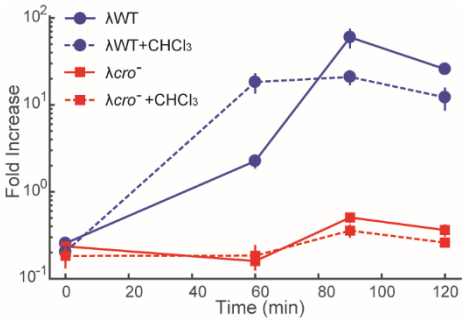

Figure 4.4 Lack of Cro results in defective lytic development.
The phage titers from supernatant or $CHCl_3$ treated samples taken at different time points after λ*cro*⁻ infection at API=0.1 were compared to the phage input and the fold change was shown. At 0 min, ~20% of both phages were detected in the supernatant, which corresponds to the unabsorbed phages. At 90 min, λWT infection leads to ~80-fold increase in phage numbers compared to the input. At 120 min, a drop is observed, which is probably due to further adsorption and infection of the released phages to the remaining host cells. For λ*cro*⁻ infection, a drop in the phage titer was detected at 60 min, possibly due further adsorption of free phages to the host cells. At 90 and 120 min, a slight increase in phage titer was observed, however, the total phage output is only ~0.4 fold compared to the input, indicating that λ*cro*⁻ is defective in cell lysis. Adding $CHCl_3$ to the samples, which can help release phage progeny inside cells, does not increase the phage titer, indicating that the number of progeny produced by λ*cro*⁻ is very low. Error bar denotes the standard error of the mean from at least two biological repeats.

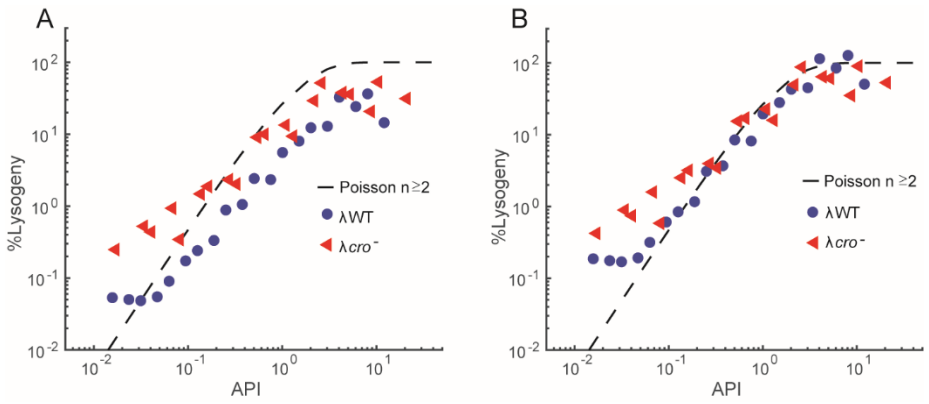

Figure 4.5 Lack of Cro results in higher frequency of lysogenization.
(A) The lysogenization frequency of cells after λWT and λ*cro*⁻ infections at different APIs. Combined data of two experiments were shown. λ*cro*⁻ infection leads to higher lysogenization frequencies across different APIs, and plateaus at the same level with λWT at high APIs. (B) The data from (A) were shifted to fit into the curve of Poisson distribution of n≥2. Both phages follow the curve, indicating that 2 or more phages are required to lysogenize the cell on average for both λWT and λ*cro*⁻.

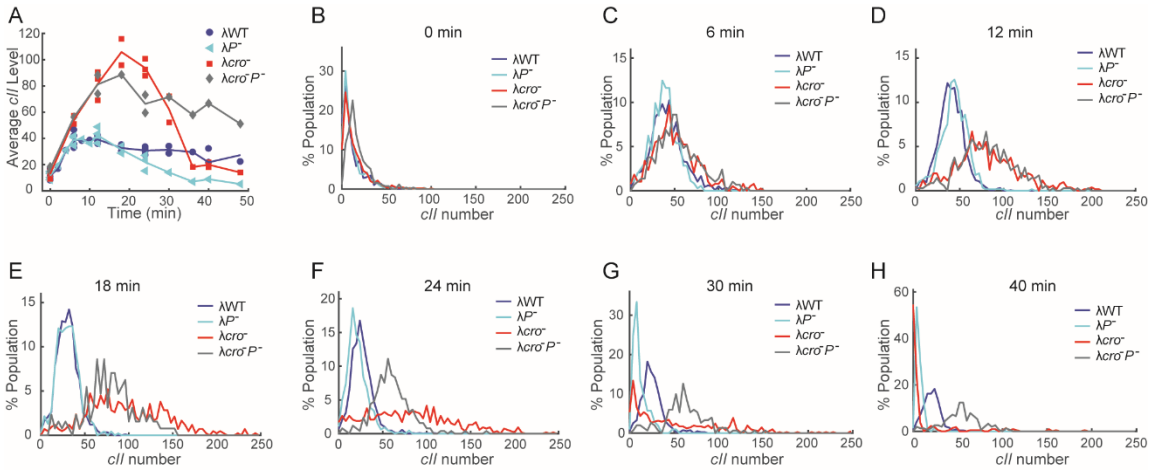

Figure 4.6 *cII* mRNA expression after infection.
(A) Average *cII* levels comparing λWT, λ*cro*⁻, λ*P*⁻, and λ*cro*⁻*P*⁻ infections. The lines were the mean of *cII* expression levels from different experiments for each phage. In the first 18 min, λWT and λ*P*⁻ have similar *cII* levels, but both are lower than λ*cro*⁻ and λ*cro*⁻*P*⁻. The distributions of single-cell *cII* mRNA levels at 0 min (B), 6 min (C), 12 min (D), 18 min (E), 24 min (F), 30 min (G), and 40 min (H) after infection were shown. Data from different experiments were combined, and only the cells that have *cII* mRNA expression were shown. For comparison, the mRNA numbers were normalized according to the cell volume of each cell. For all 4 phages, the *cII* distribution at 0 min looks similar to each other (B). λWT and λ*P*⁻ have similar *cII* distributions at 6 min (C), 12 min (D), and 18 min (E). *cII* distributions for λ*P*⁻ shift to the lower end compared to λWT after 24 min (F, G, and H). For λ*cro*⁻ and λ*cro*⁻*P*⁻, *cII* distributions are similar to each other and both have higher levels compared to λWT and λ*P*⁻ at 6 min (C) and 12 min (D). At 18 min (E) and 24 min (F), λ*cro*⁻ has a wider distribution compared to λ*cro*⁻*P*⁻. At 30 min (G) and 40 min (H), *cII* distributions for λ*cro*⁻ and λ*P*⁻ gradually shift to the left and reach a lower level compared to λWT and λ*cro*⁻*P*⁻.

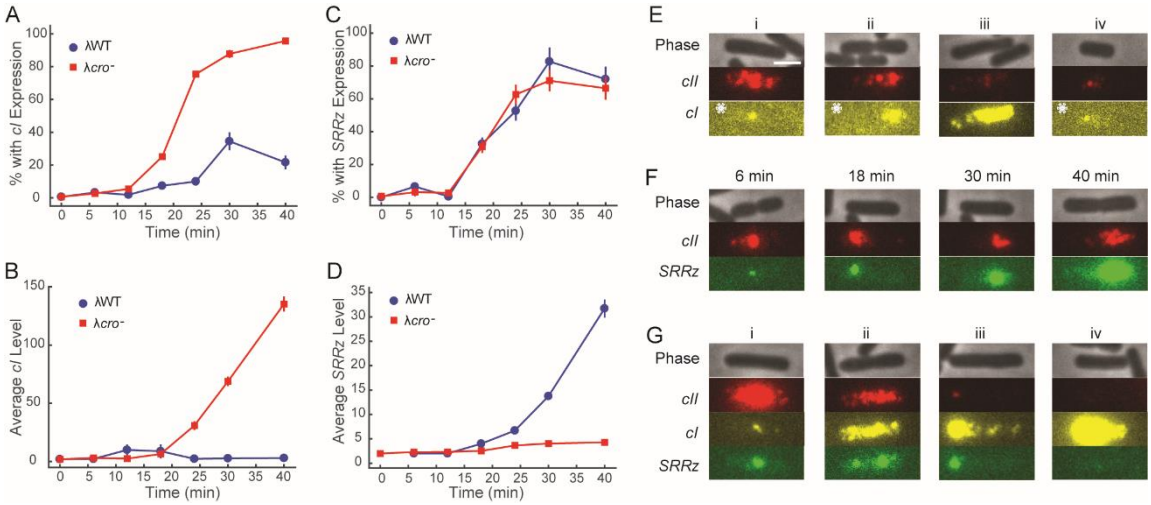

Figure 4.7 The effect of Cro on the lytic-lysogenic decision.
(A) The percentage of cells showing *cI* expression after λWT and λ*cro*⁻ infection. Only infected cells with *cII* expression were taken into account. The percentage of cells with *cI* expression reaches ~30% after infection by λWT and ~95% by λ*cro*⁻. (B) Average *cI* mRNA levels after λWT and λ*cro*⁻ infections. Only the cells with *cI* expression were included for calculation. For λWT, the average *cI* level reaches a peak at around 12-18 min and subsequently drops. For λ*cro*⁻, *cI* level keeps increasing over time after 12 min. (C) Percentage of cells with *SRRz* expression after λWT and λ*cro*⁻ infection. For both phages, the percentage starts to increase substantially after 12 min, and reaches a peak of ~70% for λ*cro*⁻ and ~80% for λWT. (D) Average *SRRz* levels after λWT and λ*cro*⁻ infection. Only the cells with *SRRz* expression were included for calculation. For λWT, *SRRz* expression starts to increase substantially after 12 min, while λ*cro*⁻ only shows moderate increase after 12 min. (E) Selected images showing cells with *cII* and *cI* expression at 18 min after λWT infection. Different levels of *cII* and *cI* expression can be observed in these cells, indicating different stages of the decision making. *: the contrast of the images was adjusted differently to allow better visualization. Unless otherwise stated, the same contrast was used for all microscopic images. (F) Selected images showing cells with *cII* and *SRRz* expression at different time points after λWT infection. Overall, the *SRRz* expression keeps increasing over time. (G) Selected images showing cells with *cII*, *cI*, and *SRRz* expression at 40 min after λ*cro*⁻ infection. Cells are at different stages of infection, and show different levels of *cII*, *cI*, and *SRRz* expression. The error bar denotes the standard error of the mean. Scale bar represents 2 μm.

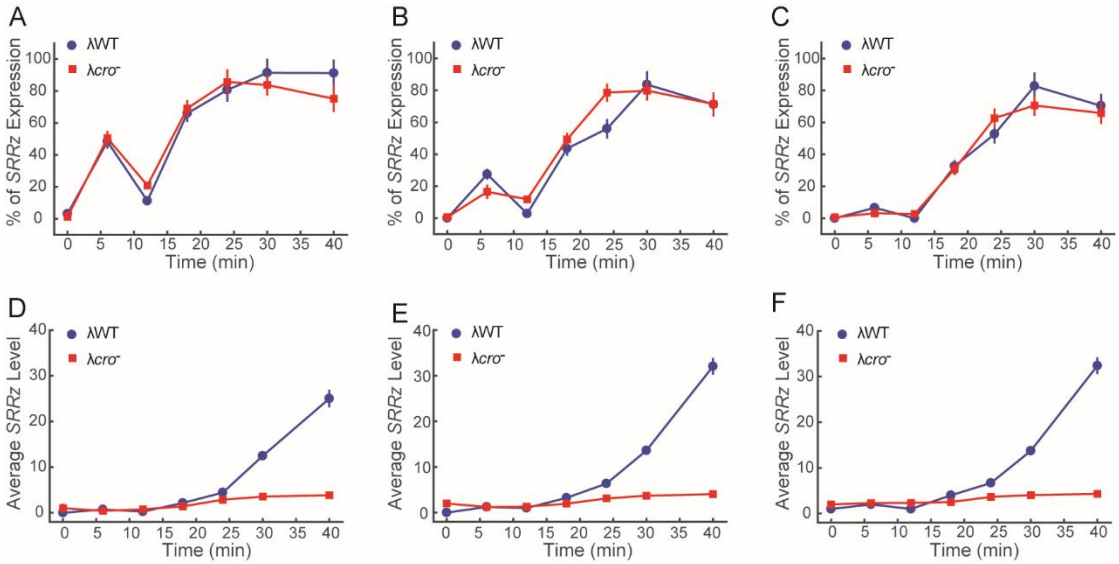

Figure 4.8 *SRRz* mRNA expression after λWT and λ*cro*⁻ phage infection.
(A) The percentage of cells showing *SRRz* expression. The cells were manually determined to have at least one *SRRz* mRNA expression by eye. For both λWT and λ*cro*⁻ infections, the percentages with *SRRz* expression at 6 min are high (~45%), which subsequently drop to ~10% at 12 min. This drop may correspond to the repression of Q by CII through paQ. After 12 min, the percentages increase substantially to more than 80% for both phages. (B) The percentage of cells showing *SRRz* expression. The cells were determined to have at least one *SRRz* mRNA expression by the mRNA number calculation methods described in Materials and Methods. The overall trend is the same as shown in (A), but the level is lower, possibly because some cells having one mRNA were miscalculated as 0 due to the variations in both the background fluorescence intensity and the single mRNA intensity. (C) The percentage of cells showing *SRRz* expression. The cells were determined to have more than one *SRRz* mRNA numbers by calculation. (D) Average *SRRz* expression levels within the population of cells as described in (A). The *SRRz* levels start to increase at 12 min for both λWT and λ*cro*⁻ infections. λWT reaches a much higher level compared to that of λ*cro*⁻. (E) Average *SRRz* levels within the population of cells as described in (B). The average *SRRz* level for λWT reaches about 35 molecules per cell after 40 min of infection, while the λ*cro*⁻ has only ~5 *SRRz* per cell on average. (F) Average *SRRz* level within the population of cells as described in (C). The overall trend is similar to the ones shown in (A) and (B).

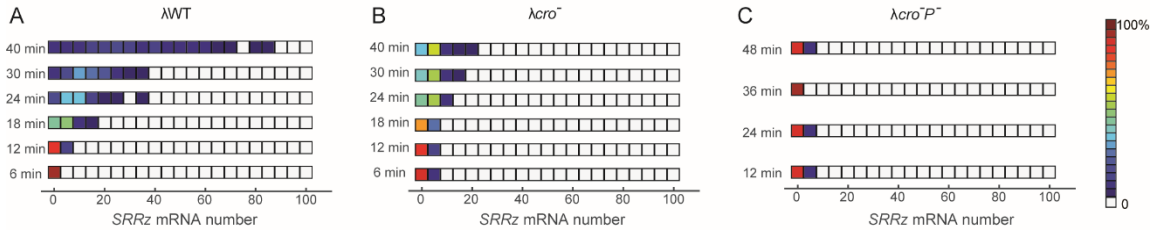

Figure 4.9 Distribution of *SRRz* mRNA number over time for different phages. Only the cells with *SRRz* expression were included. (A) The distribution of *SRRz* number for λWT. The *SRRz* level is low at the first 12 min, and starts to increase after 18 min. At 40 min, some cells reach as high as ~85 *SRRz* molecules per cell, while some cells still have low expression levels. (B) The distribution of *SRRz* number for λ*cro*$^{-}$. Overall, the *SRRz* level is lower compared to λWT. At 40 min, the majority of cells show 1~10 *SRRz* molecules, while very few cells reaches ~25 *SRRz* molecules. (C) The distribution of *SRRz* number for λ*cro*$^{-}$*P*$^{-}$. The *SRRz* expression level is low (<10) throughout the infection process.

After characterizing the *cII* gene expression profile over time and its regulation by Cro, we then examined how *cII* regulation correlates with expression of the late genes that seal the cell fates. To this end, we use smFISH to quantify *cI* and the lysis genes (*SRRz*, *S* for holin, *R* for endolysin, and *Rz* for spanin respectively), in addition to the *cII* transcript. As shown in Figure 4.7A, a low fraction of λWT infected cells show *cI* transcription at 6 min, and by 30 min after infection, about 30% of the infected cells exhibit *cI* signal (Figure 4.7A). The average *cI* level is low at 6 min, and subsequently increases to peak at around 18 min (Figure 4.7B). The *cI* mRNA level then drops, reflecting CI's negative auto-regulation (13). Moreover, our data suggest that the timing of the phage decision-making varies greatly. For example, as shown in Figure 4.7E, cells at different stages of infection can be observed at samples collected at 18 min. Some cells show low levels of *cI* transcription when the *cII* level is high (Figure 4.7E-i),

therefore they may have initiated the lysogenic pathway. Some cells, as shown in Figure 4.7E-ii and iii, may correspond to the ones that have chosen the lysogenic pathway as there are intermediate levels of *cI* expression, and the *cII* expression seems to be inhibited by CI. Cells that show low levels of both *cII* and *cI* expression are also observed (Figure 4.7E-iv), which likely correspond to fully established lysogens. In contrast to λWT, more than 95% of cells show *cI* expression when infected by λ*cro*$^-$ (Figure 4.7A), which is expected as λ*cro*$^-$ has much higher *cII* levels. The *cI* level for λ*cro*$^-$ infections continues to increase and reaches ~140 *cI* mRNAs per cell at 40 min compared to the peak average of ~10 by λWT (Figure 4.7B). This long-term increase of *cI* expression from the λ*cro*$^-$ infection is probably due to prolonged activation of the pRE promoter by CII protein, whose concentration may be very high based on the mRNA levels (Figure 4.6A). This suggests that Cro limits the production of CI in lysogenic cells by tuning *cII* expression. In this way, Cro creates a cellular environment that allows the phage DNA to be more sensitive to stimuli that affect the decision, where perhaps small changes may push the phage to choose between alternative developmental pathways.

Following the canonical understanding of lambda decision-making, if a given pathway is chosen, then the other pathway is excluded. However, higher resolution studies have indicated that individual phage DNAs can commit to different decisions in the same cell, which we call "mixed voting" (4, 111). Interestingly, we find that for λ*cro*$^-$ infected cells, where the vast majority ultimately become lysogenic indicated by high *cI* mRNA levels, most infections show *SRRz* transcription as well (Figure 4.7C and 4.6). In fact, ~70% of λ*cro*$^-$ infected cells show *SRRz* expression (Figure 4.7C), while >95% also

show *cI* expression (Figure 4.7A), indicating that a substantial amount of mixed voting must occur. This suggests that the decision-making circuit of lambda allows both pathways to develop concurrently among the population of intracellular phage DNAs, to the enforcement of the decision, but one decision wins in the end. For λWT, in the case of mixed voting, the lytic pathway almost always dominates, leading to the lytic development of the cell (4, 111). On the contrary, the lysogenic pathway always dominates for λ*cro*$^-$ infections. The *SRRz* expression for λ*cro*$^-$ infection is very low (Figure 4.7D and G), which has <5 *SRRz* molecules per cell on average even after 40 min of infection (Figure 4.7D and 4.9), while λWT infections show an average of ~33 molecules per cell (Figure 4.7D and F). Assays at the bulk level also show that the λ*cro*$^-$ infection leads to high levels of lysogeny and very low levels of progeny production from lysis (Figure 4.4 and 4.5), supporting the domination by lysogenic pathway. This indicates that λ*cro*$^-$ infected cells fail to fully execute the lytic pathway, possibly due to the over-production of CII to inhibit Q expression through paQ and CI (10). In fact, when looking at the *cII*, *cI*, and *SRRz* expression simultaneously at 40 min, we can find evidence of "mixed voting" and the dominance of lysogenic "vote" by λ*cro*$^-$ infection. Some cells have very high *cII* expression, but low levels of both *cI* and *SRRz* (Figure 4.7G-i). This possibly indicates the onset of both lysogenic and lytic pathway. At the same time, cells with moderate amounts of *cII*, *cI*, and *SRRz* are also observed, indicating simultaneous development of lytic and lysogenic pathway (Figure 4.7G-ii). Cells with high *cI* expression, and low *cII* and *SRRz* expression are also observed (Figure 4.7G-iii and iv). The low *cII* expression is most likely caused by the inhibition of pR

promoter by CI, which was produced massively as indicated by the high *cI* level. As CI also inhibits Q expression from pR promoter, we reasoned that the *SRRz* expression will be further inhibited as well, leading to the eventual winning of the lysogenic "vote". Nevertheless, the data support the idea that Cro is required for the bifurcation into the lytic or lysogenic pathways. It accomplishes its role by being a negative regulator for pR to inhibit *cII* expression, to maintain an environment in the cells that permits the development of both lytic and lysogenic pathways prior to the establishment of the chosen fate.

Lysogenic establishment requires multiple copies of phage DNA

One overlooked facet of the decision-making circuit is that, due to viral DNA replication, multiple phage DNAs exist in the cell throughout the infection, regardless of the initial phage input. Here, we investigated how the P^- mutant λP^-, defective in DNA replication, differs in its gene expression profiles and ability to make decisions. Lysogenization frequency of the λP^- mutant is lower than that of λWT at low APIs (Figure 4.10A). Its lysogenic response to the API follows a Poisson distribution of $n \geq 3$, indicating that lysogenization requires 3 or more λP^- phages on average, compared to $n \geq 2$ for λWT (Figure 4.10B) (53). This suggests that multiple copies of phage DNA are needed to lysogenize a cell. We then used smFISH to investigate if DNA replication affects the transcription of early genes and leads to different cell fates. We found that both λWT and λP^- show similar levels of *cII* mRNA (Figure 4.6A). The overall trend of λP^- is similar to λWT, especially through the first 18 minutes after infection where most of the lysogenic decisions are made, although after 24 min, the *cII* levels in λP^- are lower

(Figure 4.6A). Surprisingly, very few cells show *cI* mRNA expression in the λ*P*$^{-}$ infected cells (Figure 4.11A), and if *cI* mRNA is present, its level is lower than in λWT (Figure 4.11B), indicating that λ*P*$^{-}$ is defective in lysogenization. We then asked if the DNA replication can affect the *cII* expression at the single-cell level by changing its population distribution without affecting the population average. However, we did not observe significant differences in the distribution of *cII* mRNA between λWT and λ*P*$^{-}$, especially in the first 18 min (Figure 4.6B-E). These data suggest that the main function of DNA replication in the lysogenization process is downstream of *cII* expression.

To further explore how a single phage DNA attempts its decision-making, we tested a λ*cro*$^{-}$*P*$^{-}$ double mutant. Compared to λWT, this double mutant has higher *cII* mRNA levels (Figure 4.6A), but fewer cells showing *cI* mRNA expression (Figure 4.11A). Cells that show *cI* expression have lower mRNA levels (Figure 4.11B), suggesting that despite having ample expression of *cII*, the key gene for lysogenization, the double mutant phage cannot effectively carry out the lysogenic decision. This is supported by bulk experiments showing that λ*cro*$^{-}$*P*$^{-}$ does not lysogenize as frequently as λWT (Figure 4.12). The data again suggest that the lower lysogenization frequencies for the DNA replication deficient strains are not due to changes at the *cII* expression. Instead, it is possible that a single activated pRE promoter does not produce enough CI to establish lysogeny. Additionally, lytic gene expression in both λ*P*$^{-}$ and λ*cro*$^{-}$*P*$^{-}$ infections is very low (Figure 4.12D and 4.13). And the percentage of cells showing lytic gene expression is also low (Figure 4.11C). This suggests that although a single phage DNA may be capable of choosing a cell fate, indicated from the occasional *cI* and *SRRz*

expression, multiple copies of DNA are required to enforce both decisions. Altogether, our results suggest that DNA replication is important for the enforcement of decision-making. By providing more templates for transcription, DNA replication allows the production of enough effectors for the decisions, CI and the lysis genes.

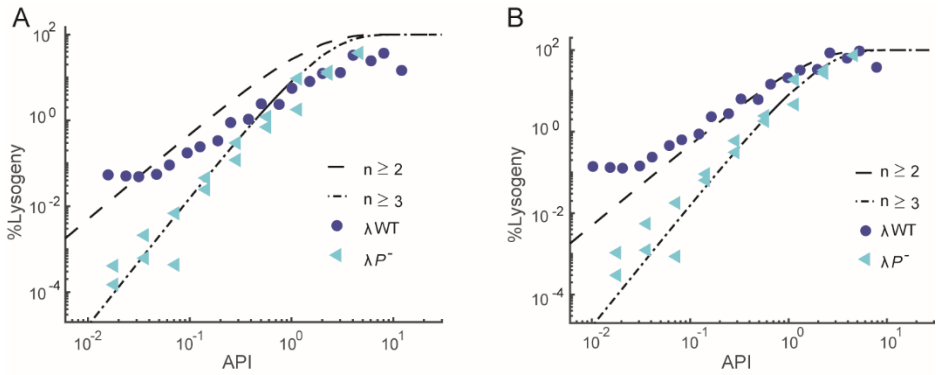

Figure 4.10 DNA replication is important for the lysogenization decision by lambda.
(A) The lysogenization frequency of cells after λWT and λ*P*⁻ infections at different APIs. Combined data of two experiments were shown. The λ*P*⁻ phage infection leads to lower lysogenization frequencies at the low APIs, and has the same level as λWT at high APIs. (B) The data from (A) were shifted to fit into the curves of Poisson distribution. λWT follows the Poisson distribution of n≥2, indicating that 2 or more phages are required to lysogenize the cell on average. λ*P*⁻ follows n≥3, indicating that the lack of DNA replication leads to different patterns of lysogenic response.

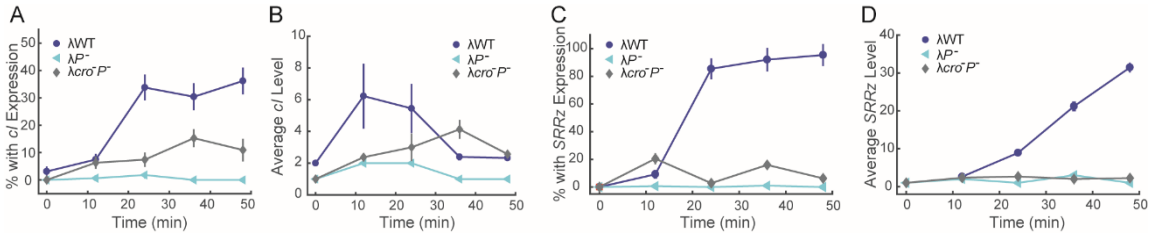

Figure 4.11 DNA replication is important for the lysogenic decision.
(A) The percentages of cells showing *cI* expression for different phage mutants. λ*P*⁻ infection leads to very low frequency of cells with *cI* expression. The percentage of cells with *cI* expression for λ*cro*⁻*P*⁻ is lower than λWT. (B) The average *cI* mRNA levels for different phage mutants. Only the cells showing *cI* expression were included for calculation. Different from λWT, the *cI* level for λ*cro*⁻*P*⁻ infection keeps increasing until 36 min, but the peak level is lower than λWT. The *cI* level for λ*P*⁻ is very low throughout the infection process. (C) Percentages of cells with *SRRz* expression comparing λWT, λ*cro*⁻*P*⁻, and λ*P*⁻ infections. For λ*P*⁻, the percentage is close to 0. λ*cro*⁻*P*⁻ shows lower percentage of cells with *SRRz* expression compared to λWT. (D) Average *SRRz* levels comparing λWT, λ*cro*⁻*P*⁻, and λ*P*⁻ infections. Only the cells with *SRRz* expression were included for calculation. For both λ*cro*⁻*P*⁻ and λ*P*⁻, the average *SRRz* levels are much lower compared to λWT. The error bar denotes the standard error of the mean.

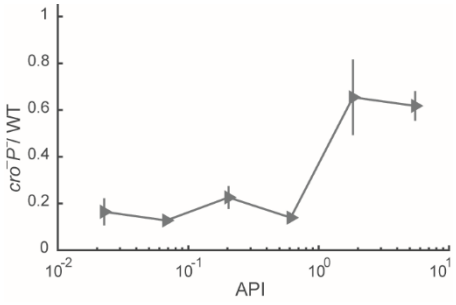

Figure 4.12 The lysogenization frequency of λ*cro*⁻*P*⁻ is lower than λWT.
At high APIs, λWT phage has only slightly higher lysogenization frequencies compared to that of λ*cro*⁻*P*⁻. As API drops, the lysogenization frequency of λ*cro*⁻*P*⁻ is only ~0.2 fold compared to λWT.

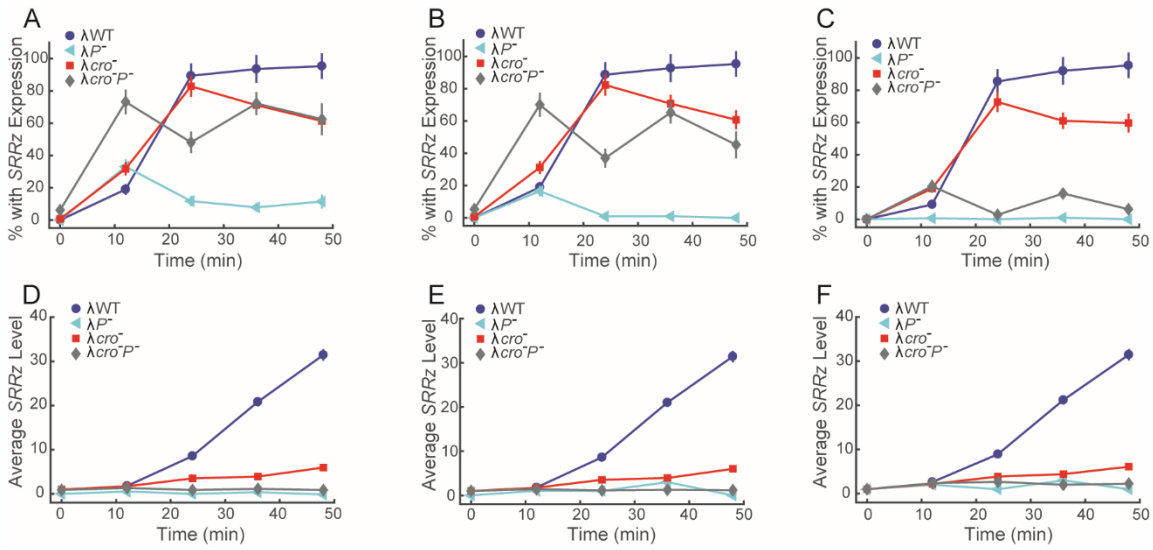

Figure 4.13 The expression level of *SRRz* for different phages.
(A) The percentage of cells showing *SRRz* expression. The cells were manually determined to have at least one *SRRz* mRNA by eye. For all phages except λ*cro*$^{-}$*P*$^{-}$, the percentages with *SRRz* expression at 12 min are already already at ~20%. For λWT and λ*cro*$^{-}$, the percentage increases substantially to ~80% for both phages after 12 min. For λ*P*$^{-}$, the percentage drops after 12 min to almost 0, indicating its inability to enter the lytic pathway. For λ*cro*$^{-}$*P*$^{-}$, ~70% cells show *SRRz* expression. (B) The percentage of cells showing *SRRz* expression. The cells were determined to have at least one *SRRz* mRNA by calculation. The overall trend is the same with shown in A, and the level is only slightly lower. (C) The percentage of cells showing *SRRz* expression. The cells were determined to have more than one *SRRz* mRNAs by calculation. Almost none of the λ*P*$^{-}$ phage infected cells showing more than one *SRRz* expression, again confirming its inability to enter the lytic pathway. The percentage for λ*cro*$^{-}$*P*$^{-}$ drops to lower than 20% compared to ~70% shown in (B), indicating that most of the cells with *SRRz* mRNA expression have only one *SRRz* after λ*cro*$^{-}$*P*$^{-}$ infection. (D) The average *SRRz* expression level within the population of cells as described in (A). The *SRRz* level starts to increase after 12 min of infection for both λWT and λ*cro*$^{-}$. λWT reaches a much higher level compared to λ*cro*$^{-}$. λ*cro*$^{-}$*P*$^{-}$ and λ*P*$^{-}$ infections show very low levels of *SRRz* expression overall, but λ*cro*$^{-}$*P*$^{-}$ has a slightly higher level than λ*P*$^{-}$. (E) The average *SRRz* level within the population of cells as described in (B). (F) The average *SRRz* level within the population of cells as described in (C). The overall trend is similar to the ones shown in (A) and (B).

If phage DNAs can make decisions without replicating, but be hindered in producing the late genes needed to execute the decisions, then we can predict some differences in decision reporters during live-cell infections in the presence and absence of phage DNA replication. We introduced the P^- mutation into our established lytic-lysogenic reporter systems to study the decision-making of λP^- phage by following the progressive development of both pathways simultaneously using live-cell fluorescence microscopy (111). Briefly, a fluorescent protein (mKO2) is inserted downstream of *cI* on the phage genome to report *cI* transcription, corresponding to lysogenic events (Figure 4.14B). Another fluorescent protein (mTurquoise2) is fused to the C-terminus of the phage capsid decoration protein, gpD. Thus mTurquoise2 fluorescence reports lytic development up to host cell lysis (Figure 4.14B). Moreover, this method allows for the quantification of the number of infecting phages on each single cell (Figure 4.14B, cyan dot at 0 min). Overall, the λP^- phage lysogenizes less frequently than λWT, as predicted by bulk experiments (Figure 4.10). Remarkably, λP^- phage infections show no lysogenization events at MOI=1 (Figure 4.14A, 0 out of 37), consistent with our smFISH data (Figure 4.11A). In the lysogenic cells obtained at MOI>1, the *cI* reporter signal is lower than in λWT (Figure 4.14B and C), indicating that fewer copies of phage DNA in the absence of DNA replication results in less *cI* transcription. Additionally, DNA replication is also required for cell lysis. We observe very low levels of the lytic reporter in the live cells (Figure 4.14C), and we did not observe any lysis events within the time window of our time-lapse movies (4 hours, cell lysis occurs at ~2 hours for λWT), in accordance the low level *SRRz* expression reported by smFISH (Figure 4.11C and D).

Taken together, these data suggest that an individual phage DNA has the agency to decide cell fates, but is compromised in its ability to complete the chosen pathway. Next we used EYFP labeled fluorescent λWT and λ*P*$^{-}$ phages to infect cells bearing a multi-copy reporter plasmid, pRE-mCherry, to report the activation of mCherry fluorescence from the pRE promoter by CII, (4, 17). This system artificially increases the copy number of pRE promoters without affecting the decision-making. We find that more than 60% of MOI=1 infections by λ*P*$^{-}$ phages are able to activate this reporter, indicating that a single phage DNA produces enough CII to commit to the lysogenic decision (Figure 4.14E and F). Interestingly, about 50% of MOI=1 λWT infected cells show pRE activation (Figure 4.14D), which is lower than λ*P*$^{-}$, indicating additional effects of DNA replication on the expression of *cII*. Nevertheless, the data together suggest that the failure of lysogenization by λ*P*$^{-}$ phages are due to insufficient CI production rather than CII, resulting in the failure to implement the lysogenic decision.

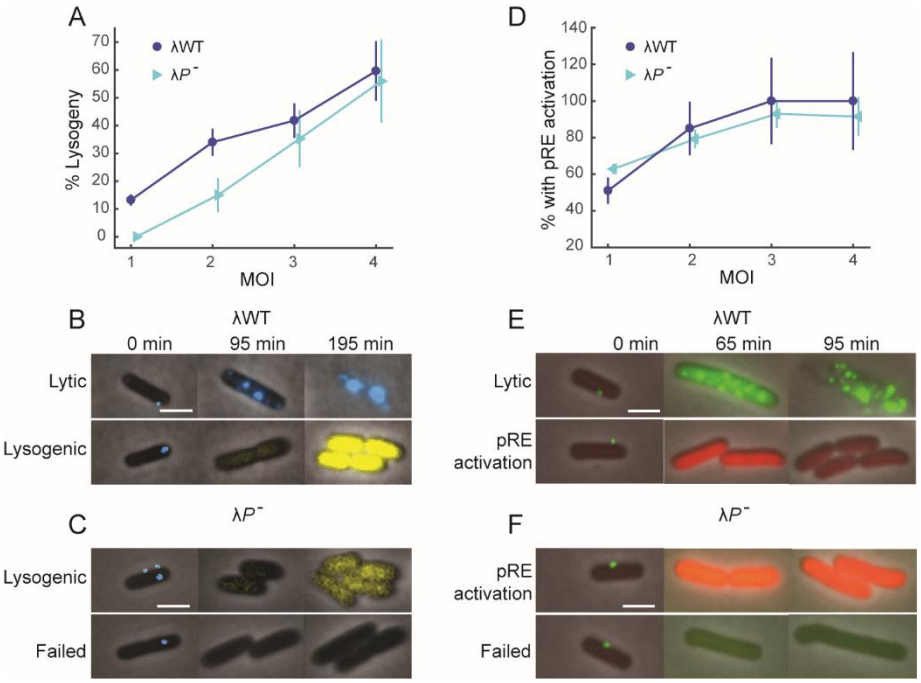

Figure 4.14 Lack of DNA replication results in failure in lysogenic establishment. (A) The lysogenization frequency of λWT and λ*P*⁻ reported by *cI* reporter. M9 medium supplemented with maltose was used for infection. For both phages, the lysogenization frequency increases with MOI. λ*P*⁻ has lower lysogenization frequencies at MOI ≤ 3, and reaches almost the same level as λWT at MOI of 4. At MOI=1, no lysogenization event is observed for λ*P*⁻. (B) Example images showing lytic and lysogenic events by λWT. Top: the cell is infected by one λWT (cyan dot at 0 min), and subsequently gpD-mTurquiose2 expression is observed. The cell eventually lyses at 195 min. Bottom: the cell is infected by one λWT (cyan dot at 0 min). Expression of *cI* reporter (yellow) is observed and the cell divides normally, indicating a successful lysogenization event. (C) Example images of lysogenic and failed infection by λ*P*⁻. Top: the cell is infected by 3 λ*P*⁻ phages (cyan dots at 0 min). The cell divides normally, and expression of the *cI* reporter (yellow) is observed, indicating cell lysogenization. Bottom: the cell is infected by one λ*P*⁻ phage (cyan dot at 0 min). The cell divides, and only minimal expression of gpD-mTurquoise2 is detected. (D) The percentages of cells showing the pRE activation for both phages. LB medium was used for infection. Both phages show increases in frequencies of pRE activation with MOI, and reach a plateau at MOI≥3. (E) Example images of lytic and lysogenic events by λWT infections at MOI=1. Top: Expression of gpD-EYFP (green) is observed and the cell lyses at 95 min. Bottom: Increase of mCherry (red) expression is observed, and the cell divides normally, indicating a successful lysogenic event.

Figure 4.14 continued.
(F) Example images showing λ*P*$^{-}$ infections at MOI=1. Top: Increase in mCherry expression is observed, indicating the activation of pRE promoter. Low levels of gpD-EYFP expression are also detected in the cell. Bottom: Only very low levels gpD-EYFP expression is observed. Division is inhibited, and the cell keeps growing longer without lysing. The error bar denotes the standard error of the mean. Scale bar represents 2 μm.

Transient pRE activation and DNA replication mediate proper cI expression for lysogenic establishment

Our data suggest that DNA replication is critical for boosting *cI* production to enforce the lysogenic decision after the activation of pRE promoter by CII. However, the detailed mechanism is unknown. DNA replication results in more templates, and in the case of λWT infections at API~0.1, the phage DNA number increases by 4.56 (±0.58) fold after 12 min of infection, and reaches 44.46 (±2.92) fold at 24 min on average, by qPCR assays (Figure 4.15). Thus it is possible that having more pRE promoters would promote a higher chance of *cI* expression under a given CII concentration, and lead to more CI production.

We next examined the *cI* expression patterns of different phage mutants to test how DNA replication affects the *cI* expression and cell lysogenization. As shown in Figure 4.16A, most of the λWT infected cells with *cI* expression have 1-10 *cI* mRNA molecules at all time points. However, at 12, 18, and 24 min, we observed that a small fraction of cells have very high *cI* levels, reaching ~100 *cI* per cell. This low frequency of cells with high *cI* expression indicates that the high *cI* expression level does not last for a very long time. Instead, *cI* production most likely reaches a high level within a

relatively short time and then rapidly decreases. This suggests that pRE is transiently activated by CII, which has a relatively short half-life (27). In this case, the inhibition of pR transcription by Cro creates a cellular environment which allows only transient activation of CI production. On the other hand, comparing to the case of one λ*P*$^{-}$ phage infection where *cI* production is rarely observed, the *cI* level in the λWT infections can reach up to ~100 per cell within a short time. This suggests that a substantial amount of phage DNAs must exist at the time of pRE activation to briefly produce these high levels of *cI*. On the other hand, higher levels of CII from the λ*cro*$^{-}$ infection would be predicted to counteract the rapid reduction of *cI* mRNA levels via prolonged pRE activation to produce an expression pattern where *cI* accumulates progressively, which we observe (Figure 4.16B). Furthermore, the *cI* expression pattern for the λ*cro*$^{-}$*P*$^{-}$ double mutant also shows a progressive increase to a fairly uniform level of *cI* over time, consistent with elevated and prolonged pRE activity, but these infections do not achieve high *cI* mRNA numbers, consistent with a lack of DNA templates (Figure 4.16C). Altogether, these data support that the levels of CII are finely tuned by Cro as to only allow transient activation of pRE to promote *cI*, and multiple phage DNAs are required to provide more pRE and pRM templates for sufficient CI production to allow lysogenic establishment.

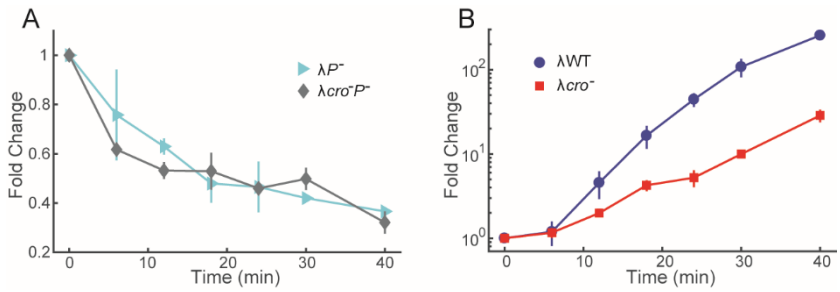

Figure 4.15 Average phage DNA copy number along time after infection.
(A) The average phage DNA copy numbers for λ*P*⁻ and λ*cro*⁻*P*⁻ were shown after normalizing to the host cell DNA number and the first time point. Along time, the number decreases, which can be due to the increase in the host DNA number, as the phage DNA number should stay relatively the same assuming minimal or no DNA replication. (B) Average phage DNA copy numbers after λWT and λ*cro*⁻ infections over time. The average phage DNA numbers for each sample were normalized first to the *E. coli* DNA number for that sample, and then the resulting number was divided by the number obtained in (A), at the corresponding time points, to eliminate the effect of increasing host DNA number. This number was further normalized to the data of the first time point, to result in the absolute phage DNA copy number changes over time. In the first 6 min, the average DNA copy numbers for both λWT and λ*cro*⁻ are the similar, however, starting at 12 min, λWT shows higher levels of phage DNA and reaches ~250 at 40 min, while λ*cro*⁻ reaches only ~28 on average. The lower level of DNA copy number in λ*cro*⁻ infection is probably due to the inhibition of DNA replication and gene expression by CI as most λ*cro*⁻ infections lead to lysogenic establishment.

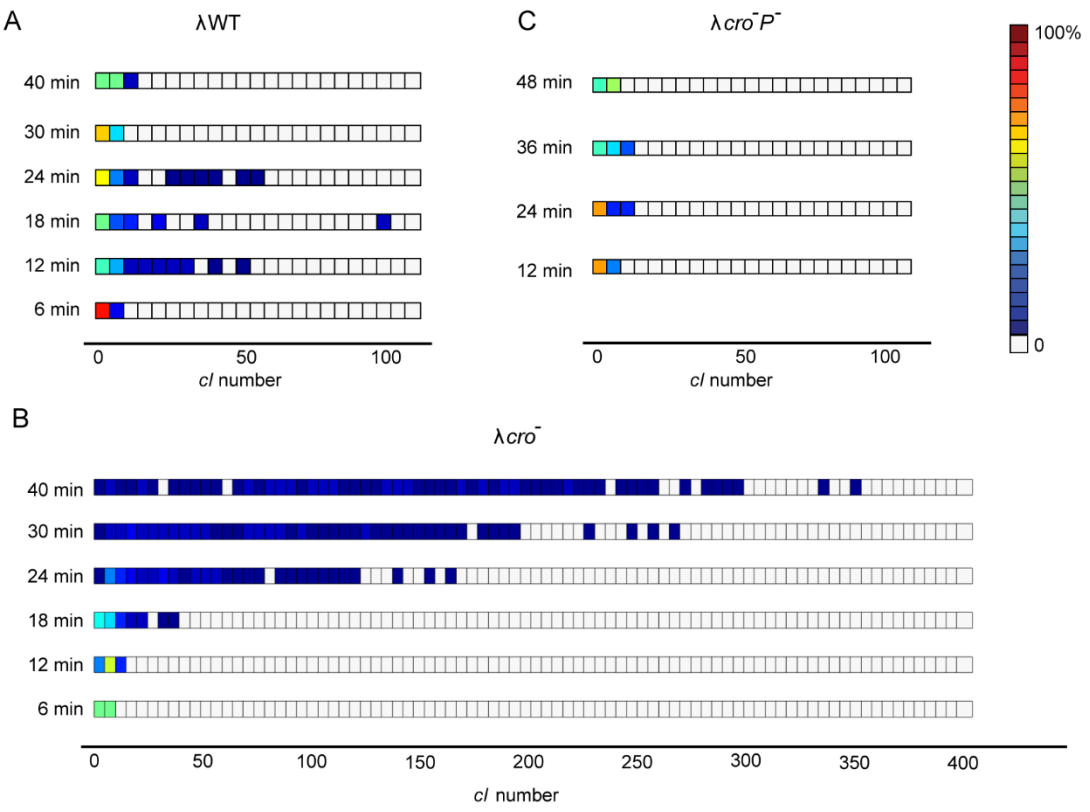

Figure 4.16 The *cI* expression patterns for different phages.
Only cells with *cI* expression were included for the analysis. (A) Distribution of *cI* mRNA level for λWT. Most of the cells have low *cI* expression at all time points. At 12-24 min, some cells have high *cI* expression levels, but the frequency is low. (B) Distribution of *cI* mRNA level for λ*cro*⁻. The *cI* level keeps increasing over time. Some cells show very high levels of *cI* expression (>100 *cI*). (C) Distribution of *cI* mRNA level for λ*cro*⁻*P*⁻. The *cI* expression level is low at all time points, and there are no cells with high expression.

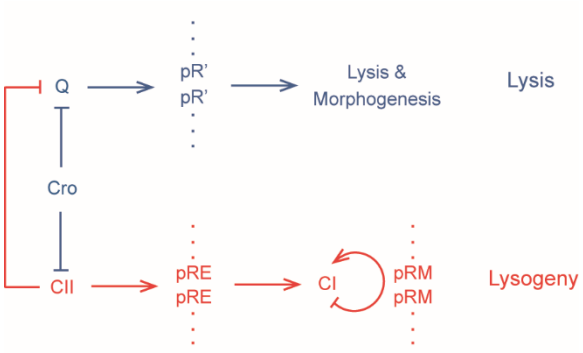

Figure 4.17 A schematic model for the lysis-lysogeny process.
Cro represses the expression of CII from the pR promoter, such that the CII concentration is relatively low and allows only transient activation of CI production from pRE promoter. After a lysogenic decision is made, multiple copies of phage DNA are required for sufficient CI production from both pRE and pRM in order to enforce the decision. If the CII level is low, the cell defaults to the lytic pathway, where multiple copies of DNA are also required for the expression of lysis and phage morphogenesis proteins. When Cro is absent, CII expression reaches a high level that is capable of continuous activation of CI production from pRE promoter. The high CII level also leads to inhibition of Q production, therefore inhibiting the lytic development and allowing only lysogenic development. Altogether, the repression by Cro and positive regulation by DNA replication allow phages to bifurcate into alternative developmental pathways and to enforce their decisions.

Discussion

The lysis-lysogeny decision-making of bacteriophage lambda has long served as a paradigm for studying stochastic cell-fate selection, mainly due to the well-established genetic networks involved. Following decades of studies, researchers have characterized the effects of each genetic component, and built models to understand this process systematically (89). However, previous experimental approaches to this system have been carried out in bulk cultures, which may obscure important aspects of this process. Here, we have applied single-cell and single-molecule techniques to examine the effects of Cro and DNA replication on the lysis-lysogeny decision-making. We provided more quantitative measurements of their effects on gene expression, decision-making, and the enforcement of the cell-fate decisions.

The role of DNA replication in the decision-making process has been largely overlooked, although bulk experimental data have long suggested an important role of DNA replication for the lysogenic pathway (53). Surprisingly, we found that the average level and single-cell distribution of pR transcription level for λWT and λ*P*$^{-}$ phages are similar to each other, despite differences in phage DNA copy number. The λ*P*$^{-}$ phages are not capable of lysogenization when a single phage infects, indicating effects of DNA replication on the downstream processes of *cII* expression. Our experimental data suggest that a single phage DNA, from our λ*P*$^{-}$ experiments, is able to produce enough CII protein to activate pRE for CI production, but an insufficient amount of CI is produced. Even the double mutant λ*cro*$^{-}$*P*$^{-}$, which expresses more *cII* than λWT on average, has lower lysogenization frequency compared to λWT. The data indicate that

the strength of pRE promoter is too weak to reliably produce an adequate amount of CI from a single copy of DNA, regardless of CII level. In this case, DNA replication fulfills the role to produce more templates for transcription (Figure 4.17). The level of DNA replication can be variable between different cells. At this stage, we don't know the copy number of phage DNA at the time when the cells are entering the lysogenic state, and whether the timing of lysogenic establishment is affected by the level of DNA replication. Future experiments allowing the quantification of phage DNA copy number will allow the examination of its correlations with cell-fate selection.

The role of Cro has been extensively studied in the CI-Cro bistable switch (13), but its function in decision-making is still nebulous. The main activity of Cro is to inhibit transcription from the pR and pL promoters. Our results show that *cII* mRNA expression in the absence of Cro is high enough that >90% of λ*cro*$^-$ infected cells go to the lysogenic pathway. Interestingly, high pR transcription also allows Q to pass the threshold and allow transcription of late genes from pR', although the resultant lytic gene expression is much lower compared to λWT. We can infer that the cellular environment in the absence of Cro is rich in CII and relatively low in Q, leading to the lack of decision diversity. In this case, Cro appears to create a balanced environment that allows phages to bifurcate into different directions (Figure 4.17). On the other hand, Cro also regulates the expression from pL promoter, where *cIII* is expressed. As CIII functions to stabilize CII protein, we therefore expect an even higher CII protein concentration in λ*cro*$^-$ infection compared to λWT.

The detection of *cII* mRNA using smFISH also allows for the observation of its intracellular location. Unlike eukaryotic cells where transcription happens in the nucleus and is separated from the cytoplasm by membranes, *E. coli* cells lack specific compartments designated for transcription. Interestingly, after phage infection, we observed that *cII* mRNAs most often locate within a specific region, forming clusters instead of exhibiting well-distributed foci as would be predicted by normal diffusion. This highly localized mRNA distribution suggests possible compartmentalization for intracellular phage progression. The bacterial cytoplasm is an extremely crowded environment with macromolecules taking up ~30% of the volume (115, 116), and has been reported to exhibit glass like properties, especially for large particles (7). It has been shown that in a crowded environment, the local mRNA production rate can exceed the diffusion rate, and the mRNAs appear in clusters (120). In our case, *cII* mRNA is part of a transcript that can be as long as 6000 nt. The mRNA might also be actively translated at the same time and associated with multiple ribosomes. Moreover, it might still reside in the vicinity or tether to its template DNA. It is therefore possible that *cII* mRNAs are part of a potentially large complex that has reduced diffusion in the crowded cytoplasm. This localized mRNA distribution may provide evidence for the "individuality" of different phages, as suggested by researchers (4, 111, 213), however, further investigation is required.

CHAPTER V

SUMMARY AND CONCLUSIONS

Phage DNA Dynamics *in vivo*

In this work, we developed a new technique to allow the tracking of single phage DNAs *in vivo* in real time. The infecting phages are prepared to have fully-methylated DNAs packaged inside their head, and are used to infect specifically engineered host cells. The host cells are *dam*$^-$ strains with constitutive expression of a protein fusion, SeqA-YFP. As SeqA specifically binds to fully-methylated or hemi-methylated DNAs, the first two copies of every initially ejected phage DNAs after replication can be tracked under the fluorescence microscope. Following the freshly ejected DNA with mini-second resolution within a few seconds, phage DNA is found to exhibit subdiffusive behavior. When the phage DNA motions are detected throughout the whole infection process, great heterogeneity in their dynamics are observed. Some phage DNAs are found to exhibit restricted motions, where they 'jiggle' around within a short radius, while some phage DNAs can traverse the whole cell within a few minutes. When the cell-fate decisions are followed at the same time, there is not strong correlation between the early phage DNA motion and the final fate. However, when a certain cell fate is chosen, phage DNA movement slows down during lytic development in general, while staying the same in lysogenic cells.

Lysis-lysogeny Coexistence

Recent research suggested that multiple phages infecting the same cell may be able to maintain their 'identity' to some degree, and make lysis-lysogeny decisions independently. However, direct experimental observation of concurrent lytic and lysogenic votes in the same cell have not been made. To investigate this possibility, we developed a DNA integration reporter system, in hope to use it in combination with lytic reporters, to dissect the behavior of single DNAs for lytic-lysogenic developments. Inserting multiple copies of *tetO* repeats in the vicinity of *E. coli attB*, the phage DNA integration site, and constitutive expression of protein fusion TetR-mCherry allows the observation of the host chromosome location and movement. Combining with the SeqA phage DNA labeling system, the DNA integration process can be followed in real time. We found that in some lytic cells, phage DNA integration events can be observed, suggesting that phage DNAs in the same cellular environment can make distinct decisions. Moreover, by tracking the movements of individual DNAs, we found that over time the *E. coli attB* locus migrates towards the polar region, where the phage DNA preferentially resides. This directed motion of *E. coli* DNA may therefore contribute to more collisions with phage DNA, therefore leading to more integration events, regardless of the cell fate choice.

DNA Replication and Cro Regulated Cell-fate Bifurcation

The role of phage DNA replication during lambda lysis-lysogeny decision making has long been over-looked, both in experimental investigations and mathematical simulations. Here combining single-cell, single-phage labeling techniques

and real time live-cell imaging, we found that phages lacking DNA replication are defective in lysogenic establishment when one single phage is infecting. Moreover, single-cell quantification of the gene activities using smFISH reveals that phage DNA replication exerts its effect in the production of the decision effectors, such as *cI* and lysis genes, rather than *cII*, the early fate-determining genes. Furthermore, the role of Cro in gene regulation is also investigated. We determined that in the decision-making process, one of the main functions of Cro is to inhibit the transcription of genes, such as *cII* and *Q*, from the pR promoter. In the absence of Cro, CII expression is high enough to repress the lytic pathway and leads to almost exclusively lysogenic development. Overall, the presence of Cro allows the cell to maintain an environment where the overall CII level allows phage bifurcation into distinct lytic-lysogenic pathways.

REFERENCES

1. Balazsi G, van Oudenaarden A, & Collins JJ (2011) Cellular decision making and biological noise: from microbes to mammals. *Cell* 144(6):910-925.
2. Perkins TJ & Swain PS (2009) Strategies for cellular decision-making. *Mol Syst Biol* 5:326.
3. St-Pierre F & Endy D (2008) Determination of cell fate selection during phage lambda infection. *Proc Natl Acad Sci U S A* 105(52):20705-20710.
4. Zeng L, *et al.* (2010) Decision making at a subcellular level determines the outcome of bacteriophage infection. *Cell* 141(4):682-691.
5. Kaern M, Elston TC, Blake WJ, & Collins JJ (2005) Stochasticity in gene expression: from theories to phenotypes. *Nat Rev Genet* 6(6):451-464.
6. Raj A & van Oudenaarden A (2008) Nature, nurture, or chance: stochastic gene expression and its consequences. *Cell* 135(2):216-226.
7. Parry BR, *et al.* (2014) The bacterial cytoplasm has glass-like properties and is fluidized by metabolic activity. *Cell* 156(1-2):183-194.
8. Greer H (1975) The kil gene of bacteriophage lambda. *Virology* 66(2):589-604.
9. Haeusser DP, *et al.* (2014) The Kil peptide of bacteriophage lambda blocks Escherichia coli cytokinesis via ZipA-dependent inhibition of FtsZ assembly. *PLoS Genet* 10(3):e1004217.
10. Oppenheim AB, Kobiler O, Stavans J, Court DL, & Adhya S (2005) Switches in bacteriophage lambda development. *Annu Rev Genet* 39:409-429.

11. Casjens SR & Hendrix RW (2015) Bacteriophage lambda: Early pioneer and still relevant. *Virology* 479-480:310-330.

12. Lewis DE, Gussin GN, & Adhya S (2016) New insights into the phage genetic switch: effects of bacteriophage lambda operator mutations on DNA looping and regulation of pR, pL, and pRM. *J Mol Biol* 428(22):4438-4456.

13. Ptashne M (2004) *Genetic Switch: Phage Lambda Revisited* (Cold Spring Harbor Laboratory Press, Woodbury, NY).

14. Court DL, Oppenheim AB, & Adhya SL (2007) A new look at bacteriophage lambda genetic networks. *J Bacteriol* 189(2):298-304.

15. Dodd IB, Shearwin KE, & Egan JB (2005) Revisited gene regulation in bacteriophage lambda. *Curr Opin Genet Dev* 15(2):145-152.

16. Sepulveda LA, Xu H, Zhang J, Wang M, & Golding I (2016) Measurement of gene regulation in individual cells reveals rapid switching between promoter states. *Science* 351(6278):1218-1222.

17. Kobiler O, *et al.* (2005) Quantitative kinetic analysis of the bacteriophage lambda genetic network. *Proc Natl Acad Sci U S A* 102(12):4470-4475.

18. Hoyt MA, Knight DM, Das A, Miller HI, & Echols H (1982) Control of phage lambda development by stability and synthesis of cII protein: role of the viral cIII and host hflA, himA and himD genes. *Cell* 31(3 Pt 2):565-573.

19. Eisen H, *et al.* (1975) The role of gene cro in phage development. *Virology* 68(1):266-269.

20. Folkmanis A, Maltzman W, Mellon P, Skalka A, & Echols H (1977) The essential role of the cro gene in lytic development by bacteriophage lambda. *Virology* 81(2):352-362.

21. Datta AB, Panjikar S, Weiss MS, Chakrabarti P, & Parrack P (2005) Structure of lambda CII: implications for recognition of direct-repeat DNA by an unusual tetrameric organization. *Proc Natl Acad Sci U S A* 102(32):11242-11247.

22. Jain D, *et al.* (2005) Crystal structure of bacteriophage lambda cII and its DNA complex. *Mol Cell* 19(2):259-269.

23. Herman C, Thevenet D, D'Ari R, & Bouloc P (1995) Degradation of sigma 32, the heat shock regulator in *Escherichia coli*, is governed by HflB. *Proc Natl Acad Sci U S A* 92(8):3516-3520.

24. Krinke L & Wulff DL (1987) OOP RNA, produced from multicopy plasmids, inhibits lambda cII gene expression through an RNase III-dependent mechanism. *Genes Dev* 1(9):1005-1013.

25. Krinke L & Wulff DL (1990) RNase III-dependent hydrolysis of lambda cII-O gene mRNA mediated by lambda OOP antisense RNA. *Genes Dev* 4(12A):2223-2233.

26. Takayama KM, Houba-Herin N, & Inouye M (1987) Overproduction of an antisense RNA containing the oop RNA sequence of bacteriophage lambda induces clear plaque formation. *Mol Gen Genet* 210(1):184-186.

27. Rattray A, Altuvia S, Mahajna G, Oppenheim AB, & Gottesman M (1984) Control of bacteriophage lambda CII activity by bacteriophage and host functions. *J Bacteriol* 159(1):238-242.

28. Banuett F, Hoyt MA, McFarlane L, Echols H, & Herskowitz I (1986) hflB, a new Escherichia coli locus regulating lysogeny and the level of bacteriophage lambda cII protein. *J Mol Biol* 187(2):213-224.

29. Cheng HH, Muhlrad PJ, Hoyt MA, & Echols H (1988) Cleavage of the cII protein of phage lambda by purified HflA protease: control of the switch between lysis and lysogeny. *Proc Natl Acad Sci U S A* 85(21):7882-7886.

30. Tomoyasu T, *et al.* (1993) Topology and subcellular localization of FtsH protein in Escherichia coli. *J Bacteriol* 175(5):1352-1357.

31. Ito K & Akiyama Y (2005) Cellular functions, mechanism of action, and regulation of FtsH protease. *Annu Rev Microbiol* 59:211-231.

32. Langklotz S, Baumann U, & Narberhaus F (2012) Structure and function of the bacterial AAA protease FtsH. *Biochim Biophys Acta* 1823(1):40-48.

33. Shotland Y, *et al.* (2000) Proteolysis of bacteriophage lambda CII by Escherichia coli FtsH (HflB). *J Bacteriol* 182(11):3111-3116.

34. Kobiler O, Koby S, Teff D, Court D, & Oppenheim AB (2002) The phage lambda CII transcriptional activator carries a C-terminal domain signaling for rapid proteolysis. *Proc Natl Acad Sci U S A* 99(23):14964-14969.

35. Schwarz E, Scherer G, Hobom G, & Kossel H (1978) Nucleotide sequence of cro, cII and part of the O gene in phage lambda DNA. *Nature* 272(5652):410-414.

36. Wulff DL & Rosenberg M (1983) Establishment of repressor synthesis. *Lambda II*, eds Hendrix RW, Roberts JW, Stahl FW, & Weisberg RA (Cold Spring Harbor Laboratory, Cold Spring Harbor, New York), pp 53-73.

37. Ho Y & Rosenberg M (1982) Characterization of the phage lambda regulatory protein cII. *Ann Microbiol (Paris)* 133(2):215-218.

38. Jones MO & Herskowitz I (1978) Mutants of bacteriophage lambda which do not requre the cIII gene for efficient lysogenization. *Virology* 88(2):199-212.

39. Herman C, Thevenet D, D'Ari R, & Bouloc P (1997) The HflB protease of Escherichia coli degrades its inhibitor lambda cIII. *J Bacteriol* 179(2):358-363.

40. Kobiler O, Rokney A, & Oppenheim AB (2007) Phage lambda CIII: a protease inhibitor regulating the lysis-lysogeny decision. *PLoS One* 2(4):e363.

41. Nickels BE, Roberts CW, Roberts JW, & Hochschild A (2006) RNA-mediated destabilization of the sigma(70) region 4/beta flap interaction facilitates engagement of RNA polymerase by the Q antiterminator. *Mol Cell* 24(3):457-468.

42. Vorobiev SM, *et al.* (2014) Structure of the DNA-binding and RNA-polymerase-binding region of transcription antitermination factor lambdaQ. *Structure* 22(3):488-495.

43. Santangelo TJ & Artsimovitch I (2011) Termination and antitermination: RNA polymerase runs a stop sign. *Nat Rev Microbiol* 9(5):319-329.

44. Roberts JW, *et al.* (1998) Antitermination by bacteriophage lambda Q protein. *Cold Spring Harb Symp Quant Biol* 63:319-325.

45. Kuznedelov K, *et al.* (2002) A role for interaction of the RNA polymerase flap domain with the sigma subunit in promoter recognition. *Science* 295(5556):855-857.

46. Murakami KS, Masuda S, & Darst SA (2002) Structural basis of transcription initiation: RNA polymerase holoenzyme at 4 A resolution. *Science* 296(5571):1280-1284.

47. Vassylyev DG, *et al.* (2002) Crystal structure of a bacterial RNA polymerase holoenzyme at 2.6 A resolution. *Nature* 417(6890):712-719.

48. Nickels BE, Roberts CW, Sun H, Roberts JW, & Hochschild A (2002) The sigma(70) subunit of RNA polymerase is contacted by the (lambda)Q antiterminator during early elongation. *Mol Cell* 10(3):611-622.

49. Nickels BE, Dove SL, Murakami KS, Darst SA, & Hochschild A (2002) Protein-protein and protein-DNA interactions of sigma70 region 4 involved in transcription activation by lambdacI. *J Mol Biol* 324(1):17-34.

50. Deighan P, Diez CM, Leibman M, Hochschild A, & Nickels BE (2008) The bacteriophage lambda Q antiterminator protein contacts the beta-flap domain of RNA polymerase. *Proc Natl Acad Sci U S A* 105(40):15305-15310.

51. Deighan P & Hochschild A (2007) The bacteriophage lambdaQ anti-terminator protein regulates late gene expression as a stable component of the transcription elongation complex. *Mol Microbiol* 63(3):911-920.

52. Echols H, Court D, & Green L (1976) On the nature of cis-acting regulatory proteins and genetic organization in bacteriophage: the example of gene Q of bacteriophage lambda. *Genetics* 83(1):5-10.

53. Kourilsky P (1973) Lysogenization by bacteriophage lambda. I. Multiple infection and the lysogenic response. *Mol Gen Genet* 122(2):183-195.

54. Tsurimoto T & Matsubara K (1981) Purified bacteriophage lambda O protein binds to four repeating sequences at the lambda replication origin. *Nucleic acids research* 9(8):1789-1799.

55. Zakrzewska-Czerwinska J, Jakimowicz D, Zawilak-Pawlik A, & Messer W (2007) Regulation of the initiation of chromosomal replication in bacteria. *FEMS Microbiol Rev* 31(4):378-387.

56. Furth ME, McLeester C, & Dove WF (1978) Specificity determinants for bacteriophage lambda DNA replication. I. A chain of interactions that controls the initiation of replication. *J Mol Biol* 126(2):195-225.

57. Zylicz M, Gorska I, Taylor K, & Georgopoulos C (1984) Bacteriophage lambda replication proteins: formation of a mixed oligomer and binding to the origin of lambda DNA. *Mol Gen Genet* 196(3):401-406.

58. Mallory JB, Alfano C, & McMacken R (1990) Host virus interactions in the initiation of bacteriophage lambda DNA replication. Recruitment of Escherichia

coli DnaB helicase by lambda P replication protein. *J Biol Chem* 265(22):13297-13307.

59. Datta I, Sau S, Sil AK, & Mandal NC (2005) The bacteriophage lambda DNA replication protein P inhibits the oriC DNA- and ATP-binding functions of the DNA replication initiator protein DnaA of *Escherichia coli*. *J Biochem Mol Biol* 38(1):97-103.

60. Biswas SB & Biswas EE (1987) Regulation of dnaB function in DNA replication in Escherichia coli by dnaC and lambda P gene products. *J Biol Chem* 262(16):7831-7838.

61. Zylicz M, Ang D, Liberek K, & Georgopoulos C (1989) Initiation of lambda DNA replication with purified host- and bacteriophage-encoded proteins: the role of the dnaK, dnaJ and grpE heat shock proteins. *EMBO J* 8(5):1601-1608.

62. Dove WF, Hargrove E, Ohashi M, Haugli F, & Guha A (1969) Replicator activation in lambda. *Jpn. J. Genet* (44):11-22.

63. Mensa-Wilmot K, Carroll K, & McMacken R (1989) Transcriptional activation of bacteriophage lambda DNA replication in vitro: regulatory role of histone-like protein HU of Escherichia coli. *EMBO J* 8(8):2393-2402.

64. Roth A, Urmoneit B, & Messer W (1994) Functions of histone-like proteins in the initiation of DNA replication at oriC of *Escherichia coli*. *Biochimie* 76(10-11):917-923.

65. Wegrzyn G, Szalewska-Palasz A, Wegrzyn A, Obuchowski M, & Taylor K (1995) Transcriptional activation of the origin of coliphage lambda DNA replication is regulated by the host DnaA initiator function. *Gene* 154(1):47-50.

66. Wegrzyn G, *et al.* (1995) Involvement of the host initiator function dnaA in the replication of coliphage lambda. *Genetics* 139(4):1469-1481.

67. Hendrix RW, Roberts JW, Stahl FW, & Weisberg RA (1983) *Lambda II* (Cold Spring Harbor Laboratory, Cold Spring Harbor, New York).

68. Better M & Freifelder D (1982) Studies on the association of E. coli phage lambda DNA and the host chromosome: lack of a role of membranes. *Virology* 119(1):159-168.

69. Taylor K & Wegrzyn G (1995) Replication of coliphage lambda DNA. *FEMS Microbiol Rev* 17(1-2):109-119.

70. Wegrzyn G, Pawlowicz A, & Taylor K (1992) Stability of coliphage lambda DNA replication initiator, the lambda O protein. *J Mol Biol* 226(3):675-680.

71. Narajczyk M, Baranska S, Wegrzyn A, & Wegrzyn G (2007) Switch from theta to sigma replication of bacteriophage lambda DNA: factors involved in the process and a model for its regulation. *Mol Genet Genomics* 278(1):65-74.

72. Kourilsky P (1974) Lysogenization by bacteriophage lambda. II. Identification of genes involved in the multiplicity dependent processes. *Biochimie* 56(11-12):1511-1516.

73. Kourilsky P & Knapp A (1974) Lysogenization by bacteriophage lambda. III. Multiplicity dependent phenomena occuring upon infection by lambda. *Biochimie* 56(11-12):1517-1523.

74. Alvarez LJ, Thomen P, Makushok T, & Chatenay D (2007) Propagation of fluorescent viruses in growing plaques. *Biotechnol Bioeng* 96(3):615-621.

75. Zeng L & Golding I (2011) Following cell-fate in E. coli after infection by phage lambda. *J Vis Exp* (56):e3363.

76. Schirmer T, Keller TA, Wang YF, & Rosenbusch JP (1995) Structural basis for sugar translocation through maltoporin channels at 3.1 A resolution. *Science* 267(5197):512-514.

77. Erni B (2006) The mannose transporter complex: an open door for the macromolecular invasion of bacteria. *J Bacteriol* 188(20):7036-7038.

78. Edgar R, *et al.* (2008) Bacteriophage infection is targeted to cellular poles. *Mol Microbiol* 68(5):1107-1116.

79. Berkane E, *et al.* (2006) Interaction of bacteriophage lambda with its cell surface receptor: an in vitro study of binding of the viral tail protein gpJ to LamB (Maltoporin). *Biochemistry* 45(8):2708-2720.

80. Wang J, Michel V, Hofnung M, & Charbit A (1998) Cloning of the *J* gene of bacteriophage lambda, expression and solubilization of the J protein: first in vitro studies on the interactions between J and LamB, its cell surface receptor. *Res Microbiol* 149(9):611-624.

81. Rothenberg E, *et al.* (2011) Single-virus tracking reveals a spatial receptor-dependent search mechanism. *Biophys J* 100(12):2875-2882.

82. Elliott J & Arber W (1978) *E. coli* K-12 *pel* mutants, which block phage lambda DNA injection, coincide with *ptsM*, which determines a component of a sugar transport system. *Mol Gen Genet* 161(1):1-8.

83. Scandella D & Arber W (1974) An *Escherichia coli* mutant which inhibits the injection of phage lambda DNA. *Virology* 58(2):504-513.

84. Chen Y (2016) Regulation of phage lysis: diverse strategies and targets. Doctoral (Texas A&M University).

85. Huber F & Erni B (1996) Membrane topology of the mannose transporter of *Escherichia coli* K12. *Eur J Biochem* 239(3):810-817.

86. Novick SL & Baldeschwieler JD (1988) Fluorescence measurement of the kinetics of DNA injection by bacteriophage lambda into liposomes. *Biochemistry* 27(20):7919-7924.

87. Novick A & Weiner M (1957) Enzyme Induction as an All-or-None Phenomenon. *Proc Natl Acad Sci U S A* 43(7):553-566.

88. Siegele DA & Hu JC (1997) Gene expression from plasmids containing the araBAD promoter at subsaturating inducer concentrations represents mixed populations. *Proc Natl Acad Sci U S A* 94(15):8168-8172.

89. Arkin A, Ross J, & McAdams HH (1998) Stochastic kinetic analysis of developmental pathway bifurcation in phage lambda-infected Escherichia coli cells. *Genetics* 149(4):1633-1648.

90. Elowitz MB, Levine AJ, Siggia ED, & Swain PS (2002) Stochastic gene expression in a single cell. *Science* 297(5584):1183-1186.

91. Cai L, Friedman N, & Xie XS (2006) Stochastic protein expression in individual cells at the single molecule level. *Nature* 440(7082):358-362.

92. Ozbudak EM, Thattai M, Kurtser I, Grossman AD, & van Oudenaarden A (2002) Regulation of noise in the expression of a single gene. *Nat Genet* 31(1):69-73.

93. Thattai M & van Oudenaarden A (2001) Intrinsic noise in gene regulatory networks. *Proc Natl Acad Sci U S A* 98(15):8614-8619.

94. Yu J, Xiao J, Ren X, Lao K, & Xie XS (2006) Probing gene expression in live cells, one protein molecule at a time. *Science* 311(5767):1600-1603.

95. Beach DL, Salmon ED, & Bloom K (1999) Localization and anchoring of mRNA in budding yeast. *Curr Biol* 9(11):569-578.

96. Bertrand E, *et al.* (1998) Localization of ASH1 mRNA particles in living yeast. *Mol Cell* 2(4):437-445.

97. Golding I & Cox EC (2004) RNA dynamics in live Escherichia coli cells. *Proc Natl Acad Sci U S A* 101(31):11310-11315.

98. Golding I, Paulsson J, Zawilski SM, & Cox EC (2005) Real-time kinetics of gene activity in individual bacteria. *Cell* 123(6):1025-1036.

99. McAdams HH & Arkin A (1999) It's a noisy business! Genetic regulation at the nanomolar scale. *Trends Genet* 15(2):65-69.

100. Rao CV, Wolf DM, & Arkin AP (2002) Control, exploitation and tolerance of intracellular noise. *Nature* 420(6912):231-237.

101. Becskei A & Serrano L (2000) Engineering stability in gene networks by autoregulation. *Nature* 405(6786):590-593.

102. Simpson ML, Cox CD, & Sayler GS (2003) Frequency domain analysis of noise in autoregulated gene circuits. *Proc Natl Acad Sci U S A* 100(8):4551-4556.

103. McAdams HH & Arkin A (1997) Stochastic mechanisms in gene expression. *Proc Natl Acad Sci U S A* 94(3):814-819.

104. Cook DL, Gerber AN, & Tapscott SJ (1998) Modeling stochastic gene expression: implications for haploinsufficiency. *Proc Natl Acad Sci U S A* 95(26):15641-15646.

105. Kemkemer R, Schrank S, Vogel W, Gruler H, & Kaufmann D (2002) Increased noise as an effect of haploinsufficiency of the tumor-suppressor gene neurofibromatosis type 1 in vitro. *Proc Natl Acad Sci U S A* 99(21):13783-13788.

106. Becskei A, Seraphin B, & Serrano L (2001) Positive feedback in eukaryotic gene networks: cell differentiation by graded to binary response conversion. *EMBO J* 20(10):2528-2535.

107. Maamar H & Dubnau D (2005) Bistability in the Bacillus subtilis K-state (competence) system requires a positive feedback loop. *Mol Microbiol* 56(3):615-624.

108. Suel GM, Garcia-Ojalvo J, Liberman LM, & Elowitz MB (2006) An excitable gene regulatory circuit induces transient cellular differentiation. *Nature* 440(7083):545-550.

109. Weinberger LS, Burnett JC, Toettcher JE, Arkin AP, & Schaffer DV (2005) Stochastic gene expression in a lentiviral positive-feedback loop: HIV-1 Tat fluctuations drive phenotypic diversity. *Cell* 122(2):169-182.

110. Weitz JS, Mileyko Y, Joh RI, & Voit EO (2008) Collective decision making in bacterial viruses. *Biophys J* 95(6):2673-2680.

111. Trinh JT, Szekely T, Shao Q, Balazsi G, & Zeng L (2017) Cell fate decisions emerge as phages cooperate or compete inside their host. *Nat. Commun.* 8(14341).

112. Dix JA & Verkman AS (2008) Crowding effects on diffusion in solutions and cells. *Annu Rev Biophys* 37:247-263.

113. Golding I & Cox EC (2006) Physical nature of bacterial cytoplasm. *Phys Rev Lett* 96(9):098102.

114. Hunter GL & Weeks ER (2012) The physics of the colloidal glass transition. *Rep Prog Phys* 75(6).

115. Cayley S, Lewis BA, Guttman HJ, & Record MT, Jr. (1991) Characterization of the cytoplasm of Escherichia coli K-12 as a function of external osmolarity. Implications for protein-DNA interactions in vivo. *J Mol Biol* 222(2):281-300.

116. Zimmerman SB & Trach SO (1991) Estimation of macromolecule concentrations and excluded volume effects for the cytoplasm of Escherichia coli. *J Mol Biol* 222(3):599-620.

117. Luby-Phelps K (2000) Cytoarchitecture and physical properties of cytoplasm: volume, viscosity, diffusion, intracellular surface area. *Int Rev Cytol* 192:189-221.

118. Wirth AJ & Gruebele M (2013) Quinary protein structure and the consequences of crowding in living cells: leaving the test-tube behind. *Bioessays* 35(11):984-993.

119. Zhou HX, Rivas G, & Minton AP (2008) Macromolecular crowding and confinement: biochemical, biophysical, and potential physiological consequences. *Annu Rev Biophys* 37:375-397.

120. Hansen MM, *et al.* (2016) Macromolecular crowding creates heterogeneous environments of gene expression in picolitre droplets. *Nat Nanotechnol* 11(2):191-197.

121. van Zon JS, Morelli MJ, Tanase-Nicola S, & ten Wolde PR (2006) Diffusion of transcription factors can drastically enhance the noise in gene expression. *Biophys J* 91(12):4350-4367.

122. Tal A, Arbel-Goren R, Costantino N, Court DL, & Stavans J (2014) Location of the unique integration site on an *Escherichia coli* chromosome by bacteriophage lambda DNA in vivo. *Proceedings of the National Academy of Sciences of the United States of America*.

123. Shao Q, Hawkins A, & Zeng L (2015) Phage DNA dynamics in cells with different fates. *Biophys J* 108(8):2048-2060.

124. Nielsen HJ, Li Y, Youngren B, Hansen FG, & Austin S (2006) Progressive segregation of the Escherichia coli chromosome. *Mol Microbiol* 61(2):383-393.

125. Nielsen HJ, Ottesen JR, Youngren B, Austin SJ, & Hansen FG (2006) The Escherichia coli chromosome is organized with the left and right chromosome arms in separate cell halves. *Mol Microbiol* 62(2):331-338.

126. Youngren B, Nielsen HJ, Jun S, & Austin S (2014) The multifork Escherichia coli chromosome is a self-duplicating and self-segregating thermodynamic ring polymer. *Genes Dev* 28(1):71-84.

127. Youngren B, Radnedge L, Hu P, Garcia E, & Austin S (2000) A plasmid partition system of the P1-P7par family from the pMT1 virulence plasmid of Yersinia pestis. *J Bacteriol* 182(14):3924-3928.

128. Siegel PJ & Schaechter M (1973) The role of the host cell membrane in the replication and morphogenesis of bacteriophages. *Annu Rev Microbiol* 27:261-282.

129. Hallick L, Boyce RP, & Echols H (1969) Membrane association by bacteriophage lambda-DNA: possible direct role of regulator gene N. *Nature* 223(5212):1239-1242.

130. Hallick LM & Echols H (1973) Genetic and Biochemical Properties of an Association Complex between Host Components and Lambda DNA. *Virology* 52(1):105-119.

131. Klaus S, Geuther R, & Noack D (1972) Membrane attachment of lambda DNA in mutants of Escherichia coli temperature sensitive in DNA replication. *Mol Gen Genet* 115(1):97-100.

132. Klaus S, Geuther R, & Noack D (1972) Kinetics of membrane association by bacteriophage lambda DNA after repressor inactivation. *Mol Gen Genet* 115(1):93-96.

133. Kolber AR & Sly WS (1971) Association of lambda bacteriophage DNA with a rapidly sedimenting Escherichia coli component. *Virology* 46(3):638-654.

134. Korn D & Thomas M (1971) Control of plasmid replication in Escherichia coli: correlation of the membrane site of DNA replication with the bacterial segregation unit. *Proc Natl Acad Sci U S A* 68(9):2047-2051.

135. Nishimoto T & Matsubara K (1972) The correlation between transcription and membrane-association of lambda DNA. *Biochem Biophys Res Commun* 46(2):349-356.

136. Sakakibara Y & Tomizawa JI (1971) Regulation of transcription of lambda bacteriophage operator mutants. *Virology* 44(3):463-472.

137. Sakaki Y, Mizuno S, & Maruo B (1971) The binding of the parental DNA from bacteriophages to the cell membrane of Escherichia coli. *Biochim Biophys Acta* 232(1):14-20.

138. Parma DH, *et al.* (1992) The Rex system of bacteriophage lambda: tolerance and altruistic cell death. *Genes Dev* 6(3):497-510.

139. Murialdo H & Siminovitch L (1972) The morphogenesis of bacteriophage lambda. IV. Identification of gene products and control of the expression of the morphogenetic information. *Virology* 48(3):785-823.

140. Hohn T & Katsura I (1977) Structure and assembly of bacteriophage lambda. *Curr Top Microbiol Immunol* 78:69-110.

141. Valenzuela MS (1975) Intermediates of the first round of lambda DNA replication are preferentially found in a rapidly sedimenting complex. *Biochem Biophys Res Commun* 65(4):1221-1228.

142. Witkiewicz H & Taylor K (1978) Lambda dna-membrane complex isolated in the CsCl density gradient. *FEBS Lett* 90(2):313-317.

143. Rudner DZ & Losick R (2010) Protein subcellular localization in bacteria. *Cold Spring Harb Perspect Biol* 2(4):a000307.

144. Bi EF & Lutkenhaus J (1991) FtsZ ring structure associated with division in Escherichia coli. *Nature* 354(6349):161-164.

145. Buskila AA, Kannaiah S, & Amster-Choder O (2014) RNA localization in bacteria. *RNA Biol* 11(8):1051-1060.

146. Miller OL, Jr., Hamkalo BA, & Thomas CA, Jr. (1970) Visualization of bacterial genes in action. *Science* 169(3943):392-395.

147. Gowrishankar J & Harinarayanan R (2004) Why is transcription coupled to translation in bacteria? *Mol Microbiol* 54(3):598-603.

148. Fisher JK, *et al.* (2013) Four-dimensional imaging of E. coli nucleoid organization and dynamics in living cells. *Cell* 153(4):882-895.

149. Bakshi S, Siryaporn A, Goulian M, & Weisshaar JC (2012) Superresolution imaging of ribosomes and RNA polymerase in live Escherichia coli cells. *Mol Microbiol* 85(1):21-38.

150. Chai Q, *et al.* (2014) Organization of ribosomes and nucleoids in Escherichia coli cells during growth and in quiescence. *J Biol Chem* 289(16):11342-11352.

151. Fusco D, *et al.* (2003) Single mRNA molecules demonstrate probabilistic movement in living mammalian cells. *Curr Biol* 13(2):161-167.

152. Forrest KM & Gavis ER (2003) Live imaging of endogenous RNA reveals a diffusion and entrapment mechanism for nanos mRNA localization in Drosophila. *Curr Biol* 13(14):1159-1168.

153. Montero Llopis P, *et al.* (2010) Spatial organization of the flow of genetic information in bacteria. *Nature* 466(7302):77-81.

154. Nevo-Dinur K, Nussbaum-Shochat A, Ben-Yehuda S, & Amster-Choder O (2011) Translation-independent localization of mRNA in E. coli. *Science* 331(6020):1081-1084.

155. Shao Q, *et al.* (2016) Lysis-lysogeny coexistence: prophage integration during lytic development. *Microbiologyopen*.

156. Grayson P, Han L, Winther T, & Phillips R (2007) Real-time observations of single bacteriophage lambda DNA ejections in vitro. *Proc Natl Acad Sci U S A* 104(37):14652-14657.

157. Van Valen D, *et al.* (2012) A single-molecule Hershey-Chase experiment. *Curr Biol* 22(14):1339-1343.

158. Hendrix RW & Duda RL (1992) Bacteriophage lambda PaPa: not the mother of all lambda phages. *Science* 258(5085):1145-1148.

159. Shao Y & Wang IN (2008) Bacteriophage adsorption rate and optimal lysis time. *Genetics* 180(1):471-482.

160. Hendrix RW (1983) *Lambda II* (Cold Spring Harbor Laboratory, Cold Spring Harbor, N.Y.) pp vii, 694 p.

161. Kourilsky P & Gros D (1976) Lysogenization by bacteriophage lambda IV inhibition of phage DNA synthesis by the products of genes cII and cIII. *Biochimie* 58(11-12):1321-1327.

162. Joh RI & Weitz JS (2011) To lyse or not to lyse: transient-mediated stochastic fate determination in cells infected by bacteriophages. *PLoS Comput Biol* 7(3):e1002006.

163. Thanbichler M & Shapiro L (2008) Getting organized--how bacterial cells move proteins and DNA. *Nat Rev Microbiol* 6(1):28-40.

164. Rothfield L, Taghbalout A, & Shih YL (2005) Spatial control of bacterial division-site placement. *Nat Rev Microbiol* 3(12):959-968.

165. Weber SC, Spakowitz AJ, & Theriot JA (2010) Bacterial chromosomal loci move subdiffusively through a viscoelastic cytoplasm. *Phys Rev Lett* 104(23):238102.

166. Herman GE & Modrich P (1981) Escherichia coli K-12 clones that overproduce dam methylase are hypermutable. *J Bacteriol* 145(1):644-646.

167. Babic A, Lindner AB, Vulic M, Stewart EJ, & Radman M (2008) Direct visualization of horizontal gene transfer. *Science* 319(5869):1533-1536.

168. Zhang N & Young R (1999) Complementation and characterization of the nested Rz and Rz1 reading frames in the genome of bacteriophage lambda. *Mol Gen Genet* 262(4-5):659-667.

169. Barondess JJ & Beckwith J (1995) bor gene of phage lambda, involved in serum resistance, encodes a widely conserved outer membrane lipoprotein. *J Bacteriol* 177(5):1247-1253.

170. Szyf M, *et al.* (1984) DNA methylation pattern is determined by the intracellular level of the methylase. *Proc Natl Acad Sci U S A* 81(11):3278-3282.

171. Datsenko KA & Wanner BL (2000) One-step inactivation of chromosomal genes in Escherichia coli K-12 using PCR products. *Proc Natl Acad Sci U S A* 97(12):6640-6645.

172. Mackay DJ & Bode VC (1976) Events in lambda injection between phage adsorption and DNA entry. *Virology* 72(1):154-166.

173. Skinner SO, Sepulveda LA, Xu H, & Golding I (2013) Measuring mRNA copy number in individual Escherichia coli cells using single-molecule fluorescent in situ hybridization. *Nat Protoc* 8(6):1100-1113.

174. St-Pierre Fo (2009) Determination of Cell Fate Selection During Phage Lambda Infection. *Ph.D. Thesis, MIT*.

175. Slominska M, Konopa G, Baranska S, Wegrzyn G, & Wegrzyn A (2003) Interplay between DnaA and SeqA proteins during regulation of bacteriophage lambda pR promoter activity. *J Mol Biol* 329(1):59-68.

176. Slominska M, Wegrzyn A, Konopa G, Skarstad K, & Wegrzyn G (2001) SeqA, the *Escherichia coli* origin sequestration protein, is also a specific transcription factor. *Mol Microbiol* 40(6):1371-1379.

177. Weber SC, Spakowitz AJ, & Theriot JA (2012) Nonthermal ATP-dependent fluctuations contribute to the in vivo motion of chromosomal loci. *Proc Natl Acad Sci U S A* 109(19):7338-7343.

178. Brendler T & Austin S (1999) Binding of SeqA protein to DNA requires interaction between two or more complexes bound to separate hemimethylated GATC sequences. *EMBO J* 18(8):2304-2310.

179. Han JS, Kang S, Kim SH, Ko MJ, & Hwang DS (2004) Binding of SeqA protein to hemi-methylated GATC sequences enhances their interaction and aggregation properties. *J Biol Chem* 279(29):30236-30243.

180. Phillips R, Kondev J, Theriot J, & Garcia HG (2013) *Physical biology of the cell* (Garland Science, New York, NY) 2nd edition. Ed.

181. Coquel AS, *et al.* (2013) Localization of protein aggregation in Escherichia coli is governed by diffusion and nucleoid macromolecular crowding effect. *PLoS Comput Biol* 9(4):e1003038.

182. Conter A, Bouche JP, & Dassain M (1996) Identification of a new inhibitor of essential division gene ftsZ as the kil gene of defective prophage Rac. *J Bacteriol* 178(17):5100-5104.

183. Lin-Chao S & Bremer H (1986) Effect of the bacterial growth rate on replication control of plasmid pBR322 in Escherichia coli. *Mol Gen Genet* 203(1):143-149.

184. Slater S, *et al.* (1995) E. coli SeqA protein binds oriC in two different methyl-modulated reactions appropriate to its roles in DNA replication initiation and origin sequestration. *Cell* 82(6):927-936.

185. Lu M, Campbell JL, Boye E, & Kleckner N (1994) SeqA: a negative modulator of replication initiation in E. coli. *Cell* 77(3):413-426.

186. Lau IF, *et al.* (2003) Spatial and temporal organization of replicating Escherichia coli chromosomes. *Mol Microbiol* 49(3):731-743.

187. Svenningsen SL, Costantino N, Court DL, & Adhya S (2005) On the role of Cro in lambda prophage induction. *Proc Natl Acad Sci U S A* 102(12):4465-4469.

188. Takeda Y, Folkmanis A, & Echols H (1977) Cro regulatory protein specified by bacteriophage lambda. Structure, DNA-binding, and repression of RNA synthesis. *J Biol Chem* 252(17):6177-6183.

189. Marr MT, Datwyler SA, Meares CF, & Roberts JW (2001) Restructuring of an RNA polymerase holoenzyme elongation complex by lambdoid phage Q proteins. *Proc Natl Acad Sci U S A* 98(16):8972-8978.

190. Nash HA (1981) Integration and excision of bacteriophage lambda: the mechanism of conservation site specific recombination. *Annu Rev Genet* 15:143-167.

191. Landy A (1989) Dynamic, structural, and regulatory aspects of lambda site-specific recombination. *Annu Rev Biochem* 58:913-949.

192. Wang X, Tang OW, Riley EP, & Rudner DZ (2014) The SMC condensin complex is required for origin segregation in Bacillus subtilis. *Curr Biol* 24(3):287-292.

193. Wang X, Possoz C, & Sherratt DJ (2005) Dancing around the divisome: asymmetric chromosome segregation in Escherichia coli. *Genes Dev* 19(19):2367-2377.

194. Powell BS, Rivas MP, Court DL, Nakamura Y, & Turnbough CL, Jr. (1994) Rapid confirmation of single copy lambda prophage integration by PCR. *Nucleic acids research* 22(25):5765-5766.

195. Sliusarenko O, Heinritz J, Emonet T, & Jacobs-Wagner C (2011) High-throughput, subpixel precision analysis of bacterial morphogenesis and intracellular spatio-temporal dynamics. *Mol Microbiol* 80(3):612-627.

196. Goedhart J, *et al.* (2012) Structure-guided evolution of cyan fluorescent proteins towards a quantum yield of 93%. *Nat Commun* 3:751.

197. Freifelder D & Levine EE (1973) Requirement for transcription in the neighborhood of the phage attachment region for lysogenization of Escherichia coli by bacteriophage lambda. *J Mol Biol* 74(4):729-733.

198. Miller HI, *et al.* (1981) Regulation of the integration-excision reaction by bacteriophage lambda. *Cold Spring Harb Symp Quant Biol* 45 Pt 1:439-445.

199. Schindler D & Echols H (1981) Retroregulation of the int gene of bacteriophage lambda: control of translation completion. *Proc Natl Acad Sci U S A* 78(7):4475-4479.

200. Freifelder D & Kirschner I (1971) The formation of homoimmune double lysogens of phage lambda and the segregation of single lysogens from them. *Virology* 44(3):633-637.

201. Freifelder D & Levine EE (1975) The formation of polylysogens during infection of Escherichia coli with bacteriophage lambda. *Virology* 63(2):428-437.

202. Maamar H, Raj A, & Dubnau D (2007) Noise in gene expression determines cell fate in *Bacillus subtilis*. *Science* 317(5837):526-529.

203. Suel GM, Kulkarni RP, Dworkin J, Garcia-Ojalvo J, & Elowitz MB (2007) Tunability and noise dependence in differentiation dynamics. *Science* 315(5819):1716-1719.

204. Acar M, Mettetal JT, & van Oudenaarden A (2008) Stochastic switching as a survival strategy in fluctuating environments. *Nat Genet* 40(4):471-475.

205. Choi PJ, Cai L, Frieda K, & Xie XS (2008) A stochastic single-molecule event triggers phenotype switching of a bacterial cell. *Science* 322(5900):442-446.

206. Leisner M, Stingl K, Frey E, & Maier B (2008) Stochastic switching to competence. *Curr Opin Microbiol* 11(6):553-559.

207. McAdams HH & Shapiro L (1995) Circuit simulation of genetic networks. *Science* 269(5224):650-656.

208. Lyubimova A, *et al.* (2013) Single-molecule mRNA detection and counting in mammalian tissue. *Nat Protoc* 8(9):1743-1758.

209. Lee C, Kim J, Shin SG, & Hwang S (2006) Absolute and relative QPCR quantification of plasmid copy number in Escherichia coli. *J Biotechnol* 123(3):273-280.

210. Zong C, So LH, Sepulveda LA, Skinner SO, & Golding I (2010) Lysogen stability is determined by the frequency of activity bursts from the fate-determining gene. *Mol Syst Biol* 6:440.

211. Bednarz M, Halliday JA, Herman C, & Golding I (2014) Revisiting bistability in the lysis/lysogeny circuit of bacteriophage lambda. *PLoS One* 9(6):e100876.

212. Schubert RA, Dodd IB, Egan JB, & Shearwin KE (2007) Cro's role in the CI Cro bistable switch is critical for lambda's transition from lysogeny to lytic development. *Genes Dev* 21(19):2461-2472.

213. Golding I (2011) Decision making in living cells: lessons from a simple system. *Annu Rev Biophys* 40:63-80.